PRESSURE DISTRIBUTION AROUND RIGID CULVERTS CONSIDERING THE SOIL-STRUCTURE INTERACTION EFFECTS

by

Eric Yvon Allard, P.Eng.

Bachelor of Science in Engineering, University of New Brunswick, 2008

A Thesis Submitted in Partial Fulfillment
of the Requirements for the Degree of

Masters of Science in Engineering

in the Graduate Academic Unit of Civil Engineering

Supervisor: Hany El Naggar, PhD, PEng, Department of Civil Engineering

Examining Board: Arun J. Valsangkar, PhD, PEng, Department of Civil Engineering
Allison B. Schriver, PhD, PEng Department of Civil Engineering
Saleh Saleh, PhD, PEng, Department of Electrical Engineering

This thesis is accepted by the Dean of Graduate Studies

THE UNIVERSITY OF NEW BRUNSWICK

February 2014

©Eric Yvon Allard, 2014

ABSTRACT

Heger's pressure distributions are considered a fundamental tool in the design of reinforced concrete culverts per the direct design method. However, there are some factors known to affect soil-structure interaction that are neglected when utilizing Heger's pressure distributions. These factors include the effect of the trench geometry, the relative stiffness of the existing and backfill soil, and the burial depth of the structure. This thesis presents a detailed finite-element analysis parametric study that investigates the accuracy and applicability of Heger's pressure distributions for culverts in partial trench installations when the aforementioned factors are considered. Additionally, a detailed pseudo-static finite-element analysis parametric study investigating the applicability and accuracy of the simplified seismic load combination presented in the Canadian Highway Bridge Design Code is presented.

ACKNOWLEDGEMENTS

I would like to thank Dr. El Naggar for his constant support, guidance, encouragement, and patience. Without his help, I would not have completed this thesis.

I would also like to thank everyone at HILCON Limited, especially Jeff Martin and James Wood, for the support and encouragement in completing my Masters.

I would also like to thank Heidi for her understanding, patience and encouragement as this endeavor consumed many of my evenings and weekends.

Finally, I want to thank the New Brunswick Innovations Foundation for providing the funds used for purchasing some of the software necessary for much of my analysis.

Table of Contents

ABSTRACT ii
ACKNOWLEDGEMENTS iii
Table of Contents iv
List of Tables vi
List of Figures vii
Chapter 1 - Introduction 1
1.1 Statement of the Problem 1
1.2 Thesis Objectives 4
1.3 Scope and Organization of the Thesis 4
1.4 References 5
Chapter 2 - Literature Review 7
2.1 Indirect Design of Reinforced Concrete Culvert 7
2.2 Direct Design of Reinforced Concrete Culvert 16
2.3 Comparison of Current Design Standards 20
2.3.1 Limit-States Design Implementation Comparison 20
2.3.2 Seismic Load Combination 22
2.3.3 Miscellaneous Differences 23
2.3.4 Potential Errors and Inconsistencies between Standards 24
2.3.5 References 27
Chapter 3 - Numerical Analysis – Static Load Case 29
3.1 General 29
3.2 Finite-Element Analysis Model 30
3.2.1 Geometry 30
3.2.2 Finite-Element Mesh Elements 32
3.2.3 Material Properties 32
3.2.4 Staged Analysis 34
3.2.5 Results 37
3.3 Heger Pressure Distribution Model 47
3.3.1 Geometry and Finite-Element Mesh 47
3.3.2 Elements 49
3.3.3 Materials 51
3.3.4 Pressure Distribution 51
3.3.5 Validation 51
3.3.6 Results 59
3.4 Finite-Element Analysis / Heger Comparison 67
3.4.1 Bending Moments 67
3.4.2 Axial Thrusts 72
3.4.3 Shear Forces 76
3.5 Comparison of Required Flexural Reinforcing Steel at Ultimate Limit States .. 78
3.6 Summary and Conclusion 80
3.7 References 82
Chapter 4 - Numerical Analysis – Seismic Load Case 83
4.1 General 83

4.2 Simplified Method per CHBDC 84
4.3 Pseudo-Static Analysis of in-Plane Seismic Stresses 85
4.4 Finite-Element Analysis Model 86
4.4.1 Staged Analysis 87
4.4.2 Results 90
4.5 Summary and Conclusion 128
4.6 References 129
Chapter 5 - Chapter 5 – Summary and Conclusions 131
5.1 General 131
5.1.1 Numerical Analysis – Static Load Case 132
5.1.2 Numerical Analysis – Seismic Load Case 133
5.2 Recommended Further Study 134
5.3 Practical Considerations 134
Bibliography 136
Curriculum Vitae

List of Tables

Table 2.1 - Design Values of Settlement Ratio (ACPA, 1980). 11
Table 2.2 - Bedding Factors for Dead Load (after AASHTO). 15
Table 2.3 - Bedding Factors for Live Load (after AASHTO). 16
Table 3.1 - Soil Properties Considered in the Analysis 33
Table 3.2 - SIDD Earth Load Coefficients for Type 1 Installations 54
Table 3.3 - SIDD Earth Load Coefficients for Type 2 Installations 55
Table 3.4 - SIDD Earth Load Coefficients for Type 3 Installations 56
Table 3.5 - SIDD Earth Load Coefficients for Type 4 Installations 57
Table 3.6 - SIDD Coefficients for Self-Weight of Culvert 58
Table 3.7 - Comparison of Required Flexural Reinforcement 80
Table 4.1 - Comparison of Seismic Bending Moments with 3 m burial depth. 101
Table 4.2 - Comparison of Seismic Bending Moments with 6 m burial depth. 102
Table 4.3 - Comparison of Seismic Bending Moments with 12 m burial depth. 103
Table 4.4 - Comparison of Seismic Axial Thrusts with 3 m burial depth. 113
Table 4.5 - Comparison of Seismic Axial Thrusts with 6 m burial depth. 114
Table 4.6 - Comparison of Seismic Axial Thrusts with 12 m burial depth. 115
Table 4.7 - Comparison of Seismic Shear Forces with 3 m burial depth. 125
Table 4.8 - Comparison of Seismic Shear Forces with 6 m burial depth. 126
Table 4.9 - Comparison of Seismic Shear Forces with 12 m burial depth. 127

List of Figures

Figure 2.1 - Indirect Design Geometry Definition Sketch (ACPA, 1980). 10
Figure 2.2 - Sample Design Chart for Embankment Fill Load Calculation (ACPA, 1980). 12
Figure 2.3 - Effective Supporting Length of Culvert (ASCE, 2001). 13
Figure 2.4 - Three-Edge Bearing Test (ACPA, 1980). 14
Figure 2.5 - Heger Pressure Distributions and Coefficients (ASCE, 2000). 18
Figure 3.1 – Geometry of the considered problem. 32
Figure 3.2 - Staged Installation Sequence 35
Figure 3.3 - Bending Moments in Culvert with 3 m Fill (FEA) 38
Figure 3.4 - Bending Moments in Culvert with 6 m Fill (FEA) 39
Figure 3.5 - Bending Moments in Culvert with 12 m Fill (FEA) 40
Figure 3.6 – Axial Thrust in Culvert with 3 m Fill (FEA) 41
Figure 3.7 – Axial Thrust in Culvert with 6 m Fill (FEA) 42
Figure 3.8 – Axial Thrust in Culvert with 12 m Fill (FEA) 43
Figure 3.9 – Shear Force in Culvert with 3 m Fill (FEA) 44
Figure 3.10 – Shear Force in Culvert with 6 m Fill (FEA) 45
Figure 3.11 – Shear Force in Culvert with 12 m Fill (FEA) 46
Figure 3.12 - Model Geometry and Restraint Conditions 49
Figure 3.13 - Bending Moments in Culvert with 3 m Fill (SIDD) 59
Figure 3.14 - Bending Moments in Culvert with 6 m Fill (SIDD) 60
Figure 3.15 - Bending Moments in Culvert with 12 m Fill (SIDD) 61
Figure 3.16 – Axial Thrust in Culvert with 3 m Fill (SIDD) 62
Figure 3.17 – Axial Thrust in Culvert with 6 m Fill (SIDD) 63
Figure 3.18 – Axial Thrust in Culvert with 12 m Fill (SIDD) 64
Figure 3.19 – Shear Force in Culvert with 3 m Fill (SIDD) 65
Figure 3.20 – Shear Force in Culvert with 6 m Fill (SIDD) 66
Figure 3.21 – Shear Force in Culvert with 12 m Fill (SIDD) 67
Figure 3.22 – Bending Moment in Culvert with 3 m Fill (Comparison) 68
Figure 3.23 – Bending Moment in Culvert with 6 m Fill (Comparison) 70
Figure 3.24 – Bending Moment in Culvert with 12 m Fill (Comparison) 71
Figure 3.25 – Axial Thrust in Culvert with 3 m Fill (Comparison) 73
Figure 3.26 – Axial Thrust in Culvert with 6 m Fill (Comparison) 74
Figure 3.27 – Axial Thrust in Culvert with 12 m Fill (Comparison) 75
Figure 3.28 – Shear Force in Culvert with 3 m Fill (Comparison) 76
Figure 3.29 – Shear Force in Culvert with 6 m Fill (Comparison) 77
Figure 3.30 – Shear Force in Culvert with 12 m Fill (Comparison) 78
Figure 4.1 - Results of the Ground Response Analyses (El Naggar, 2008) 86
Figure 4.2 - Staged Installation Sequence 88
Figure 4.3 - Bending Moments in Culvert with 3 m Fill, MSZ (PS) 92
Figure 4.4 - Bending Moments in Culvert with 3 m Fill, G1 (PS) 93
Figure 4.5 - Bending Moments in Culvert with 6 m Fill, MSZ (PS) 94
Figure 4.6 - Bending Moments in Culvert with 6 m Fill, G1 (PS) 95
Figure 4.7 - Bending Moments in Culvert with 12 m Fill, MSZ (PS) 96

Figure 4.8 - Bending Moments in Culvert with 12 m Fill, MSZ (PS) 97
Figure 4.9 – Axial Thrust in Culvert with 3 m Fill, MSZ (PS) 104
Figure 4.10 – Axial Thrust in Culvert with 3 m Fill, G1 (PS) 105
Figure 4.11 – Axial Thrust in Culvert with 6 m Fill, MSZ (PS) 106
Figure 4.12 – Axial Thrust in Culvert with 6 m Fill, G1 (PS) 107
Figure 4.13 – Axial Thrust in Culvert with 12 m Fill, MSZ (PS) 108
Figure 4.14 – Axial Thrust in Culvert with 12 m Fill, G1 (PS) 109
Figure 4.15 – Shear Force in Culvert with 3 m Fill, MSZ (PS) 116
Figure 4.16 – Shear Force in Culvert with 3 m Fill, G1 (PS) 117
Figure 4.17 – Shear Force in Culvert with 6 m Fill, MSZ (PS) 118
Figure 4.18 – Shear Force in Culvert with 6 m Fill, G1 (PS) 119
Figure 4.19 – Shear Force in Culvert with 12 m Fill, MSZ (PS) 120
Figure 4.20 – Shear Force in Culvert with 12 m Fill, G1 (PS) 121

Chapter 1 - Introduction

1.1 Statement of the Problem

The design of reinforced concrete culverts is usually performed using the direct design method and the Heger pressure distributions since their introduction in the late 1980's. The wider availability of computers capable of performing finite element analysis and the introduction of programs used to automate much of the analysis has led to wide adoption of direct design methods; largely supplanting the Marston-Spangler design methods previously used.

The Marston-Spangler method, which is known as the "Indirect Design" method since the introduction of the "Direct Design", was developed in 1933 and is based on semi-empirical observation of hundreds of destructive tests (ACPA, 2011). The indirect design method involves using Marston-Spangler procedure for estimating the earth load on the culvert and converting it to an equivalent three-edge-bearing (TEB) test load using empirical "bedding factors" based on one of four standard installation types. Despite its satisfactory performance, the TEB method does not offer flexibility in the design and specification of reinforced concrete culverts. Moreover, TEB tests to validate the design can become increasingly difficult as the culvert capacity and diameter increase. Reinforced concrete culverts with diameters in excess of 3.0 m are frequently specified as alternatives to small bridges and several precast concrete manufacturers do not have TEB testing equipment that can accommodate culverts over 2.4 m in diameter.

In contrast to the Marston-Spangler method, the direct design method is far less empirical. It involves applying a pressure distribution to a numerical model of the structure and determining the bending moment, axial thrust, and shear force around the perimeter of culvert. As a consequence, structural design can be performed using conventional and well established reinforced concrete design methods (Kurdziel and McGrath, 1991).

While several pressure distributions such as the Paris, Olander, and Modified Olander have been used in the past, the pressure distribution widely used today was developed by F.J. Heger of Simon, Gumpertz & Heger Inc (SGH) and bears his name (Heger, 1988). In the 1970's, the American Concrete Pipe Association (ACPA) initiated a research program to improve the standard design practice and update or replace the Marston-Spangler design method (ASCE, 2000). As part of his research, Heger developed SPIDA (Soil Pipe Interaction Design and Analysis), a finite-element analysis program to analyze the soil-structure interaction effects and resulting pressure distribution on the culvert (Heger et al., 1985). SPIDA allowed Heger to develop four "Standard Installations for Direct Design" (SIDD) requiring varying levels of installation effort and determined corresponding pressure distributions for each (Heger, 1988). SGH, in conjunction with the Federal Highway Administration (FHWA) and ACPA, have also developed the software PipeCAR to simplify the analysis as the pressure distributions are not trivial to apply to a structural model nor are they conducive to simplified closed-form solutions (McGrath et al., 1988). This research formed the basis for ASCE 15-93 – Standard Practice for Direct Design of Buried Precast Concrete Pipe Using Standard Installations (SIDD), which is the basis of

Section 12.10 in the AASHTO LRFD Bridge Design Specifications and Section 7.8 of the Canadian Highway Bridge Design Guide (CHBDC).

While Heger's pressure distributions appear to lead to reasonable results, a review of the factors affecting the magnitude of the pressure applied to the structure reveals that several factors known to affect the soil-structure interaction appear to have been neglected. These factors include the trench geometry, the relative stiffness of the existing and backfill soil, and the depth of fill above the culvert. Upon review of the available literature, it appears that Heger's pressure distributions were prepared for the case of positive projecting embankments and the beneficial effects of soil arching ignored altogether (Heger, 1988). As a result, Heger's pressure distribution may lead to conservative results where conditions differ from those assumed in their preparation, such as trench installations where a sufficiently high depth of fill is present to mobilize significant soil arching action. While the case of positive projecting embankments is a reasonable assumption in new constructions, it may lead to excessively conservative results where a culvert is being replaced in an existing embankment.

ASCE 15-98 and the AASHTO LRFD Bridge Design Specifications do not consider seismic effects in the design of reinforced concrete culverts. A simplified seismic design check is presented in CHBDC; where the lack of comparisons with results obtained by other detailed methods, such as finite-element analysis, is still a source for reluctance in its application.

1.2 Thesis Objectives

The objective of the research presented in this thesis is to determine when Heger's pressure distributions and its associated simplified design tools such as PipeCAR can be successfully applied and when a more sophisticated, site-specific, finite-element analysis may lead to more appropriate results. This thesis also investigates the force effects in the structure caused by seismic events. Such effects are quantified by employing a pseudo-static finite-element analysis and are compared with seismic design requirements presented in CHBDC.

1.3 Scope and Organization of the Thesis

This thesis comprises:

(1) A review of available literature and codes governing the structural design of reinforced concrete culvert;

(2) The analysis of static force effects in reinforced concrete culverts installed in partial trench conditions using finite-element methods;

(3) The analysis of seismic force effects in reinforced concrete culverts installed in trench conditions using finite-elements methods.

The layout and organization of the thesis is summarized below:

Chapter 2 reviews the available literature on the topic. A historical overview of the design of reinforced concrete culverts is presented, as well as an overview of the development of current design practice. Finally, relevant design codes are compared to each other.

Chapter 3 presents the development and results of a finite-elements analysis parametric study which is conducted to determine forces in the culvert walls under static loading conditions. Results are compared with those obtained using Heger's pressure distributions.

Chapter 4 presents the development and results of a finite-elements analysis parametric study which is performed to determine forces in the culvert walls under pseudo-static seismic loading. Results are compared with those obtained while applying CHBDC simplified seismic design requirements to the static analysis developed in Chapter 3.

Chapter 5 presents a summary and conclusions of the findings presented in this thesis

1.4 References

American Association of State Highway and Transportation Officials (AASHTO). (2004). *AASHTO LRFD bridge design specifications.* (SI Units, Third Edition). Washington, DC: American Association of State Highway and Transportation Officials.

American Concrete Pipe Association (ACPA). (2011). *Concrete pipe design manual*. Vienna, Va.: American Concrete Pipe Association (ACPA).

American Society of Civil Engineers (ASCE). (2000). *Standard practice for direct design of buried precast concrete pipe using standard installations (SIDD)* American Society of Civil Engineers.

Canadian Standards Association (CSA). (2006). *CAN/CSA-S6-06 - Canadian highway bridge design code*. Mississauga, Ont.: Canadian Standards Association.

Heger, F. J. (1985). Proportioning reinforcement for buried concrete pipe. ASCE Proceedings. Advances in Underground Pipeline Engineering, Madison, WI, 543-553.

Heger, F. J. (1988). New installation designs for buried concrete pipe. Pipeline Infrastructure, Proceedings, 117-135.

Heger, F. J., Liepins, A. A., & Selig, E. T. (1985). SPIDA: An analysis and design system for buried concrete pipe. ASCE Proceedings. Advances in Underground Pipeline Engineering, Madison, WI, 143-154.

Kurdziel, J. M., & McGrath, T. J. (1991). SPIDA method for reinforced concrete pipe design. *Journal of Transportation Engineering, 117*(4), 371-381.

Marston, A. (1930). *The theory of external loads on closed conduits in the light of the latest experiments.* (Bulletin 96, Iowa Engineering Experiment Station).Iowa State College.

McGrath, T. J., Tigue, D. B., & Heger, F. J. (1988). PIPECAR and BOXCAR microcomputer programs for the design of reinforced concrete pipe and box sections. *Transportation Research Record,* (1191), 99-105.

Spangler, M. (1933). *The supporting strength of rigid pipe culverts.* (Bulletin 112, Iowa Engineering Experiment Station). Iowa State College.

Chapter 2 - Literature Review

2.1 Indirect Design of Reinforced Concrete Culvert

The classical theory of loads on buried rigid culvert structures was published by Anson Marston of Iowa State University in 1930. In his paper, he described what he called the "Marston load", which consists of the weight of the soil above the culvert plus or minus the friction on the edges of the column of soil above the culvert caused by the relative displacement of the soil above and directly adjacent of the culvert. Two cases could be established based on Marston's work:

1- Trench installations, where the friction on the edge of the soil column creates a reduction in the apparent weight of the soil on the culvert.

2- Positive projecting embankment, where the friction on the edge of the soil column creates an increase in the apparent weight of the soil on the culvert.

In a 1933 paper titled "The Supporting Strength of Rigid Pipe Culverts", Merlin Grant Spangler expanded Marston's work by developing four standard bedding configurations and a general equation for the bedding factor. The bedding factor is an experimentally developed empirical factor relating the results of a three-edge bearing test to anticipated loads in the installed condition.

The Marston-Spangler approach has undergone several updates by the ACPA. The historical A, B, C, and D bedding configurations developed by Spangler have been replaced by Standard Installations for Direct Design (SIDD) Types 1, 2, 3, and 4, which better define

the installation geometry and compaction requirements (ACPA, 2011). Furthermore, the bedding factor equations have been refined to consider lateral earth pressure on the culvert, which cause bending moments counter to those caused by the vertical loads. In its current form, the Marston-Spangler method is known as the Indirect Design method and is presented in many design codes and reference manuals. An overview of the Indirect Design method per ACPA's 1980 and 2011 editions of the Concrete Pipe Design Manual, as it relates to a positive-projecting embankment, is presented below.

In order to apply the Indirect Design method, one must first calculate the loads on the culvert. The loads generally considered are the weight of the earth fill, weight of the fluid inside the culvert, and live load.

Figure 1 shows a definition sketch for the geometry and parameters considered for the indirect design method. The weight of the earth fill on the culvert is calculated with equation [2.1]. The term C_c is defined in equations [2.2] and [2.3]. The plane of equal settlement (H_e) is dependent on the settlement ratio (r_{sd}), as well as on the projection ratio (p). The settlement ratio is defined as the relative settlement between the prism of fill directly above the culvert and the adjacent soil and is expressed per equation [2.4]. Recommended values of r_{sd} to be used for design are presented in the available literature as summarized in Table 2.1. The projection ratio (p) is the vertical distance the culvert projects above the original ground divided by its outside diameter.

$$\boldsymbol{W_c = C_c \gamma B_c^2} \qquad \textbf{[2.1]}$$

$$C_c = \frac{e^{2K\mu\frac{H}{B_c}}-1}{2K\mu} \text{ when } H \le H_e \quad \textbf{[2.2]}$$

$$C_c = \frac{e^{2K\mu\frac{H}{B_c}}-1}{2K\mu} + \left(\frac{H}{B_c} - \frac{H_e}{B_c}\right) e^{2K\mu\frac{H_e}{B_c}} \text{ when } H > He \quad \textbf{[2.3]}$$

$$r_{sd} = \frac{(s_m + s_g) - (s_f + d_c)}{s_m} \quad \textbf{[2.4]}$$

$$\mu = \tan\varphi' \quad \textbf{[2.5]}$$

The parameter K in equations [2.2] and [2.3] represents the Rankin lateral earth pressure coefficient, μ is the coefficient of friction along the plane where differential settlements occur and is defined in equation [2.5], where φ' is the soil's internal angle of friction. Remaining variables are defined in Figure 2.1.

Numerical solutions for calculating the plane of equal settlements (H_e) are necessary to calculate C_c. However, it is usually more convenient to use the graphical solutions presented in ACPA's Concrete Culvert Design Manual to determine the apparent fill load (W_c) directly, skipping the intermediate calculations. A sample design chart is presented in Figure 2.2 below. Calculation of W_c with the design charts is performed in the following steps:

Step 1: Calculate the projection ratio, p;

Step 2: Choose the appropriate settlement ratio, r_{sd}, from the provided table;

Step 3: Choose the appropriate design chart based on the product of r_{sd} p;

Step 4: Find the appropriate height of fill, H, on the abscissa;

Step 5: Follow this value vertically until it reaches the diameter of the culvert under consideration;

Step 6: Read the value of W_c for this location from the ordinate;

Step 7: Scale the results for the in-situ soil unit weight (charts are compiled for a soil unit weight of 100 pounds per cubic foot).

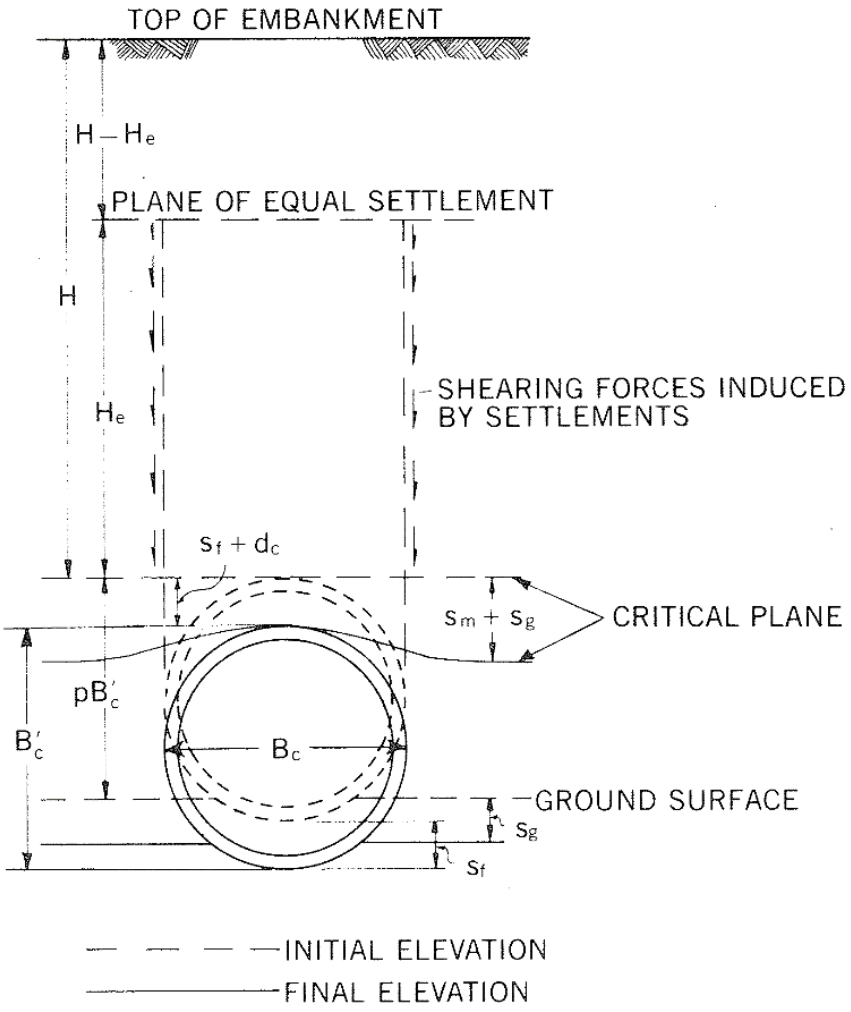

Figure 2.1 - Indirect Design Geometry Definition Sketch (ACPA, 1980).

Table 2.1 - Design Values of Settlement Ratio (after ACPA, 1980).

Installation and Foundation Condition	Settlement Ratio, r_{sd}	
	Usual Range	Design Value
Positive Projecting	0.0 to +1.0	
Rock or Unyielding Soil	+1.0	+1.0
*Ordinary Soil	+0.5 to +0.8	+0.7
Yielding Soil	0.0 to +0.5	+0.3
Zero Projecting		0
Negative Projecting	-1.0 to 0.0	
p' = 0.5		-0.1
p' = 1.0		-0.3
p' = 1.5		-0.5
p' = 2.0		-1.0
Induced Trench	-2.0 to 0.0	
p' = 0.5		-0.5
p' = 1.0		-0.7
p' = 1.5		-1.0
p' = 2.0		-2.0

**The value of the settlement ratio depends in the degree of compaction of the fill material adjacent to the sides of the pipe. With good construction methods resulting in proper compaction of bedding and sidefill materials, a settlement ratio design value of +0.5 is recommended.*

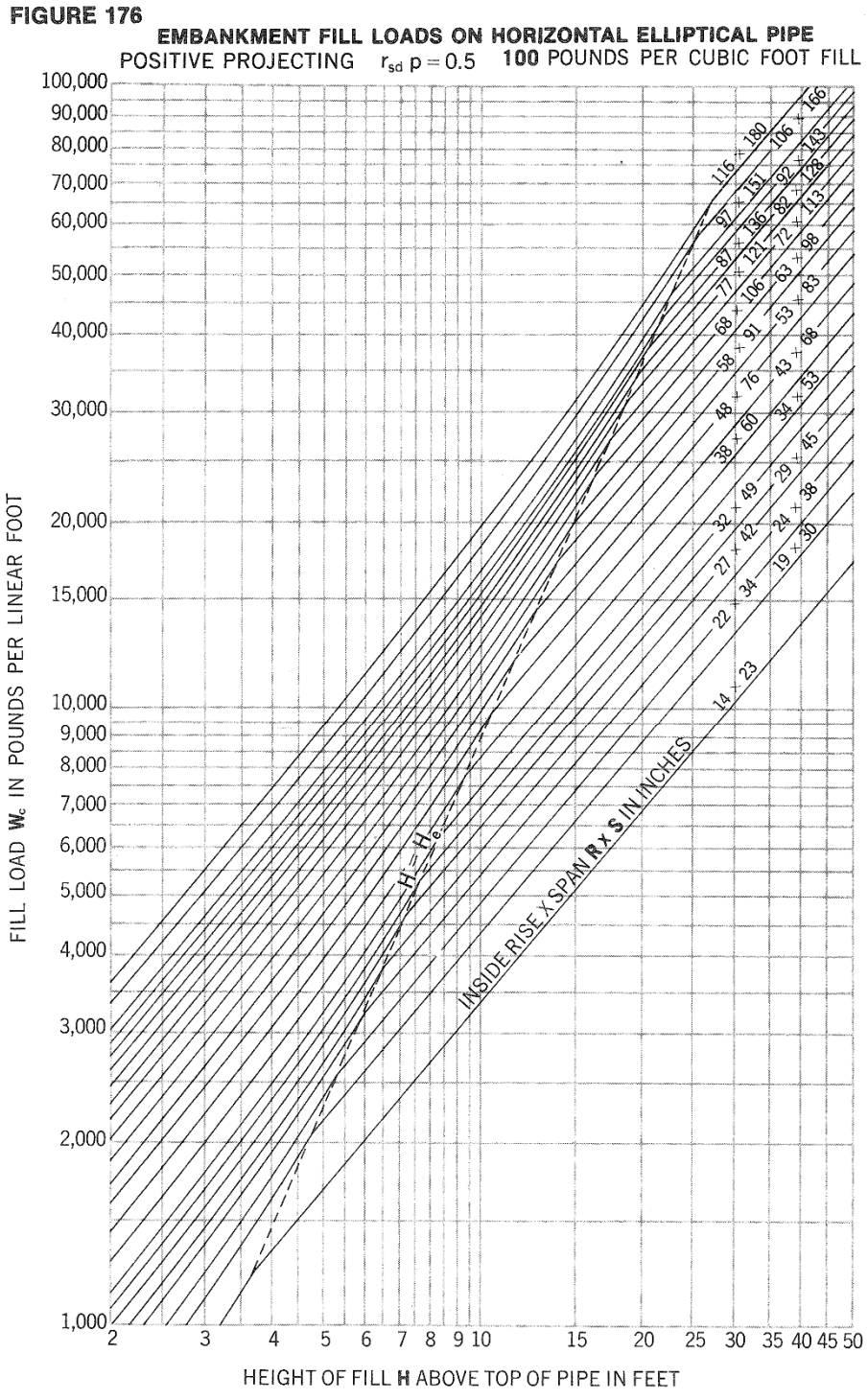

Figure 2.2 - Sample Design Chart for Embankment Fill Load Calculation (ACPA, 1980).

The weight of the fluid inside the culvert (W_F) is calculated by multiplying the area inside the culvert and the unit weight of the fluid. Historically, this weight has been neglected as it only becomes a significant portion of the dead load for large diameter culverts under shallow embankments.

The live load on the culvert resulting from traffic loading (W_L) is calculated by distributing the vehicle axle load through the fill at a ratio of 1.75:1 to the elevation corresponding to the top of the culvert. The resulting pressure is multiplied by the diameter and length of the culvert over which this pressure acts. The resulting load is then divided by the "effective" supporting length (L_e) of the culvert to get a more convenient load per unit length. The "effective" supporting length of culvert is the length of the projected load area at an elevation that is three-quarters of the culvert's outside diameter from its top surface as illustrated in Figure 2.3.

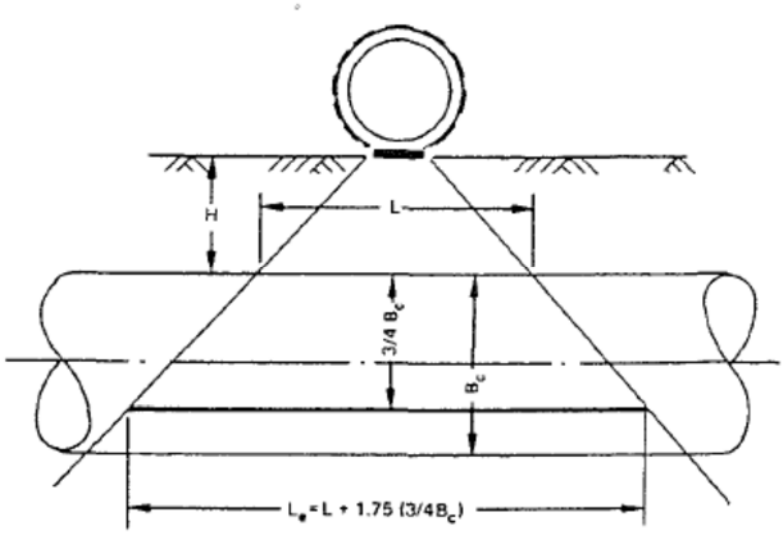

Figure 2.3 - Effective Supporting Length of Culvert (ASCE, 2001).

As the Indirect Design method leads to a minimum performance specification, culverts must be tested to ensure they satisfy the design loads. This validation is carried out using three-edge bearing (TEB) testing, which entails placing culvert segments in a machine that supports the culvert at the invert and applies a load at the crown using hydraulic jacks. The load is increased gradually until the formation of a 0.01 inch (0.3 mm) crack with a continuous length of one foot (305 mm), which is the basis of the minimum test load.

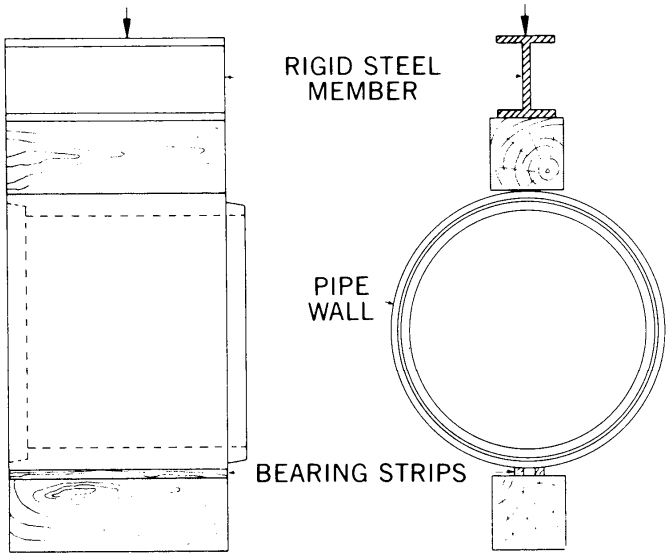

Figure 2.4 - Three-Edge Bearing Test (ACPA, 1980).

The performance of the culvert in the installed condition is related to the results of the TEB testing using bedding factors (B_f). The fundamental definition of the bedding factor is the ratio of the bending moment observed at the invert of the culvert during three-edge bearing (TEB) testing causing a 0.01 inch (either 0.25 mm or 0.3 mm are used in SI standards) crack to that observed in the installed condition. The Indirect Design method, as presented

in the 2004 AASHTO LRFD Bridge Design Specifications (AASHTO), provides separate bedding factors for the live and dead loads. However, historical design practice used a single bedding factor to be applied to the sum of all loads. Moreover, AASHTO provides tables where bedding factors can be chosen based on the culvert diameter, height of fill, and standard installation type. Bedding factors per AASHTO are presented in Tables 2.2 and 2.3.

The required TEB strength is calculated by dividing loads by their respective bedding factors, that is:

$$\boldsymbol{TEB} = \frac{\boldsymbol{W_c + W_f}}{\boldsymbol{B_f}} + \frac{\boldsymbol{W_L}}{\boldsymbol{B_{f,LL}}} \qquad \textbf{[2.6]}$$

Table 2.2 - Bedding Factors for Dead Load (after AASHTO).

Nominal Culvert Diameter, mm	Standard Installations			
	Type 1	Type 2	Type 3	Type 4
300	4.4	3.2	2.5	1.7
600	4.2	3.0	2.4	1.7
900	4.0	2.9	2.3	1.7
1800	3.8	2.8	2.2	1.7
3600	3.6	2.8	2.2	1.7

Table 2.3 - Bedding Factors for Live Load (after AASHTO).

Fill Height, mm	Culvert Diameter, mm										
	300	600	900	1200	1500	1800	2100	2400	2700	3000	3600
150	2.2	1.7	1.4	1.3	1.3	1.1	1.1	1.1	1.1	1.1	1.1
300	2.2	2.2	1.7	1.5	1.4	1.3	1.3	1.3	1.1	1.1	1.1
450	2.2	2.2	2.1	1.8	1.5	1.4	1.4	1.3	1.3	1.3	1.1
600	2.2	2.2	2.2	2.0	1.8	1.5	1.5	1.4	1.4	1.3	1.3
750	2.2	2.2	2.2	2.2	2.0	1.8	1.7	1.5	1.4	1.4	1.3
900	2.2	2.2	2.2	2.2	2.2	2.2	1.8	1.7	1.5	1.5	1.4
1050	2.2	2.2	2.2	2.2	2.2	2.2	1.9	1.8	1.7	1.5	1.4
1200	2.2	2.2	2.2	2.2	2.2	2.2	2.1	1.9	1.8	1.7	1.5
1350	2.2	2.2	2.2	2.2	2.2	2.2	2.2	2.0	1.9	1.8	1.7
1500	2.2	2.2	2.2	2.2	2.2	2.2	2.2	2.2	2.0	1.9	1.8
1650	2.2	2.2	2.2	2.2	2.2	2.2	2.2	2.2	2.2	2.0	1.9
1800	2.2	2.2	2.2	2.2	2.2	2.2	2.2	2.2	2.2	2.1	2.0
1950	2.2	2.2	2.2	2.2	2.2	2.2	2.2	2.2	2.2	2.2	2.2

Culvert strengths are often expressed as “D-Loads” where the TEB strength is divided by the culvert inside diameter. Divisions based on the D-Load are the basis of the culvert classes (I, II, III, IV, and V) as designated in ASTM C76, which allow for some standardization. In Canada, CAN/CSA-A257 divides the culverts based on their D-Load in units of N/m/mm (Newtons per metre length of culvert per millimetre inside diameter). Common classifications include 50 D, 65 D, 100 D, and 140 D.

2.2 Direct Design of Reinforced Concrete Culvert

In the 1970’s, the American Concrete Culvert Association (ACPA) initiated a research program to improve the standard design practice and update or replace the Marston-Spangler design method (ASCE, 2000).

With the availability of new mathematical models capable of representing the non-linear soil behaviour, as well as the wider availability of personal computers, Frank Heger developed SPIDA (Soil Pipe Interaction Design and Analysis). SPIDA is a finite-element analysis program to analyze the soil-structure interaction effects and resulting pressure distribution on the culvert. His results are presented in his 1985 paper entitled "SPIDA: An Analysis and Design System for Reinforced Concrete Pipe".

Heger employed SPIDA to develop four "Standard Installations for Direct Design" (SIDD) that require varying levels of installation effort and supervision. Furthermore, Heger determined corresponding pressure distributions for each standard installation (see Figure 2.5). The geometry, soil properties, compaction requirements and supervision requirements for SIDD installations are defined in more detail than the historical Marston-Spangler installations. This detailed prescriptive approach can offer improved consistency and predictability in the applied loads on the culvert. The installations range from Type 1 to Type 4. Type 1 requires high quality, well graded sand, compacted to 95% Standard Proctor density in the haunch and outer bedding area. Type 4 which requires little to no compaction and allows for the use of most in-situ materials. Quality control measures such as supervision and testing must also be sufficient to achieve the required installation quality for each standard installation type. Types 2 and 3 fall between the two extremes described above (Heger, 1988).

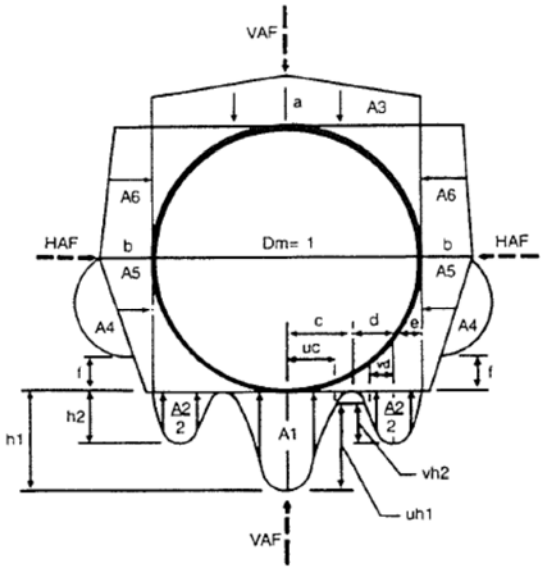

Installation Type	VAF	HAF	A1	A2	A3	A4	A5	A6	a	b	c	e	f	u	v
1	1.35	0.45	0.62	0.73	1.35	0.19	0.08	0.18	1.40	0.40	0.18	0.08	0.05	0.80	0.80
2	1.40	0.40	0.85	0.55	1.40	0.15	0.08	0.17	1.45	0.40	0.19	0.10	0.05	0.82	0.70
3	1.40	0.37	1.05	0.35	1.40	0.10	0.10	0.17	1.45	0.36	0.20	0.12	0.05	0.85	0.60
4	1.45	0.30	1.45	0.00	1.45	0.00	0.11	0.19	1.45	0.30	0.25	0.00	-	0.90	-

NOTES:

1. VAF and HAF are vertical and horizontal arching factors. These coefficients represent nondimensional total vertical and horizontal loads on the pipe, respectively. The actual vertical and horizontal earth loads are (VAF) x (PL) and (HAF) x (PL), respectively, where PL is the prism load.

2. PL, the prism load, is the weight of the column of earth cover over the pipe outside diameter and is calculated as:

$$English\ units\ PL = \left[\frac{wD_0}{12}\right]\left[H + \left(\frac{0.107D_0}{12}\right)\right]$$

$$SI\ units\ PL = \left[\frac{wD_0}{1{,}000}\right]\left[H + \left(\frac{0.107D_0}{1{,}000}\right)\right]$$

3. Coefficients A1 through A6 represent the integration of nondimensional vertical and horizontal components of soil pressure under the indicated portions of the component pressure diagrams (i.e., the area under the component pressure diagrams). The pressures are assumed to vary either parabolically or linearly, as shown, with the nondimensional magnitudes at governing points represented by h_1, h_2, uh_1, vh_2, a, and b. Nondimensional horizontal and vertical dimensions of component pressure regions are defined by c, d, e, uc, vd, and f coefficients.

4. d is calculated as (0.5-c-e).
   h_1 is calculated as (1.5A1) / (c) (1+u).
   h_2 is calculated as (1.5A2) / [(d) (1+v)+(2e)].

Figure 2.5 - Heger Pressure Distributions and Coefficients (ASCE, 2000).

Attempts to recreate Heger's pressure distribution has revealed that the equation for non-dimensional coefficient "h_1", presented above, likely should have an additional set of

parentheses around the term "(c)(1+u)" to ensure the intended order of operations is followed.

Unlike Indirect Design, which is a performance-type specification, Direct Design is performed by applying the appropriate Heger pressure distribution to a numerical model of the culvert. The resulting bending moments, shear forces, and axial thrusts are then used to calculate the required flexural and shear reinforcement around the culvert's perimeter using conventional, well established reinforced concrete design methods (Kurdziel and McGrath, 1991). This research formed the basis for ASCE 15-93 – Standard Practice for Direct Design of Buried Precast Concrete Culvert Using Standard Installations (SIDD), which is the basis of Section 12.10 in the AASHTO LRFD Bridge Design Specifications and Section 7.8 of the Canadian Highway Bridge Design Guide (CHBDC).

As Heger's pressure distributions are not trivial to apply to a structural model nor are they conducive to simplified closed-form solutions, SGH, in cooperation with FHWA and ACPA, developed the software PipeCAR to automate much of the analysis. After the user defines the culvert geometry, material properties, and installation conditions, PipeCAR performs the analysis and presents the user with minimum flexural reinforcement areas at the crown, invert, and springline, as well as a minimum shear reinforcement configuration (McGrath et al., 1988). PipeCAR is widely used by practicing engineers as a standard design tool.

2.3 Comparison of Current Design Standards

ASCE 15-93 - Standard Practice for Direct Design of Buried Precast Concrete Culvert Using Standard Installations (SIDD) is based on Heger's work as part of ACPA's research program. It has been updated to ASCE 15-98 in 2000 and forms the basis of Section 12.10 in the AASHTO LRFD Bridge Design Specifications and Section 7.8 of the Canadian Highway Bridge Design Guide (CHBDC). While AASHTO and CHBDC share the same source material, they were modified so as to be consistent with remaining design codes from their respective regions. Most notable is the use of different implementations of the Limit-States Design (LSD) philosophy and the seismic load combination included in CHBDC. A few other minor differences can be identified. Finally, inconsistencies and possible errors identified in the applicable codes will be discussed.

2.3.1 Limit-States Design Implementation Comparison

LSD is a design approach that was developed to replace the older Allowable Stress Design philosophy, in which the ratio of the nominal resistance to stresses of a structural member is compared with a minimum global factor of safety. The LSD approach was derived statistically to provide a more consistent safety level than was present with the previous approaches, allowing for more efficient and safe designs. Instead of a global factor of safety, partial factors are applied to the loads and resistances. The magnitude of the load and resistance factors is dependent on the variability of said loads and resistances, as well as the anticipated failure mechanism (Galambos and Gavindras, 1977). Load-Resistance Factor Design (LRFD) is the implementation of LSD that has been adopted in the United States. For the purpose of this thesis, LSD will refer to the approach implemented in

Canadian standards. While the LSD and LRFD are based on the same theoretical background and produce similar results, there exist some key differences that will be discussed below.

The resistance of composite materials such as reinforced concrete is handled differently in LRFD and LSD. In LRFD, a resistance factor is applied directly to the nominal resistance of the member whereas in LSD, partial resistance factors are applied to each of the component materials. Take, for example, the bending moment resistance of a reinforced concrete beam-column. AASHTO's implementation of LRFD specifies a resistance factor of 0.9 for flexure whereas CHBDC's implementation of LSD specifies resistance factors of 0.9 for the reinforcing steel and 0.75 for the concrete. Attempting to express CHBDC's resistance factors as a single "equivalent" factor can lead to a significant range of values depending on the reinforcement ratio, axial load, and the concrete strength. As the reinforcement ratio and axial compressive stress increase, and the concrete strength decreases, concrete crushing failure becomes more probable and the overall equivalent resistance factor tends more towards the concrete's resistance factor. Conversely, as the reinforcement ratio and axial compression decrease and the concrete strength increases, reinforcing steel yield becomes the probable failure mode and the overall equivalent resistance factor tends more towards the steel's resistance factor (Allen, 1975).

2.3.2 Seismic Load Combination

In addition to the Ultimate Limit States (ULS) consisting of the self-weight of the structure, the earth load, live load, and water load, CHBDC Clause 7.8.4.1 specifies that another ULS combination be evaluated. This load combination consists of the self-weight of the structure, the earth load, and the earthquake load. Reviewing ASCE 15-98, AASHTO, and PipeCAR outputs it does not appear any such provisions are present elsewhere.

Clause 7.8.4.4 presents a simplified method for calculating seismic effects. It states that "the additional force effects due to earthquake loads shall be accounted for by multiplying the force effects due to self-weight and earth load […] by the vertical acceleration ratio, A_V, specified in Clause 7.5.5.1". Clause 7.5.5.1 states that A_V shall be set equal to two-thirds of the horizontal ground acceleration, A_H, where A_H is the zonal acceleration ratio (A) determined per Clause 4.4.3.

Clause 4.4.3 provides two methods of obtaining the zonal acceleration ratio, but cautions against using either for sites close to active faults or where peak horizontal acceleration values (PHA), obtained from the Geology Survey of Canada, exceed 0.40. If either of the aforementioned conditions are true, CHBDC advises to consult with a specialized consultant for an appropriate value of zonal acceleration ratio for use in structural design. Barring the aforementioned restrictions, the zonal acceleration can be obtained directly from Tables A3.1.1 - Climatic and environmental data, or 4.1 - Seismic performance zones, of CHBDC.

As the depth of fill above the structure increases, the dead load rapidly becomes the dominant design force. This is largely due to the area over which the live load is applied increasing exponentially with depth, resulting in a matching decrease in the applied live load pressure. As a result, with increasing depth of fill, the seismic load combination, which further increases the dead loads, becomes increasingly likely to become the governing ULS combination.

2.3.3 Miscellaneous Differences

Dynamic load allowance (DLA) as it is called in CHBDC, or Impact Factor (IM) as it is called in AASHTO, is an additional factor applied to the live loads to account for the dynamic, moving nature of vehicular traffic. CHBDC and AASHTO requirements are similar in that the DLA reduces with increasing depth of fill due to the dampening properties of the soil. The equations presented in the respective codes lead to similar results with one exception: CHBDC and AASHTO specify lower bounds of 0.10 and 0, respectively. As a result, irrespective of the height of fill, the live load effects must be increased by at least ten percent when designing to CHBDC requirements.

In addition to the load factors presented in Section 3 – Loads of CHBDC, Clause 7.8.7.1 (a), states that "[an] installation factor of 1.1, in addition to the other load factors, shall be included in the multiplication to obtain the factored load effects due to earth load on the culvert and conduit shapes with curved bottoms". Load factors for axial thrust should be left as 1.0 per Clause 7.8.7.1 (b).

2.3.4 Potential Errors and Inconsistencies between Standards

As previously stated, attempts to recreate Heger's pressure distribution has revealed that the equation for non-dimensional coefficient "h_1" presented above should have an additional set of parentheses around the term "(c)(1+u)" to ensure the intended order of operations is followed. This was confirmed by fitting parabolic segments through known points in Heger's pressure distribution (h_1, uh_1, c, and uc) and performing the numerical integration of the area "A1". This operation was performed using the coefficient "h_1" calculated as presented in the literature, that is to say with only the "c" term in the denominator, and with the "(c)(1+u)" term in the denominator. The calculated area for "A1" matched the published value only in the latter case, confirming that there are missing parentheses in the published equation.

The flexural steel equation, as presented in the CHBDC Commentary Clause C7.8.8.1.1, is based on the analogous equations presented in AASHTO and ASCE, but was modified to reflect the Canadian implementation of LSD and is presented as equation [2.7] below.

$$A_s = \frac{g\varphi_s d - N_u - \sqrt{g[g(\varphi_s d)^2 - N_u(2\varphi_s d - h) - 2M_u]}}{f_y} \quad \textbf{[2.7]}$$

Where: $g = \alpha_1 \varphi_c f'_c$

α_1 = Concrete equivalent stress block coefficient

φ_s = Resistance factor for reinforcing steel

φ_c = Resistance factor for concrete

f'_c = Concrete compressive strength

f_y = Reinforcing steel yield strength

d = Distance from centroid of reinforcing steel to compressive face

h = Wall thickness

N_u = Factored axial thrust at ULS

M_u = Factored bending moment at ULS

The equation, as presented in CHBDC, however, does not include the "f_y" in the denominator, leading to erroneous results.

Design equations in ASCE 15-98 are presented in both SI units and US Customary Units, however it appears some errors were made in the conversion. Equation (12) in the original document appears as presented in equation [2.8] below.

$$j \cong 0.74 + 0.1\frac{e}{d} \quad \textbf{[2.8]}$$

Where: e = Eccentricity from reinforcing steel centroid, $\left(\frac{M_s}{N_s} + d - \frac{h}{2}\right)$

M_s = Bending moment at serviceability limit state

N_s = Axial thrust at serviceability limit state

In Appendix B, where the SI equations are presented, the equation has a factor of 0.254 instead of the original 0.1 in front of the "e/d" term. As "e" and "d" both have units of length, the resulting division renders that term dimensionless. As a result, no unit conversion should be necessary. This was confirmed with AASHTO, which presents the equation with the value 0.1 in the SI Units edition of the LRFD Bridge Design Specifications.

The equation for the crack control factor as presented in AASHTO, presented as equation [2.9] below, is inconsistent with the analogous equations presented in ASCE 15-98 and CHBDC.

$$F_{cr} = \frac{B_1 \varphi}{5250\ d\ A_s}\left(\frac{M_s + N_s\left(d - \frac{h}{2}\right)}{ij} - 0.083 C_1 b h^2 \sqrt{f'_c}\right) \quad \textbf{[2.9]}$$

Where: $B_1 = \sqrt[3]{\frac{25.4\ t_b S_1}{2n}}$

$$i = \frac{1}{\left(1 - \frac{jd}{e}\right)}$$

A_s = Area of reinforcing steel in tension face

C_1 = Coefficient considering reinforcement type

S_1 = Spacing of circumferential reinforcement

n = Coefficient for number of layers of reinforcing in tension face

φ = Resistance factor for flexure

t_b = Clear concrete cover over reinforcement

The resistance factor, φ, is included in the denominator rather than numerator in the analogous equations presented in both ASCE 15-98 and CHBDC. The crack control factor is used to predict the average maximum crack width and a value of 1.0 corresponds to an average maximum crack width of 0.25 mm. Values of F_{cr} in excess of 1.0 indicate that average maximum crack widths in excess of 0.25 mm are expected to occur. As a result, it

appears reasonable to have the resistance factor in the denominator to avoid underestimating the probability of crack widths in excess of the 0.25 mm target value.

2.3.5 References

Allen, D. (1975). Limit states design - A probabilistic study. *Canadian Journal of Civil Engineering, 2*(36), 36-49.

American Association of State Highway and Transportation Officials (AASHTO). (2004). *AASHTO LRFD bridge design specifications.* (SI Units, Third Edition). Washington, DC: American Association of State Highway and Transportation Officials.

American Concrete Pipe Association (ACPA). (1980). *Concrete pipe design manual*. Vienna, Va.: American Concrete Pipe Association (ACPA).

American Concrete Pipe Association (ACPA). (2011). *Concrete pipe design manual*. Vienna, Va.: American Concrete Pipe Association (ACPA).

American Society of Civil Engineers (ASCE). (2000). *Standard practice for direct design of buried precast concrete pipe using standard installations (SIDD)* American Society of Civil Engineers.

Canadian Standards Association (CSA). (2003). *CAN/CSA-A257 - Standards for concrete pipe and manhole sections.* CSA Group.

Canadian Standards Association (CSA). (2006). *CAN/CSA-S6-06 - Canadian highway bridge design code*. Mississauga, Ont.: Canadian Standards Association.

Galambos, T., & Ravindras, M. (1977). The basis for load and resistance factor design criteria of steel building structures. *Canadian Journal of Civil Engineering, 4*, 178-189.

Heger, F. J. (1988). New installation designs for buried concrete pipe. Pipeline Infrastructure, Proceedings, 117-135.

Heger, F. J., Liepins, A. A., & Selig, E. T. (1985). SPIDA: An analysis and design system for buried concrete pipe. ASCE Proceedings. Advances in Underground Pipeline Engineering, Madison, WI, 143-154.

Kurdziel, J. M., & McGrath, T. J. (1991). SPIDA method for reinforced concrete pipe design. *Journal of Transportation Engineering, 117*(4), 371-381.

Marston, A. (1930). *The theory of external loads on closed conduits in the light of the latest experiments.* (Bulletin 96, Iowa Engineering Experiment Station).Iowa State College.

McGrath, T. J., Tigue, D. B., & Heger, F. J. (1988). PIPECAR and BOXCAR microcomputer programs for the design of reinforced concrete pipe and box sections. *Transportation Research Record,* (1191), 99-105.

Spangler, M. (1933). *The supporting strength of rigid pipe culverts.* (Bulletin 112, Iowa Engineering Experiment Station). Iowa State College.

Chapter 3 - Numerical Analysis – Static Load Case

3.1 General

The performance of buried structures is usually of a complex nature as it is very much dependant on the soil structure interaction. This interaction is affected by several factors including soil properties, installation quality, compaction requirements, and finally, the considered geometry. Such factors are considered in Heger's pressure distributions by the use of "Standard Installations for Direct Design" (SIDD), which is a prescriptive approach describing four standard installations with varying levels of installation effort (Heger, 1988). While SIDD pressure distributions appear to produce reasonable results in various successful applications since their introduction, a review of factors affecting the magnitude of the pressure applied to the structure reveals that several factors known to affect the soil-structure interaction have not been considered. These factors include the trench geometry, the relative stiffness of the existing and backfill soil, and the effect of the depth of fill above the culvert on the vertical arching factor. A close literature review shows that Heger's pressure distributions are prepared for the case of positive projecting embankments and the beneficial effects of soil arching are ignored altogether (Heger, 1988).

The previous discussion suggests that Heger's pressure distribution may lead to conservative results where conditions vary from those assumed in their preparation. Such varying conditions may include trench installations where a sufficiently high depth of fill is present to mobilize significant soil arching action. While the case of positive projecting

embankments is usually a reasonable assumption in new constructions, it may lead to conservative results where a culvert is being replaced in an existing embankment.

The objective of this analysis is to determine the magnitude of bending moments, axial thrusts, and shear forces around the perimeter of a buried reinforced concrete culvert in a partial trench installation using finite-element analysis. A parametric study will be performed for varying the installation depth as well as the ratio of the stiffness of the backfill to that of the existing embankment material. Finite-element analysis results will be compared with results obtained using Heger's pressure distribution to determine when Heger's pressure distributions can be expected to yield reasonable results and when it may be advisable to employ more refined analysis methods to obtain more economical designs.

3.2 Finite-Element Analysis Model

In order to investigate the soil-structure interaction, numerical models were prepared using the two dimensional finite element package Plaxis 2D (Brinkgreve, 2008).

3.2.1 Geometry

The culvert geometry used in the analysis consists of a 2.1 m inside diameter with a wall thickness of 0.2 m per ASTM Specification C76, "B" wall thickness.

The culvert was assumed to be installed in a trench 3.7 m wide at its base with walls extending vertically for 1.2 m before sloping away from the structure at 1:1. Three heights of fill above the culvert were evaluated: D1 = 3 m, D2 = 6 m, and D3 = 12 m, representing low, medium, and high embankments, respectively.

The primary focus is to investigate trench in frictional soil, however, due to stability issue for the 12 m case and still maintain a slop of 1:1, a value of 5 kPa for cohesion was assumed. For design purposes, the embankment stability of the 6 m and 12 m cases should be investigated as with 1:1 side slopes, they may result in a factor of safety barely at or less than 1.3, which is the minimum practical factor of safety for trench excavations. In such cases, it may be necessary to reduce the slope to achieve an acceptable factor of safety. In this chapter, those embankment depths are included in the parametric study solely to show the effect of the high depth of fill on the predictions of the Heger pressure distributions.

The base of the excavation was located 0.25 m below the bottom of the culvert and the bedding material was assumed to extend 0.5 m above this location, resulting in an approximately 60° arc over which the culvert is supported during installation. Lateral boundaries were provided approximately 35 m in each direction from the centre of the culvert and the bottom boundary was provided 30 m below the ground surface to minimize their effect on the analysis.

The ground water table was assumed to be located well below the base of the culvert and accordingly, the effect of the water table was neglected in this analysis. Figure 3.1 presents the geometry of the considered problem.

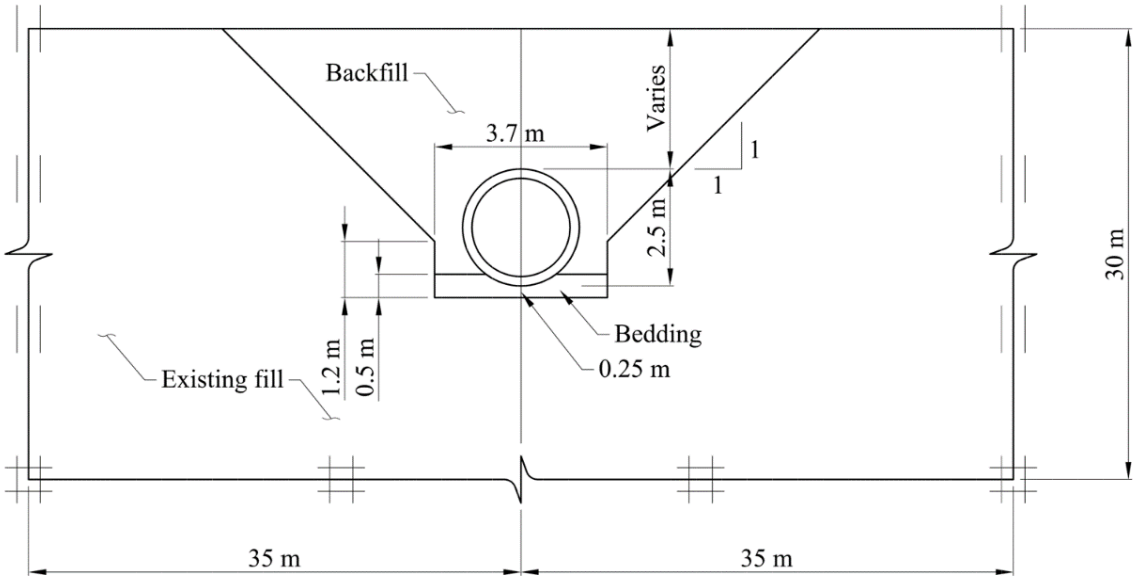

Figure 3.1 – Geometry of the considered problem.

3.2.2 Finite-Element Mesh Elements

The soil continuum was modeled using Plaxis' 15-node, plane strain elements. Soil was assumed to conform to the Mohr-Coulomb failure criteria (elasto-plastic stress-strain relationship). The culvert wall was modeled using elastic beam elements (Brinkgreve, 2008).

3.2.3 Material Properties

In addition to studying the effect of the height of the embankment's effect on the anticipated forces in the culvert, the relative stiffnesses of the existing soil to that of the culvert backfill was investigated. Soil properties used in the analysis are as presented in Table 3.1.

Table 3.1 - Soil Properties Considered in the Analysis

	φ	E (MPa)	ν	c (kPa)
Existing	36°	90	0.3	5
Group 1	36°	90	0.3	-
Group 2	33°	30	0.3	-
Group 3	39°	150	0.3	-

Where φ is the internal angle of friction, E is the modulus of elasticity, ν is Poisson's ratio, and c is the soil's cohesion.

The assumed "existing" soil was given a nominal cohesion of 5 kPa so as to prevent stability-related finite-element analysis failure during the excavation stage of the analysis. Backfill material was assumed to be cohesionless (c = 0) material.

Soil "Group 1" (G1), "Group 2" (G2), and "Group 3" (G3) represent moderately compacted fill, poorly compacted fill, and highly compacted fill, respectively. Each soil was given a consistent unit weight of 18.5 kN/m^3 to isolate the effect of the relative stiffness of the existing soil to that of the backfill on the soil-structure interaction. Realistically, the soil unit weight would vary from approximately 17 kN/m^3 for the poorly compacted fill to approximately 22 kN/m^3 for the highly compacted fill.

Concrete Modulus of Elasticity (E) was taken as 30 GPa, calculated per the equation [3.1] as presented in Clause 8.4.1.7 of CHBDC with a concrete compressive strength (f'_c) of 45 MPa and a density (γ_c) of 2300 kg/m^3.

$$E_c = (3000\sqrt{f'_c} + 6900)(\gamma_c/2300)^{1.5} \quad \textbf{[3.1]}$$

The resulting compressive and flexural stiffnesses for the culvert section were calculated as follows: EA = $6x10^6$ kN/m and EI = $20x10^3$ kN-m^2/m.

3.2.4 Staged Analysis

In order to simulate the culvert installation procedure, the analysis was performed in four stages.

Stage 1: Existing, undisturbed soil;

Stage 2: Excavation of the trench;

Stage 3: Installation of the bedding material and culvert;

Stage 4: Backfilling of structure.

A graphical representation of the above stages is presented in Figure 3.2.

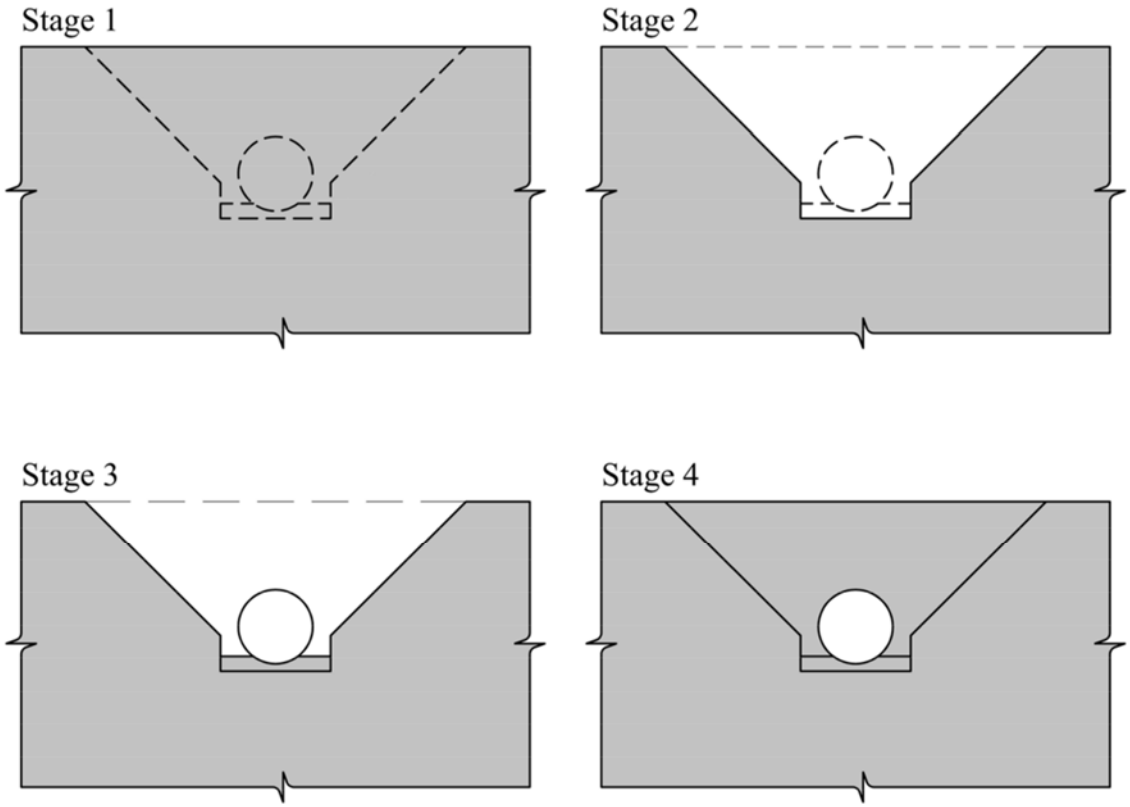

Figure 3.2 - Staged Installation Sequence

Within Plaxis 2D, a staged analysis is accomplished by defining individual stages and activating or deactivating soil "clusters" or culvert "geometry lines" and by changing material properties of specified clusters to represent each of the aforementioned stages. Pre-existing stresses and strains at the beginning of each of the stages correspond to those present at the end of the previous stage, where applicable.

3.2.4.1 Analysis Stage 1: Existing, Undisturbed Soil

Analysis Stage 1 consists of the entire soil continuum assigned with "Existing" soil properties and the beam elements representing the culvert geometry deactivated. The

purpose of this stage is to determine the pre-existing stresses in the soil continuum (installing the original in-situ stresses).

3.2.4.2 Analysis Stage 2: Excavation

Analysis Stage 2 is performed by deactivating all of the soil clusters in the areas representing the bedding material, the area enclosed by the culvert, and the backfill area. Its purpose is to determine the changes in strains and stresses in the pre-existing soil as a result of the excavation.

3.2.4.3 Analysis Stage 3: Bedding Material and Culvert Installation

Analysis Stage 3 is performed by activating the clusters representing the bedding material and changing their material properties to those representing the respective backfill material used in the analysis. Geometry lines representing the culvert walls are activated. The purpose of this stage is to simulate the installation of the culvert and that it's self-weight is initially supported mostly its invert, causing increased load effects at that location.

3.2.4.4 Analysis Stage 4: Backfilling

Analysis Stage 4 is performed by activating the clusters representing the backfill material and changing their material properties to those representing the respective backfill material used in the analysis. While pre-existing stresses are carried over from the previous stage, displacements are reset to zero to isolate soil settlements that occur after backfilling from those that occur prior to backfilling.

3.2.5 Results

Analysis was performed for each combination of backfill material stiffness and heights of fill. Bending moments, shear forces, and axial thrust numerical results around the culvert circumference were extracted from each of the Plaxis 2D models and stored in a spreadsheet for ease of comparison. Results were grouped according to depth of fill and presented graphically with the abscissa representing the angle from the invert along the culvert half circumference in degrees and the ordinate representing the bending moment, axial thrust, or shear force in units of kN-m/m, kN/m, and kN/m, respectively.

3.2.5.1 Bending Moment

The bending moments are presented on the ordinate with positive values indicating that the inside face of the culvert is in tension. Conversely, negative values indicate the outside face is in tension. Results are presented in Figures 3.3 through 3.5.

The legend identifies results as follows: Backfill soil properties are identified with “G1”, “G2”, and “G3”, representing Group 1, 2, and 3 soils, respectively; The height of fill above the culvert is identified with “D1”, “D2”, and “D3”, representing 3 m, 6 m, and 12 m height of fill above the culvert, respectively; The “S0” indicates that seismicity was not considered in these analyses.

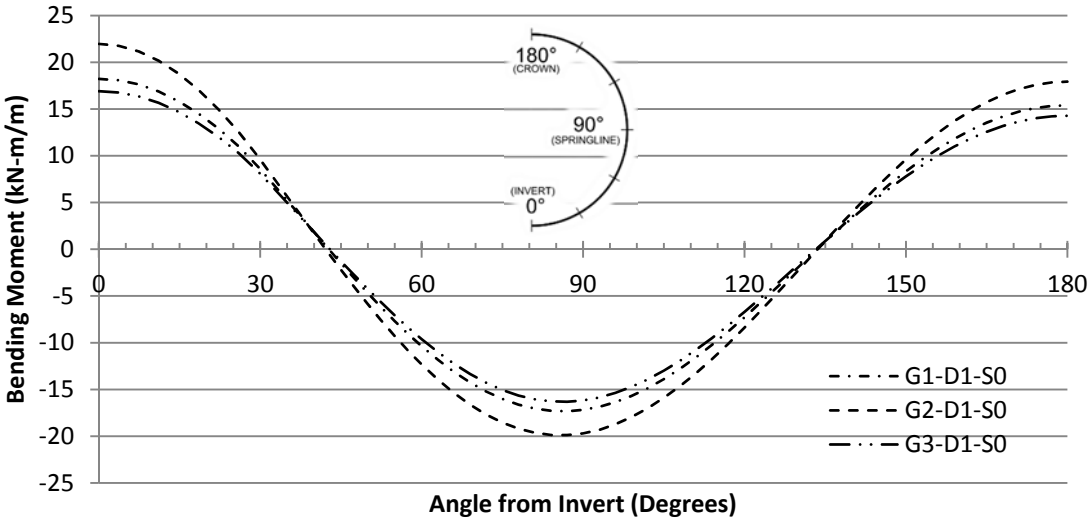

Figure 3.3 - Bending Moments in Culvert with 3 m Fill (FEA)

Figure 3.3 presents the variation of the bending moments around the circumference of culverts having a burial depth of 3 m. Considering Figure 3.3, it is evident that increasing backfill soil stiffness results in a reduction in bending moments around the entire perimeter of the culvert. Compared to Group 1 (moderately compacted) backfill, Group 2 (loosely compacted) backfill results in an increase of 20.5% at the invert, 14.6% near the springline and 16.4% at the crown. Group 3 (well compacted) backfill results in a decrease of 7.2% at the invert, 5.9% near the springline and 7.2% at the crown.

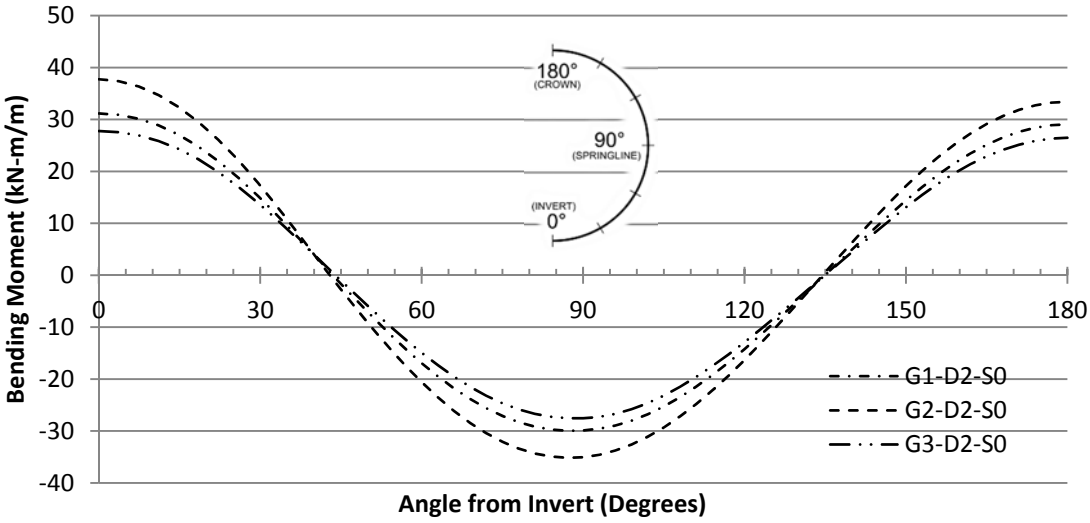

Figure 3.4 - Bending Moments in Culvert with 6 m Fill (FEA)

Figure 3.4 presents the variation of the bending moments around the circumference of culverts having a burial depth of 6 m. Figure 3.4 shows similar results to those observed in Figure 3.3. Compared to Group 1 backfill, Group 2 backfill results in an increase of 21.1% at the invert, 17.2% near the springline and 15.1% at the crown. Group 3 backfill results in a decrease of 10.9% at the invert, 7.8% near the springline and 8.9% at the crown.

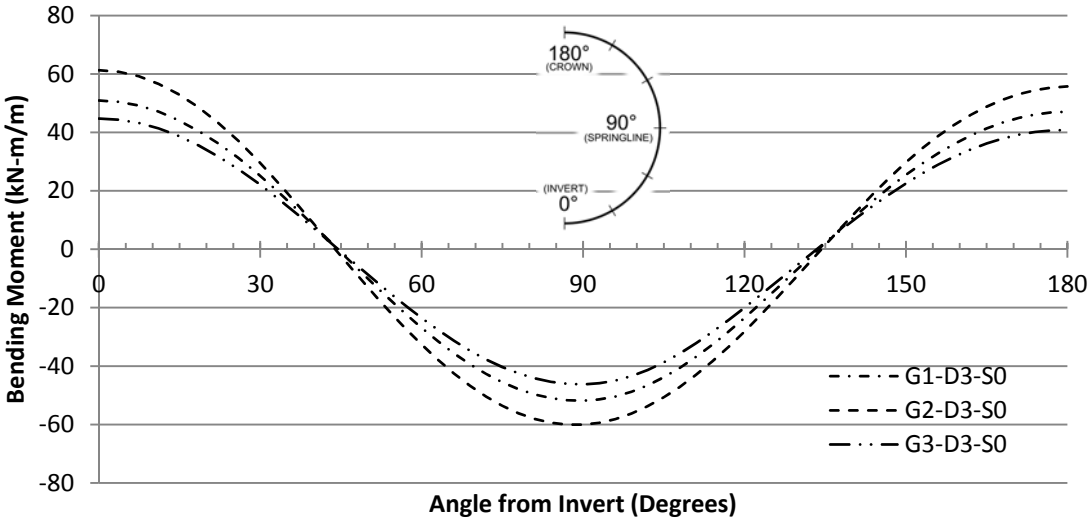

Figure 3.5 - Bending Moments in Culvert with 12 m Fill (FEA)

Figure 3.5 presents the variation of the bending moments around the circumference of culverts having a burial depth of 12 m. Figure 3.5 shows similar results to those observed in Figures 3.3 and 3.4. Compared to Group 1 backfill, Group 2 backfill results in an increase of 20.4% at the invert, 15.8% near the springline and 18.4% at the crown. Group 3 backfill results in a decrease of 12.1% at the invert, 10.8% near the springline and 13.3% at the crown.

Finally, we can conclude that as the stiffness of the backfill increases, it attracts a larger proportion of the load and consequently, a lesser proportion of the load is carried by the culvert. This results in a proportional reduction in the bending moments in the culvert walls.

3.2.5.2 Axial Thrust

Positive values in the axial thrust results indicate compression. Results are presented as Figures 3.6 through 3.8. The legend is identical to that used in the bending moment analysis.

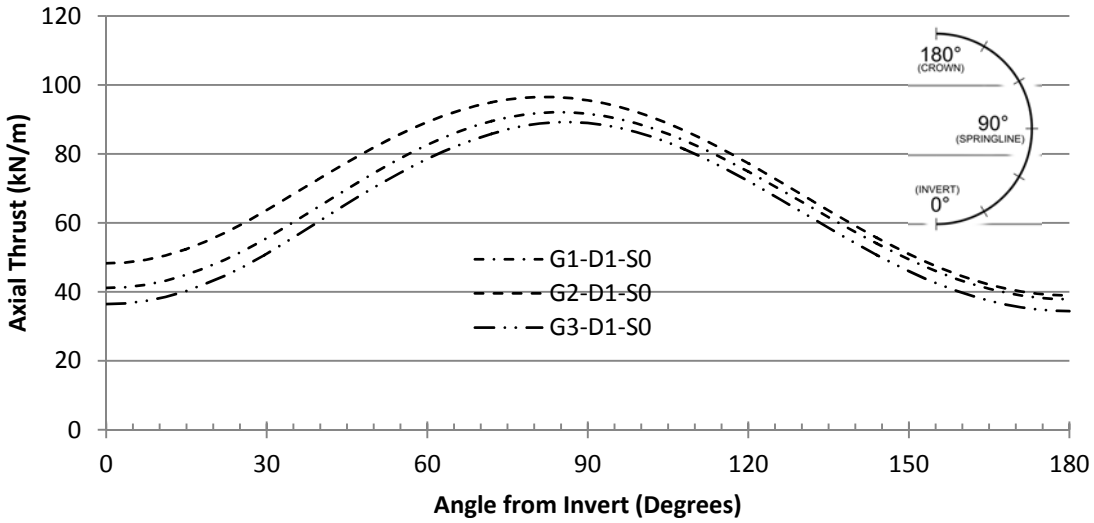

Figure 3.6 – Axial Thrust in Culvert with 3 m Fill (FEA)

Figure 3.6 presents the variation of the axial thrust around the circumference of culverts having a burial depth of 3 m. Considering Figure 3.6, it is evident that increasing backfill soil stiffness results in a reduction in axial thrust around the entire perimeter of the culvert. Compared to Group 1 backfill, Group 2 backfill results in an increase of 17.4% at the invert, 4.3% near the springline and 2.8% at the crown. Group 3 backfill results in a decrease of 11.4% at the invert, 2.9% near the springline and 9.2% at the crown.

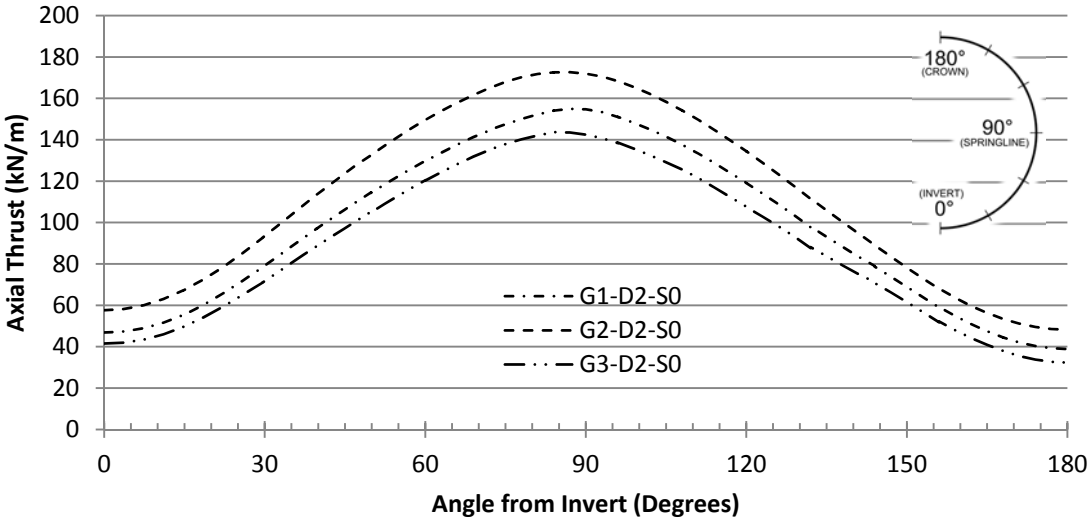

Figure 3.7 – Axial Thrust in Culvert with 6 m Fill (FEA)

Figure 3.7 presents the variation of the axial thrust around the circumference of culverts having a burial depth of 6 m. The results presented in Figure 3.7 shows a similar trend as in Figure 3.6. Compared to Group 1 backfill, Group 2 backfill results in an increase of 22.9% at the invert, 11.1% near the springline and 23.9% at the crown. Group 3 backfill results in a decrease of 11.4% at the invert, 7.9% near the springline, and 17.0% at the crown.

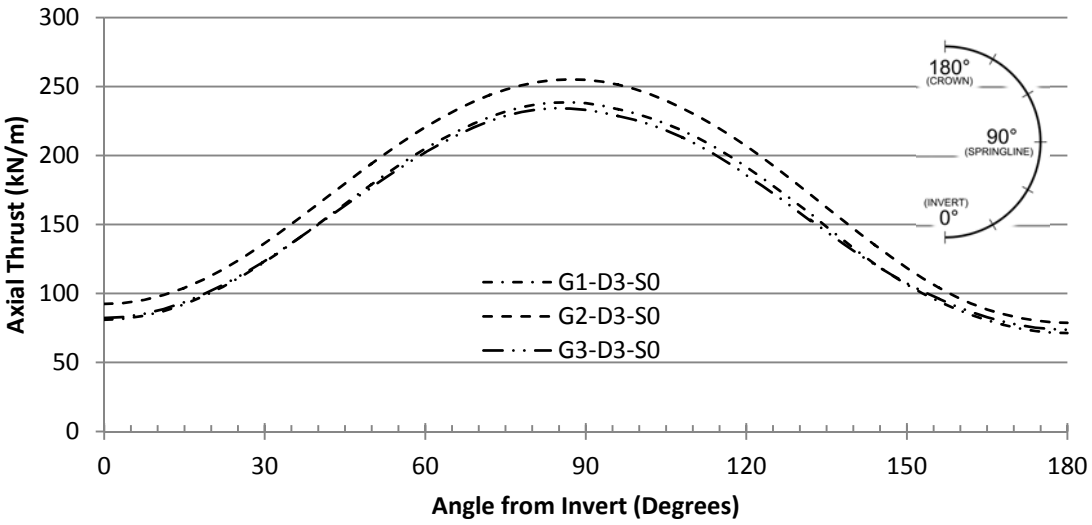

Figure 3.8 – Axial Thrust in Culvert with 12 m Fill (FEA)

Figure 3.8 presents the variation of the axial thrust around the circumference of culverts having a burial depth of 12 m. Again here, the same trend was found to hold as observed in Figures 3.6 and 3.7 for the Group 2 backfills. Compared to Group 1 backfill, Group 2 backfill results in an increase of 14.3% at the invert, 7.1% near the springline and 10.3% at the crown.

Group 3 backfill behaves somewhat differently than the established pattern. Compared to Group 1 results, Group 3 backfill results in an increase of 1.6% at the invert, a decrease of 2.0% near the springline and an increase of 3.3% at the crown. The minimal changes in axial thrust may indicate that soil arching has been fully mobilized with the Group 1 backfill and that further increases in the backfill stiffness have minimal effect on the axial thrust in the culvert wall.

3.2.5.3 Shear Force

Results of the shear force analyses are presented as Figures 3.9 through 3.11. The absolute maximum shear values are located near the haunch, approximately 37 to 45 degrees from the invert, depending on the height of fill. The legend is identical to that used in the bending moment and axial thrust analyses.

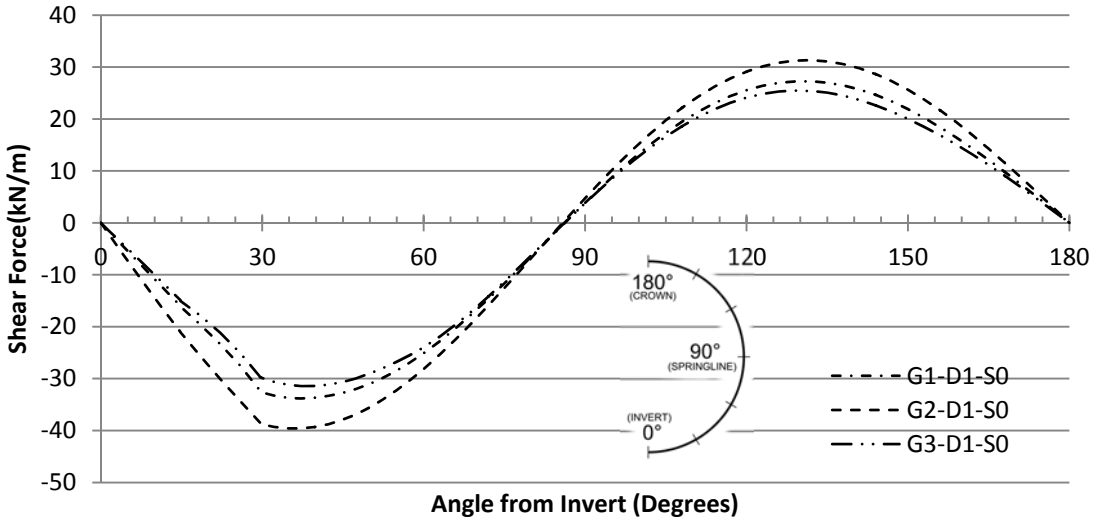

Figure 3.9 – Shear Force in Culvert with 3 m Fill (FEA)

Figure 3.9 presents the variation of the shear force around the circumference of culverts having a burial depth of 3 m. Figure 3.9 shows that increasing backfill soil stiffness results in a reduction in shear forces around the entire perimeter of the culvert. Compared to Group 1 backfill, Group 2 backfill results in an increase of 17.0%. Group 3 backfill results in a decrease of 7.1%. Results were compared approximately 37 degrees from the invert. The discontinuity in the graph around 30 degrees from the invert is a result of the self-weight

of the culvert on the bedding, which is a relatively significant portion of the total load at this height of fill.

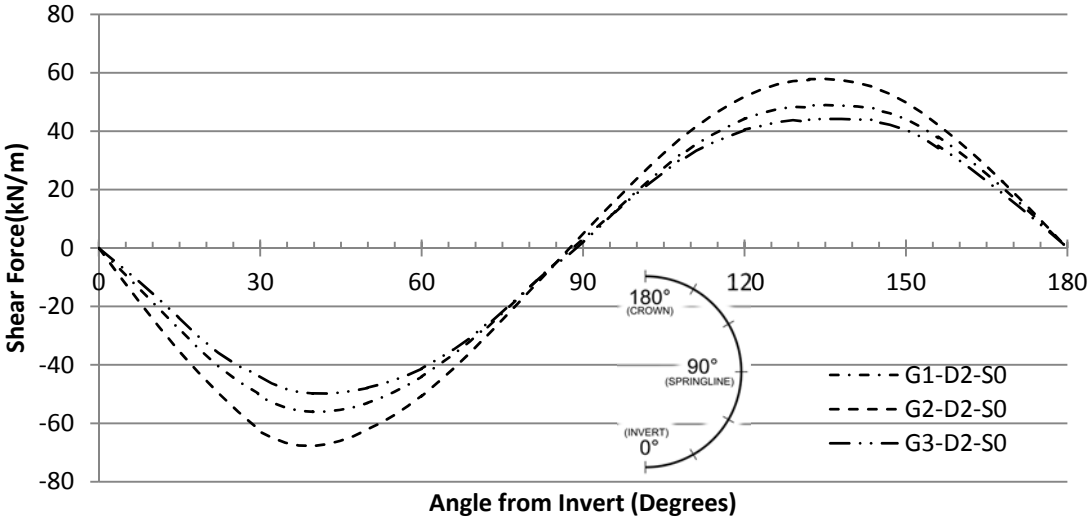

Figure 3.10 – Shear Force in Culvert with 6 m Fill (FEA)

Figure 3.10 presents the variation of the shear force around the circumference of culverts having a burial depth of 6 m. As can be seen from Figure 3.10, a similar trend to that observed in Figure 3.9 was found to hold. For instance, compared to Group 1 backfill, Group 2 backfill results in an increase of 20.9% and Group 3 backfill results in a decrease of 11.3%. Results were compared approximately 40 degrees from the invert.

The discontinuity in the graph observed in Figure 3.9 is far less evident here as it was caused by the self-weight of the culvert on the bedding and that portion of the total load becomes relatively insignificant with a height of fill of 6 m.

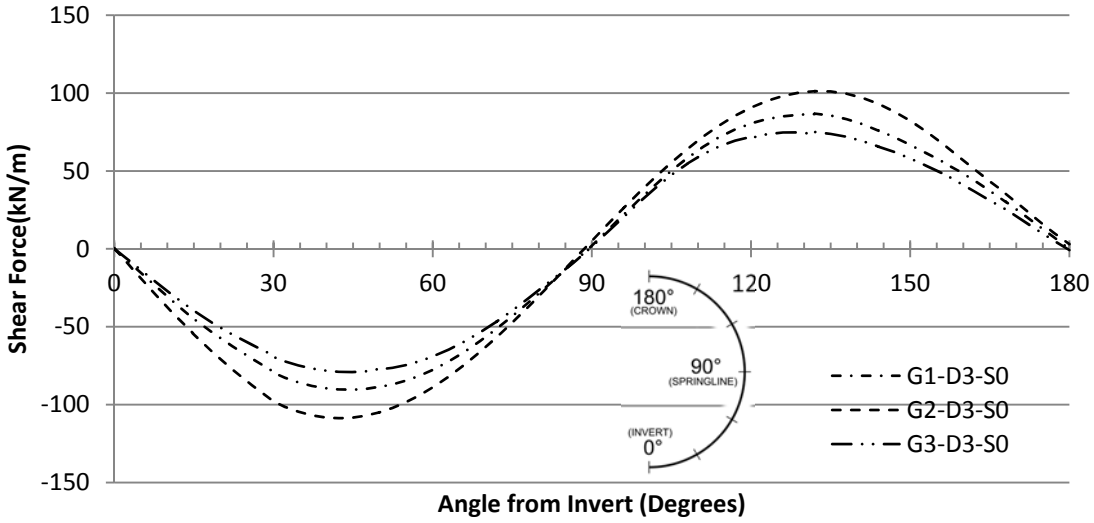

Figure 3.11 – Shear Force in Culvert with 12 m Fill (FEA)

Figure 3.11 presents the variation of the shear force around the circumference of culverts having a burial depth of 12 m. Considering Figure 3.11, results are similar to those observed in Figures 3.9 and 3.10. For example, compared to Group 1 backfill, Group 2 backfill results in an increase of 19.8% and Group 3 backfill results in a decrease of 12.5%. Results were compared approximately 45 degrees from the invert.

The discontinuity in the graph observed in Figure 3.9 is not evident here as it was caused by the self-weight of the culvert on the bedding and that portion of the total becomes relatively insignificant with a height of fill of 12 m.

3.3 Heger Pressure Distribution Model

In order to recreate the load effects resulting from Heger's pressure distributions, numerical models were prepared using LUSAS Bridge (Irving, 1985). LUSAS Bridge was chosen for this task for a few key features, including the ability to apply pressures with varying intensity based on the geometry of a circular arc. Such varying pressures were selected in order to achieve a close approximation of the parabolic pressure distribution with few segments. This eliminated the need to approximate the pressure distribution with a series of short linearly varying pressure segments that would have been necessary for other analysis packages. Moreover, LUSAS Bridge allowed loads to be applied to a simple straight line segment and projected to the culvert geometry, which was useful with curved surfaces as each element forming the surface had a different projected length in the axes used during the analysis.

3.3.1 Geometry and Finite-Element Mesh

The analysis was performed for a culvert with a mean diameter of 1 m. This was done to ensure the ability to validate results by direct comparison with those presented in ASCE 15-98. In addition, this analysis was intended to produce results that could easily be scaled to any diameter, burial depth, and soil unit weight.

As the culvert and pressure distribution were symmetric about the vertical axis, only half of the culvert was modeled. Restraints used in the analysis were as follows:

1. The node at the crown was fixed against horizontal translation and rotation, and was free to translate in the vertical direction;

2. The node at the invert was fixed against horizontal and vertical translation, as well as rotation.

The culvert geometry was approximated using straight line segments corresponding to five degree arcs about its centre.

Figure 3.12 shows the model geometry, boundary conditions, and the applied loads corresponding to the SIDD Type 1 pressure distribution.

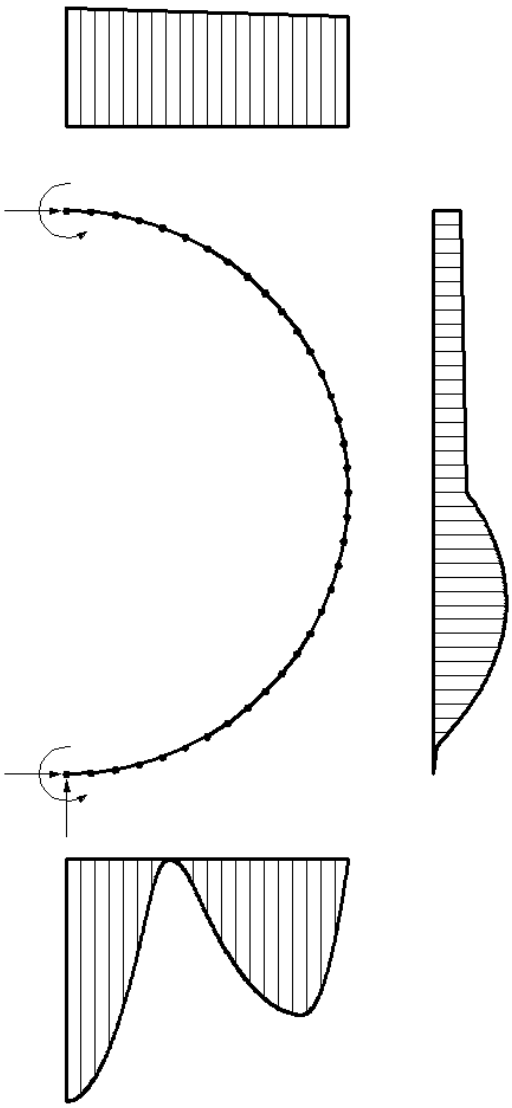

Figure 3.12 - Model Geometry and Restraint Conditions.

3.3.2 Elements

Analysis was performed using “two-dimensional thick beam” elements with “linear interpolation” from the LUSAS element library. The finite element mesh further divided the straight line segments into ten elements, providing a resolution of 0.5 degrees along the

perimeter of the culvert. Geometric properties, such as the moment of inertia and cross-sectional area, corresponded to a 1 m length of culvert with a 100 mm wall thickness.

The wall thickness used in the analysis corresponds to a "B" culvert wall thickness per American Society for Testing and Materials (ASTM) Specifications C76. As ASTM C76 does not include a standard culvert having these dimensions, the wall thickness was determined as follows:

1. The equation describing the relationship between the pipe diameter and wall thickness was determined by performing a curve fitting through internal diameter / wall thickness pairs of standard culvert sizes and is presented as equation [3.2].

$$\boldsymbol{t = \frac{d_i}{12} + 25} \qquad \textbf{[3.2]}$$

2. The analysis is performed on the basis of "mean" diameter. The mean and internal diameters are related by the wall thickness as presented in equation [3.3].

$$\boldsymbol{d_m = d_i + t} \qquad \textbf{[3.3]}$$

3. Combining the above two relationships, the wall thickness can be expressed as a function of the mean diameter of the pipe as presented in equation [3.4].

$$\boldsymbol{t = \frac{d_m + 300}{13}} \qquad \textbf{[3.4]}$$

Where: t = Wall thickness (mm)

d_i = Internal diameter (mm)

d_m = Mean diameter (mm)

3.3.3 Materials

Concrete Modulus of Elasticity (E) was taken as 30 GPa, calculated per the equation [3.1] as presented in Clause 8.4.1.7 of CHBDC with a concrete compressive strength (f'_c) of 45 MPa and a density (γ_c) of 2300 kg/m^3.

3.3.4 Pressure Distribution

Heger's pressure distributions were recreated by fitting parabolic or linear segments through the known points presented in the table of coefficients (Figure 2.5).

For the pressure distribution at the bottom of the culvert, parabolic segments were assumed to have a first derivative of zero at the invert, at a distance "c" from the invert, and at a distance "c+d" from the invert. The two parabolic segments adjacent to each inflection points ("uc" and "c+d-vd" from the invert) were assumed to have matching first derivatives at said points. Parabolic equations were validated by performing their numerical integration and comparing with values for "A1" and "A2".

The pressure distributions at the top and side of the culvert were relatively trivial to calculate as most segments are simple, linearly varying pressures. Given the pressure at one end of the segment and the total resultant force of said segment, the pressure at the other end could easily be calculated.

3.3.5 Validation

Results of the analysis were validated using Tables C-3.1 to C-3.4 of ASCE 15-98. The tables present a list of coefficients that allow the easy calculation of bending moments,

axial thrusts, and shear forces at critical locations such as the invert, crown, and springline under the influence of the earth load, culvert self-weight, weight of fluid inside the culvert, and the traffic load for each standard installation type. Bending moments, axial thrusts, and shear forces are calculated per equations [3.5], [3.6], and [3.7].

$$M_i = C_{mi} W_i D_m / 2 \quad \textbf{[3.5]}$$

$$N_i = C_{ni} W_i \quad \textbf{[3.6]}$$

$$V_i = C_{vi} W_i \quad \textbf{[3.7]}$$

C_{mi}, C_{ni}, and C_{vi} are coefficients corresponding to bending moment, axial thrust, and shear force, respectively and are obtained from the tables. The symbol "i" in the equations can represent either "p" for culvert self-weight, "e" for earth load, "f" for fluid load, or "L" for live load. "W_e" represents the weight of the soil above the culvert and "W_p" represents the self-weight of the culvert. Fluid load and live load were not considered in this analysis. "D_m" is the mean diameter of the culvert.

Results of the LUSAS analysis of Heger's pressure distributions and the self-weight of the culvert were found to correspond very closely to the coefficients presented in the ASCE 15-98 tables with most values coming within 2.5% or less of one another. Using the results of the analysis, coefficients tables similar to those presented in ASCE 15-98 were prepared, but instead of presenting resulting results at five locations (invert, springline, crown, and

at the upper and lower haunches) as is done in ASCE 15-98, coefficients are presented at five degree increments along the culvert's circumference.

This allowed for the rapid calculation of results for different culvert diameters and heights of fill. Coefficients tables are presented as Tables 3.2 to 3.6 where, as with the graphs, the angle represents the circumference starting at the invert. Coefficients F_x, F_y, and M_z represent axial thrust, shear, and bending moment, respectively. Positive values for the coefficient F_x indicate compression and positive values for the coefficient M_z indicate the inside face of the culvert is in tension. Also presented within the tables, within parentheses and with a bold font, are the corresponding coefficients for the tables presented in the ASCE 15-98 Commentary used for validation. Validation coefficients are not presented for the shear coefficients as their provided locations do not coincide with five degree increments presented in the tables.

Table 3.2 - SIDD Earth Load Coefficients for Type 1 Installations

Angle	F_x	F_y	M_z
0	0.179 **(0.188)**	0.001	0.093 **(0.091)**
5	0.186	-0.074	0.090
15	0.229	-0.162	0.068
20	0.249	-0.154	0.053
25	0.262	-0.133	0.041
30	0.277	-0.119	0.030
35	0.298	-0.117	0.020
40	0.331	-0.119	0.009
45	0.364	-0.131	-0.001
50	0.381	-0.129	-0.012
55	0.401	-0.126	-0.023
60	0.449	-0.119	-0.034
65	0.464	-0.113	-0.045
70	0.478	-0.105	-0.055
75	0.491	-0.084	-0.063
80	0.495	-0.068	-0.071
85	0.498	-0.047	-0.076
90	0.500 **(0.500)**	-0.021	-0.079 **(-0.077)**
95	0.501	0.008	-0.079
100	0.501	0.037	-0.077
105	0.500	0.067	-0.072
110	0.446	0.094	-0.065
115	0.442	0.120	-0.056
120	0.437	0.147	-0.044
125	0.390	0.145	-0.032
130	0.376	0.179	-0.018
135	0.333	0.167	-0.003
140	0.295	0.150	0.012
145	0.281	0.175	0.026
150	0.251	0.149	0.040
155	0.216	0.125	0.052
160	0.187	0.096	0.063
165	0.189	0.109	0.072
170	0.170	0.075	0.079
175	0.158	0.038	0.083
180	0.154 **(0.157)**	-0.001	0.084 **(0.083)**

Table 3.3 - SIDD Earth Load Coefficients for Type 2 Installations

Angle	F_x	F_y	M_z
0	0.162 **(0.169)**	0.001	0.124 **(0.122)**
5	0.172	-0.106	0.120
15	0.227	-0.220	0.090
20	0.257	-0.228	0.070
25	0.277	-0.206	0.051
30	0.297	-0.187	0.034
35	0.318	-0.173	0.018
40	0.353	-0.169	0.003
45	0.379	-0.164	-0.012
50	0.405	-0.161	-0.026
55	0.430	-0.152	-0.039
60	0.457	-0.129	-0.051
65	0.473	-0.116	-0.063
70	0.486	-0.102	-0.072
75	0.494	-0.074	-0.080
80	0.497	-0.053	-0.086
85	0.499	-0.030	-0.090
90	0.500 **(0.500)**	-0.002	-0.092 **(-0.090)**
95	0.500	0.027	-0.090
100	0.498	0.057	-0.086
105	0.494	0.088	-0.080
110	0.439	0.114	-0.071
115	0.433	0.140	-0.060
120	0.425	0.167	-0.047
125	0.376	0.165	-0.032
130	0.360	0.197	-0.017
135	0.315	0.185	-0.001
140	0.274	0.167	0.016
145	0.259	0.190	0.032
150	0.226	0.164	0.047
155	0.189	0.137	0.060
160	0.159	0.106	0.073
165	0.159	0.116	0.082
170	0.140	0.080	0.089
175	0.128	0.041	0.093
180	0.124 **(0.126)**	-0.001	0.095 **(0.094)**

Table 3.4 - SIDD Earth Load Coefficients for Type 3 Installations

Angle	F_x	F_y	M_z
0	0.159 **(0.163)**	0.001	0.152 **(0.150)**
5	0.171	-0.137	0.147
15	0.241	-0.286	0.110
20	0.274	-0.294	0.085
25	0.301	-0.274	0.060
30	0.324	-0.248	0.037
35	0.345	-0.229	0.016
40	0.378	-0.214	-0.003
45	0.403	-0.202	-0.021
50	0.422	-0.186	-0.038
55	0.445	-0.167	-0.053
60	0.468	-0.141	-0.067
65	0.482	-0.121	-0.079
70	0.489	-0.099	-0.088
75	0.499	-0.067	-0.096
80	0.500	-0.041	-0.101
85	0.501	-0.014	-0.103
90	0.500 **(0.500)**	0.016	-0.103 **(-0.103)**
95	0.498	0.047	-0.100
100	0.494	0.077	-0.095
105	0.489	0.108	-0.086
110	0.432	0.134	-0.075
115	0.424	0.160	-0.063
120	0.414	0.185	-0.048
125	0.364	0.183	-0.032
130	0.346	0.214	-0.015
135	0.300	0.200	0.002
140	0.259	0.180	0.020
145	0.242	0.202	0.037
150	0.209	0.173	0.053
155	0.172	0.145	0.067
160	0.141	0.112	0.080
165	0.142	0.121	0.090
170	0.122	0.083	0.098
175	0.110	0.042	0.102
180	0.106 **(0.107)**	0.000	0.104 **(0.103)**

Table 3.5 - SIDD Earth Load Coefficients for Type 4 Installations

Angle	F_x	F_y	M_z
0	0.128 **(0.128)**	0.001	0.192 **(0.191)**
5	0.140	-0.129	0.186
15	0.222	-0.334	0.146
20	0.273	-0.390	0.115
25	0.316	-0.387	0.081
30	0.357	-0.371	0.048
35	0.383	-0.342	0.017
40	0.411	-0.308	-0.012
45	0.432	-0.275	-0.037
50	0.450	-0.241	-0.060
55	0.470	-0.201	-0.079
60	0.482	-0.166	-0.095
65	0.491	-0.130	-0.108
70	0.498	-0.095	-0.117
75	0.504	-0.051	-0.124
80	0.505	-0.016	-0.127
85	0.504	0.019	-0.127
90	0.500 **(0.504)**	0.052	-0.124 **(-0.127)**
95	0.494	0.085	-0.118
100	0.487	0.117	-0.109
105	0.478	0.148	-0.097
110	0.416	0.172	-0.083
115	0.405	0.196	-0.067
120	0.393	0.220	-0.049
125	0.339	0.213	-0.030
130	0.319	0.242	-0.010
135	0.271	0.224	0.009
140	0.230	0.199	0.029
145	0.211	0.218	0.047
150	0.180	0.185	0.064
155	0.142	0.155	0.080
160	0.111	0.119	0.093
165	0.115	0.125	0.104
170	0.095	0.085	0.111
175	0.083	0.043	0.116
180	0.079 **(0.079)**	0.000	0.117 **(0.118)**

Table 3.6 - SIDD Coefficients for Self-Weight of Culvert

Angle	F_x	F_y	M_z
0	0.078 **(0.077)**	0.000	0.201 **(0.225)**
5	0.104	-0.294	0.189
15	0.193	-0.422	0.120
20	0.225	-0.391	0.085
25	0.252	-0.357	0.052
30	0.275	-0.322	0.022
35	0.295	-0.285	-0.004
40	0.309	-0.248	-0.028
45	0.320	-0.210	-0.048
50	0.326	-0.173	-0.064
55	0.329	-0.136	-0.078
60	0.327	-0.100	-0.088
65	0.322	-0.065	-0.095
70	0.314	-0.032	-0.099
75	0.302	-0.001	-0.101
80	0.287	0.028	-0.099
85	0.270	0.054	-0.096
90	0.250 **(0.249)**	0.078	-0.090 **(-0.091)**
95	0.228	0.098	-0.082
100	0.205	0.115	-0.073
105	0.181	0.129	-0.062
110	0.156	0.139	-0.051
115	0.131	0.147	-0.038
120	0.106	0.150	-0.025
125	0.081	0.151	-0.012
130	0.057	0.149	0.001
135	0.034	0.143	0.014
140	0.012	0.135	0.026
145	-0.008	0.124	0.037
150	-0.025	0.111	0.048
155	-0.041	0.096	0.057
160	-0.054	0.079	0.064
165	-0.064	0.060	0.070
170	-0.072	0.041	0.075
175	-0.076	0.021	0.077
180	-0.078 **(-0.077)**	0.000	0.078 **(0.079)**

3.3.6 Results

Using the prepared coefficient table, bending moments, axial thrusts, and shear forces were calculated for each of the fill heights and the four Heger standard installation types.

3.3.6.1 Bending Moment

As with the finite-element analysis results, the bending moments are presented on the ordinate with positive values indicating that the inside face of the culvert is in tension. The abscissa represents the culvert half circumference in units of degrees with 0° representing the culvert invert and 180° the crown. Results are presented as Figures 3.13 to 3.15.

The legend identifies results as follows: The height of fill above the culvert is identified with “D1”, “D2”, and “D3”, representing 3 m, 6 m, and 12 m, respectively; The Heger SIDD installation type is identified with “T1”, “T2”, “T3”, and “T4” for SIDD Types 1 through 4, respectively.

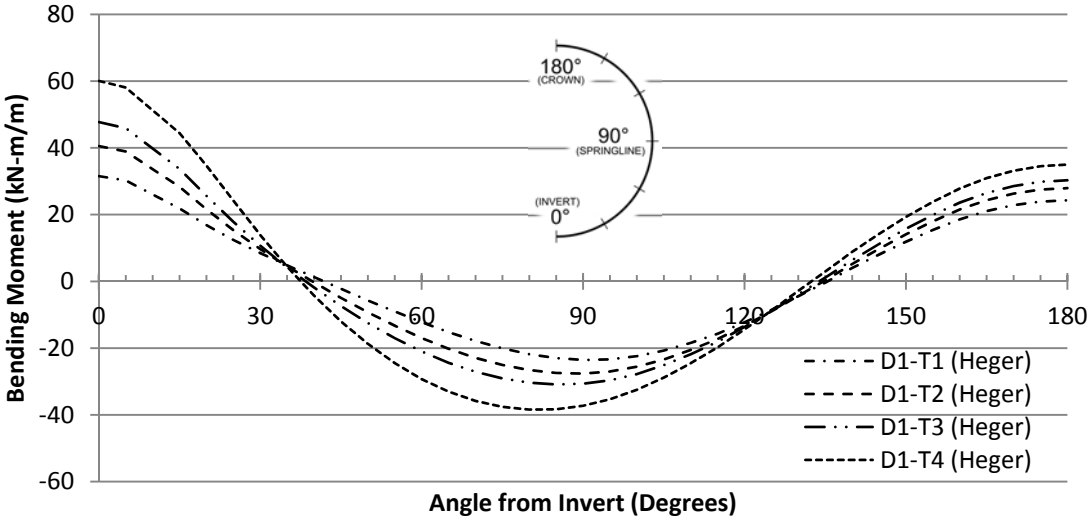

Figure 3.13 - Bending Moments in Culvert with 3 m Fill (SIDD)

Figure 3.13 presents the variation of the bending moments around the circumference of culverts having a burial depth of 3 m. As expected with standard installations for direct design (SIDD), increasing installation quality results in a decrease in bending moments along the entire culvert circumference. Comparing results at the invert, we get values of 31.6 kNm, 40.6 kNm, 47.7 kNm, and 60.1 kNm for SIDD Types 1, 2, 3, and 4, respectively.

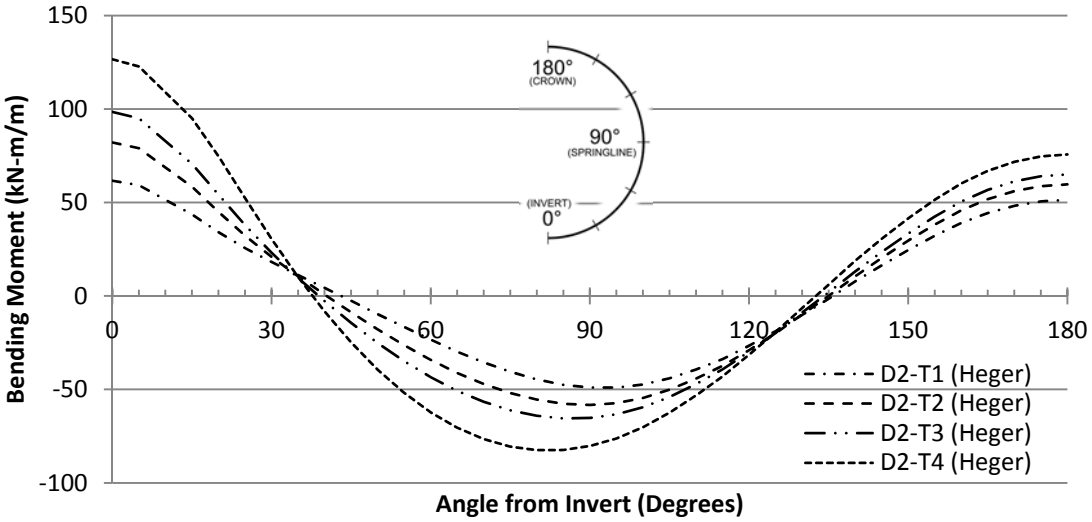

Figure 3.14 - Bending Moments in Culvert with 6 m Fill (SIDD)

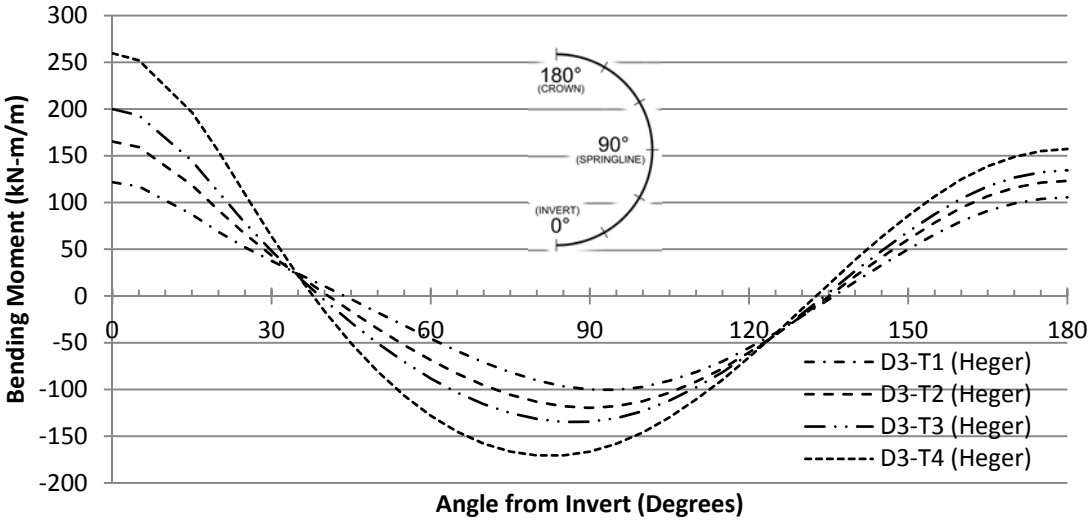

Figure 3.15 - Bending Moments in Culvert with 12 m Fill (SIDD)

Figures 3.14 and 3.15 present the variation of the bending moments around the circumference of culverts having burial depths of 6 m and 12 m, respectively. The same pattern observed in Figure 3.13 is repeated in Figures 3.14 and 3.15 with the exception that the difference between the different installation types becomes even greater with increasing depth of fill. This is explained by the fact that the portion of the bending moments resulting from the culvert self-weight is constant regardless of the installation type. As the height of fill increases, the difference in the bending moments between the different installation types trends more towards the difference in the earth pressure alone. Comparing results at the invert, we get values of 61.7 kNm, 82.2 kNm, 98.5 kNm, and 126.7 kNm for SIDD Types 1, 2, 3, and 4, respectively for 6 m burial depth and 121.8 kNm, 165.4 kNm, 200.1 kNm, and 259.8 kNm for 12 m burial depth.

3.3.6.2 Axial Thrust

Positive values in the axial thrust results indicates compression. Results are presented as Figures 3.16 to 3.18. The legend is identical to that used in the bending moment analysis.

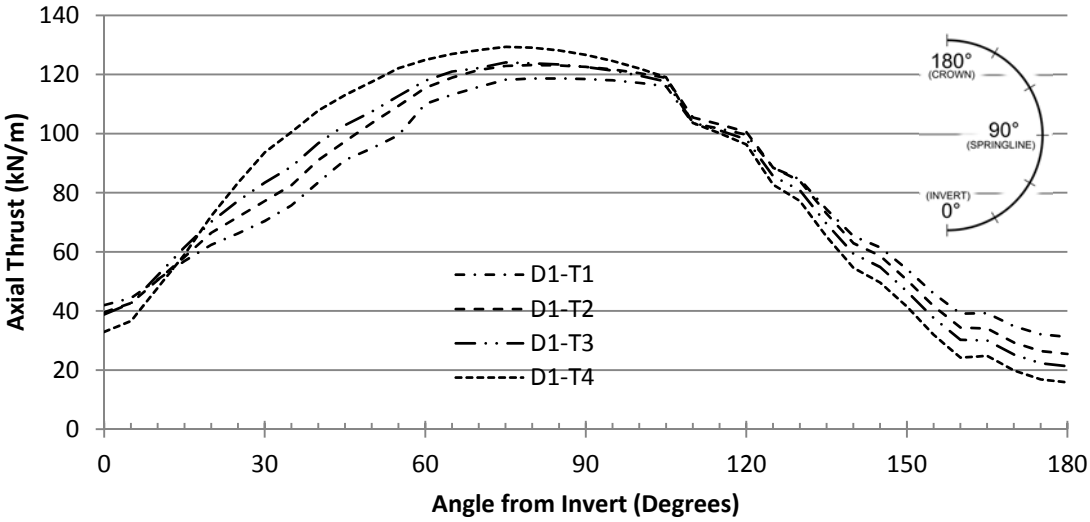

Figure 3.16 – Axial Thrust in Culvert with 3 m Fill (SIDD)

Figure 3.16 presents the variation of the axial thrust around the circumference of culverts having a burial depth of 3 m. Looking at the figure, it can be seen that the maximum axial thrust is located just below the springline at approximately 80 degrees from the invert. Maximum axial thrusts are 118.7 kN, 123.2 kN, 124.1 kN, and 129.4 kN for SIDD Types 1, 2, 3, and 4, respectively. The difference between results for each of the standard installations is closely proportional to the differences between their respective vertical arching factors, which are 1.35 for Type 1, 1.40 for Types 2 and 3, and 1.45 for Type 4.

The minimum axial thrusts are located at the invert and crown and follow a pattern similar to their respective horizontal arching factors, which are 0.45 for Type 1, 0.40 for Type 2, 0.37 for Type 3, and 0.30 for Type 4.

Figures 3.17 and 3.18 present the variation of the axial thrust around the circumference of culverts having burial depths of 6 m and 12 m, respectively. Very similar patterns to those observed in Figure 3.16 can be seen below. Maximum axial thrusts are 259.0 kN, 268.6 kN, 269.5 kN, and 281.4 kN for SIDD Types 1, 2, 3, and 4, respectively for the 6 m burial depth and 540.5 kN, 559.6 kN, 561.1 kN, and 586.2 kN for the 12 m burial depth.

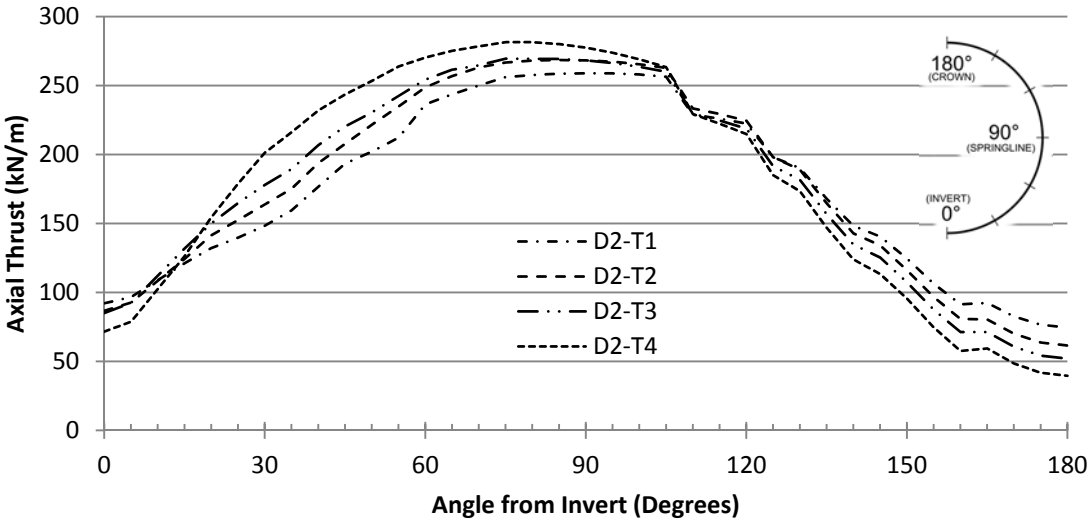

Figure 3.17 – Axial Thrust in Culvert with 6 m Fill (SIDD)

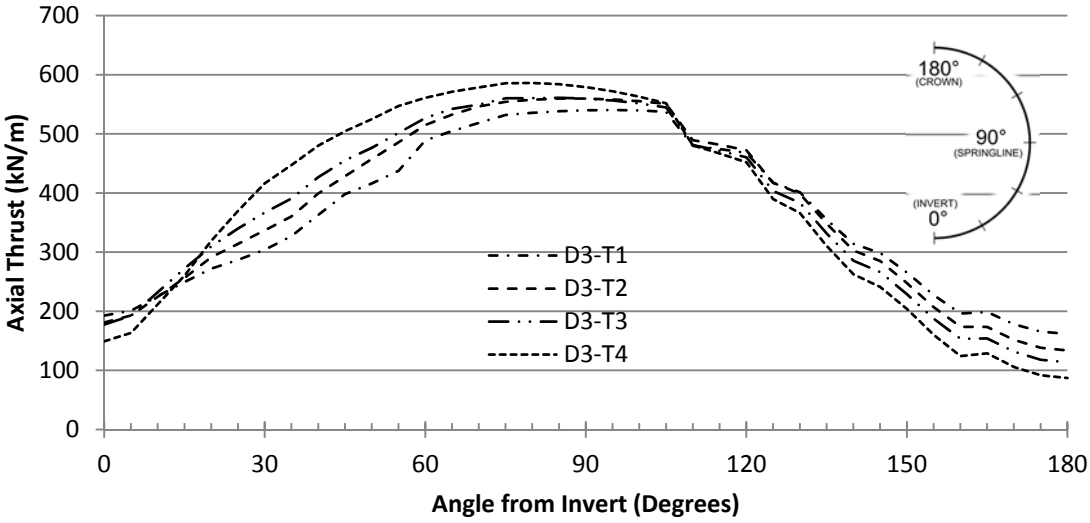

Figure 3.18 – Axial Thrust in Culvert with 12 m Fill (SIDD)

3.3.6.3 Shear Force

Results of the shear force analyses are presented as Figures 3.19 to 3.21. The absolute maximum shear values are located approximately 15 or 20 degrees from the invert, depending on the standard installation type. The legend is identical to that used in the bending moment and axial thrust analyses.

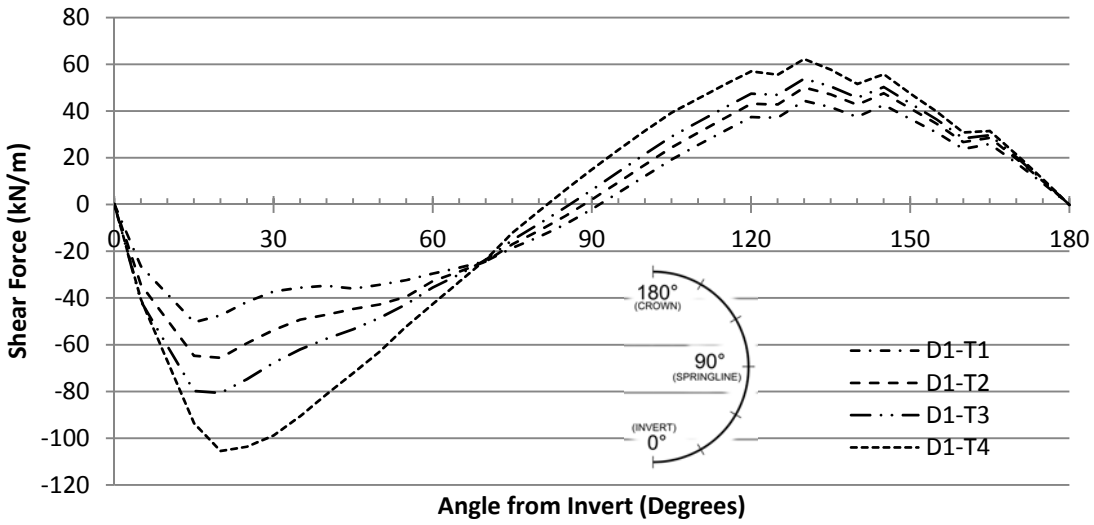

Figure 3.19 – Shear Force in Culvert with 3 m Fill (SIDD)

Figure 3.19 presents the variation of the shear forces around the circumference of culverts having a burial depth of 3 m and shows that the absolute maximum shear force is located in the lower haunch area approximately fifteen to twenty degrees from the invert. The graphs also clearly show the effect of the increasing haunch compaction with standard installation Types 3, 2, and 1. The pressure area "A2" as presented in Heger's pressure distributions becomes increasingly significant, diverting increasing amounts of the concentrated bearing pressure from directly below the invert, resulting in significantly reduced maximum shear forces. This is most evident in installation Type 4, where due to the complete lack of compaction, the pressure area "A2" is not considered to provide any support, resulting in the culvert being supported below the invert only. Comparing results at the lower haunch, we get values of 50.3 kN, 65.5 kN, 80.6 kN, and 105.5 kN for SIDD Types 1, 2, 3, and 4, respectively.

Some undulations are present in the graphs between 120 and 165 degrees from the invert, but as the shear forces at the haunch area has been validated with the tables provided in ASCE 15-98, it should not be necessary to refine the analysis further.

Figures 3.20 and 3.21 present the variation of the axial thrust around the circumference of culverts having burial depths of 6 m and 12 m, respectively. Very similar patterns to those observed in Figure 3.19 were identified in Figures 3.20 and 3.21. Comparing results at the lower haunch, we get values of 95.9 kN, 132.0 kN, 166.4 kN, and 223 kN for SIDD Types 1, 2, 3, and 4, respectively for 6 m burial depth and 187.2 kN, 264.9 kN, 338 kN, and 458.2 kN for 12 m burial depth.

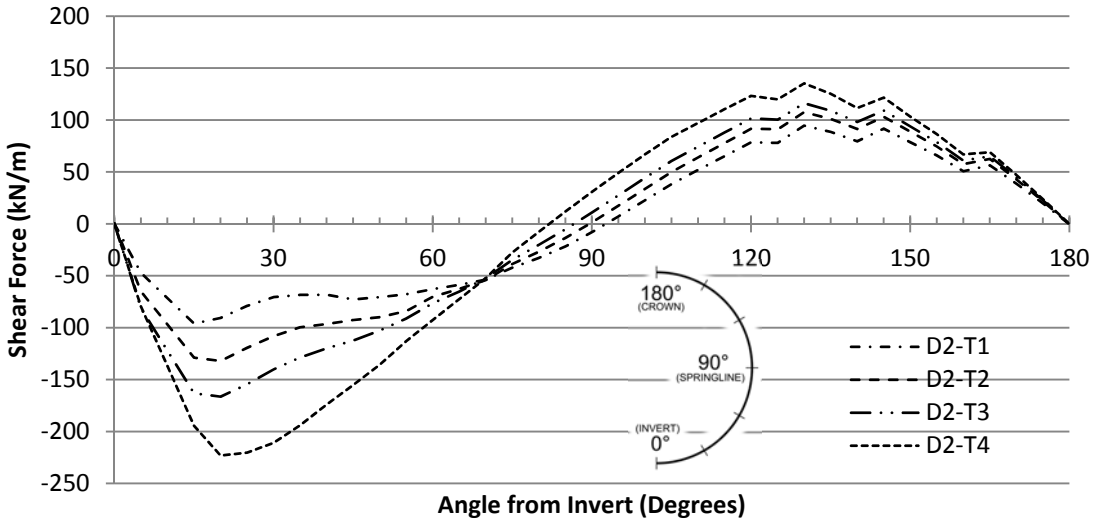

Figure 3.20 – Shear Force in Culvert with 6 m Fill (SIDD)

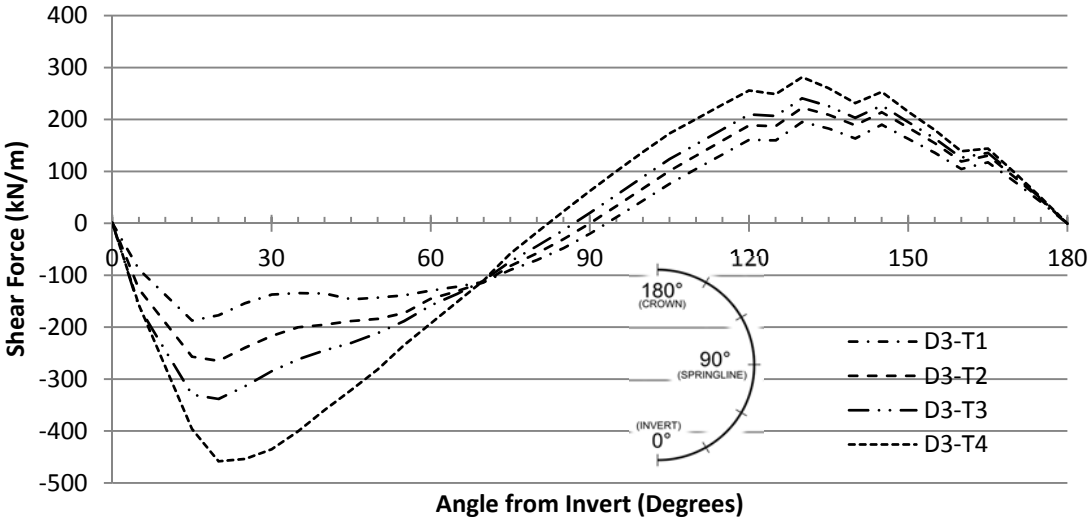

Figure 3.21 – Shear Force in Culvert with 12 m Fill (SIDD)

3.4 Finite-Element Analysis / Heger Comparison

The load effects resulting from the Heger pressure distributions and the finite-element analysis are compared below. As all of the finite-element analysis results are somewhat idealized in that they do not consider poor installation bedding conditions, only the Type 1 standard installation will be compared. This is because the Type 1 standard installation most closely approximates an idealized installation.

3.4.1 Bending Moments

As with all previous results, the bending moments are presented on the ordinate with positive values indicating that the inside face of the culvert is in tension. The abscissa represents the culvert half circumference in units of degrees with 0° representing the culvert

invert and 180° the crown. The legend is identical to that used previously. Comparisons of bending moment predictions are presented in Figures 3.22 to 3.24.

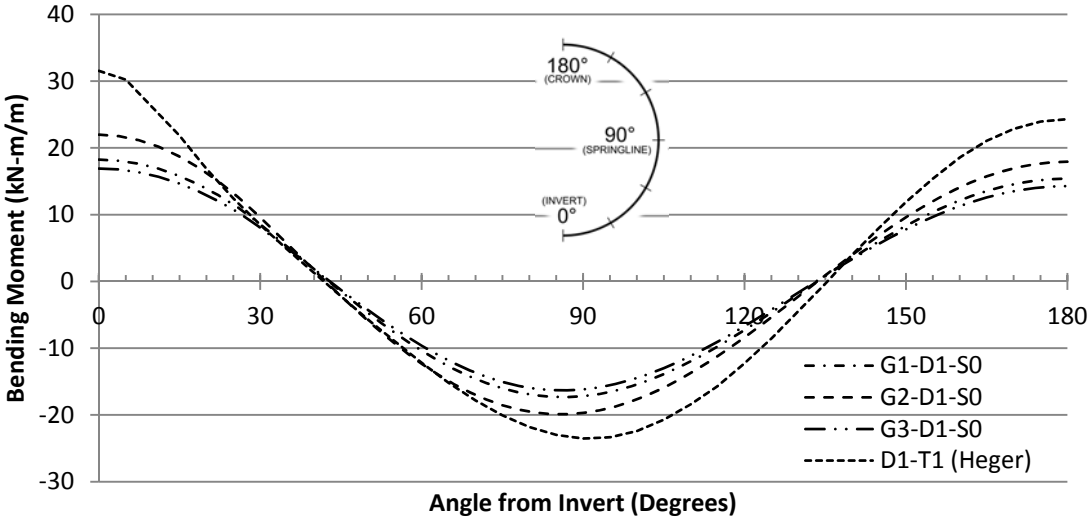

Figure 3.22 – Bending Moment in Culvert with 3 m Fill (Comparison)

Figure 3.22 presents the variation of the bending moment around the circumference of the culvert having a burial depth of 3 m. It can be seen from Figure 3.22 that the same pattern is evident in the finite-element analysis and the SIDD analysis: Bending moments are positive at the invert and crown and negative at the springline. The finite element analysis and SIDD Type 1 results differ in two important ways. The magnitude of the bending moments is greater at all key points in the SIDD installation than in the finite-element results. This is likely due to the value of the vertical arching factor in Heger's pressure distribution, which is a constant 1.35 for a Type 1 installation, which is overestimating the actual value. In reality, vertical arching factor should change depending on the height of

fill, the trench geometry, and the stiffness of the existing embankment soil. As a result, the constant value presented in Heger's pressure distribution may be a conservative oversimplification. Additionally, the distribution of the bending moments differs in that there is higher bending moment at the invert in the SIDD installation. The bending moment at the invert is approximately twenty-three percent greater than that at the crown in the finite-element analysis results compared to approximately thirty percent with the SIDD Type 1 installation. This difference is likely due to the fact that the finite-element analysis is highly idealized in how the culvert is supported at the invert. Heger's pressure distribution, on the other hand, was devised in such a way that it better considers the installation condition by providing several zones having varying stiffnesses to more accurately simulate the installation and compaction at the invert and haunches (Heger, 1988).

Comparing at the invert, the SIDD Type 1 installation results are approximately seventy-three percent greater than those calculated with Group 1 backfill material. This significant difference is likely due to the combination of the two factors discussed above.

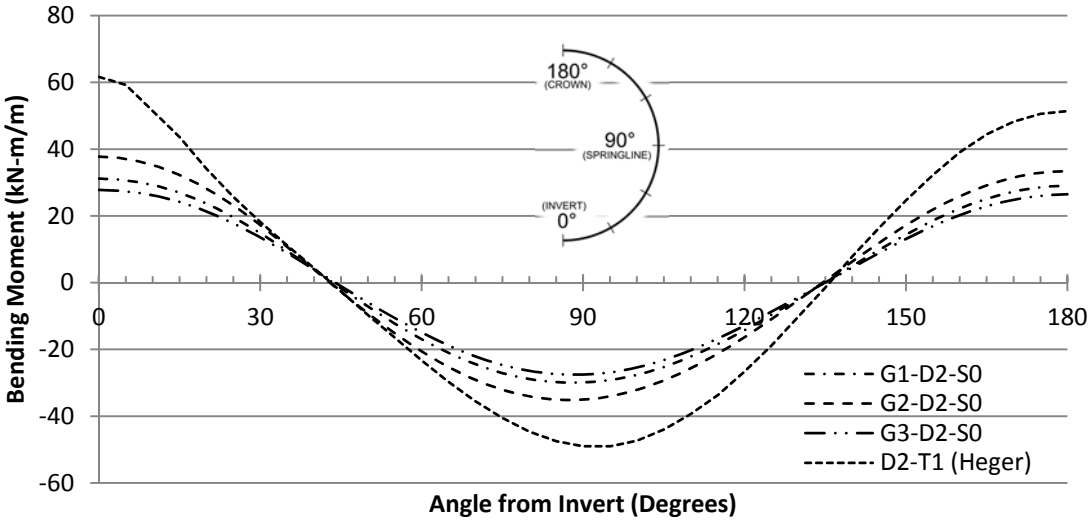

Figure 3.23 – Bending Moment in Culvert with 6 m Fill (Comparison)

Figure 3.23 presents the variation of the bending moment around the circumference of culverts having a burial depth of 6 m. It can be seen from Figure 3.23 that the SIDD Type 1 installation results are approximately ninety-eight percent greater than those calculated with Group 1 backfill material at the invert. The increasing difference between the SIDD results and the finite-element analysis with increasing depth further indicates that increased depth increases the amount of soil arching resulting in a lower value of the vertical arching factor than assumed by Heger.

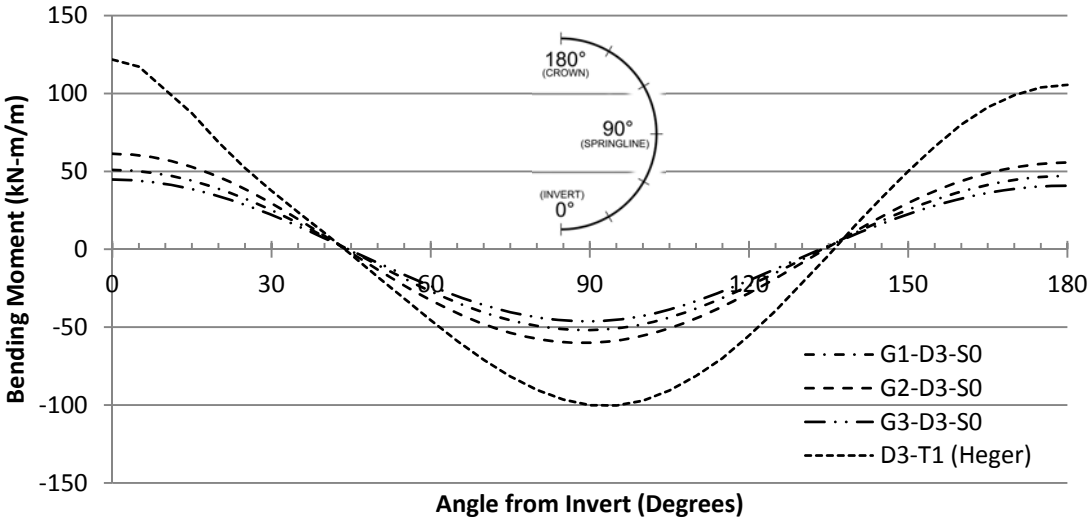

Figure 3.24 – Bending Moment in Culvert with 12 m Fill (Comparison)

Figure 3.24 presents the variation of the bending moment around the circumference of culverts having a burial depth of 12 m. It can be seen from Figure 3.24 that the SIDD Type 1 installation results are approximately 139 percent greater than those calculated with Group 1 backfill material at the invert. Again, the increasing difference between the SIDD results and the finite-element analysis with increasing depth further indicates that increased depth increases the amount of soil arching resulting in a lower value of the vertical arching factor than assumed by Heger.

In applying Heger's pressure distribution, the applied pressure, and resultantly, the bending moments, increases linearly with increasing depth of fill. Comparing G1-D1-S0 with G1-D2-S0 at the invert, doubling the depth of fill above the culvert from 3 m to 6 m has resulted in a 70.8% increase in the bending moment. Comparing G1-D2-S0 with

G1-D3-S0, doubling the height of fill above the culvert a second time, results in an increase of 63.5% at the invert. This is indicative that increasing soil arching is occurring with increasing depth of fill; a factor not considered by the constant value of the vertical arching factor used in Heger's pressure distribution.

3.4.2 Axial Thrusts

As with all previous results, the axial thrusts are presented on the ordinate with positive values indicating compression. The abscissa represents the culvert half circumference in units of degrees with 0° representing the culvert invert and 180° the crown. The legend is identical to that used previously. Comparisons of axial thrust are presented in Figures 3.25 to 3.27.

Looking at Figures 3.25 to 3.27, the same pattern is evident in the finite-element analysis and the SIDD analysis: The culvert wall is in compression over its entire length with increasing values near the springline.

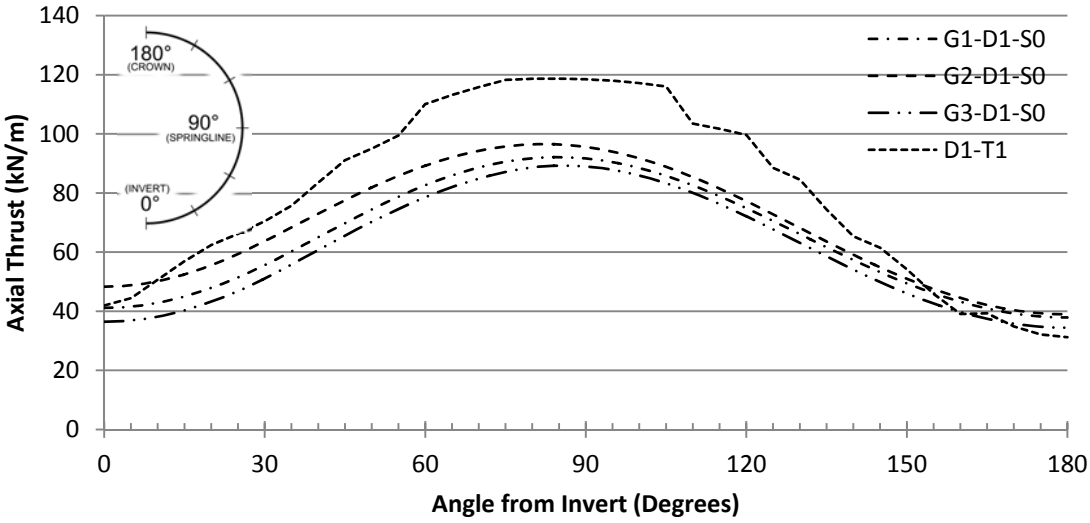

Figure 3.25 – Axial Thrust in Culvert with 3 m Fill (Comparison)

Figure 3.25 presents the variation of the axial thrust around the circumference of culverts having a burial depth of 3 m. It can be seen from Figure 3.25 that SIDD Type 1 results are approximately twenty-nine percent greater than those obtained with the finite-element analysis using Group 1 backfills when compared near the springline. The axial thrusts calculated per SIDD Type 1 are approximately the same at the invert and eighteen percent lower at the crown.

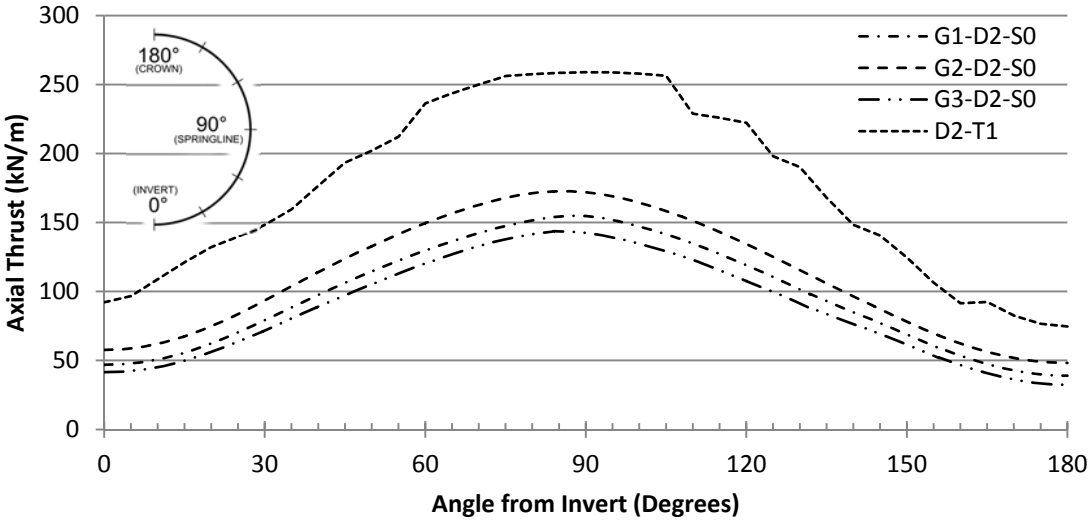

Figure 3.26 – Axial Thrust in Culvert with 6 m Fill (Comparison)

Figure 3.26 presents the variation of the axial thrust around the circumference of culverts having a burial depth of 6 m. It can be seen from Figure 3.26 that SIDD Type 1 results are approximately sixty-seven percent greater than those obtained with the finite-element analysis using Group 1 backfills when compared near the springline. The axial thrusts calculated per SIDD Type 1 are approximately ninety-seven and ninety-one percent greater at the invert and crown, respectively.

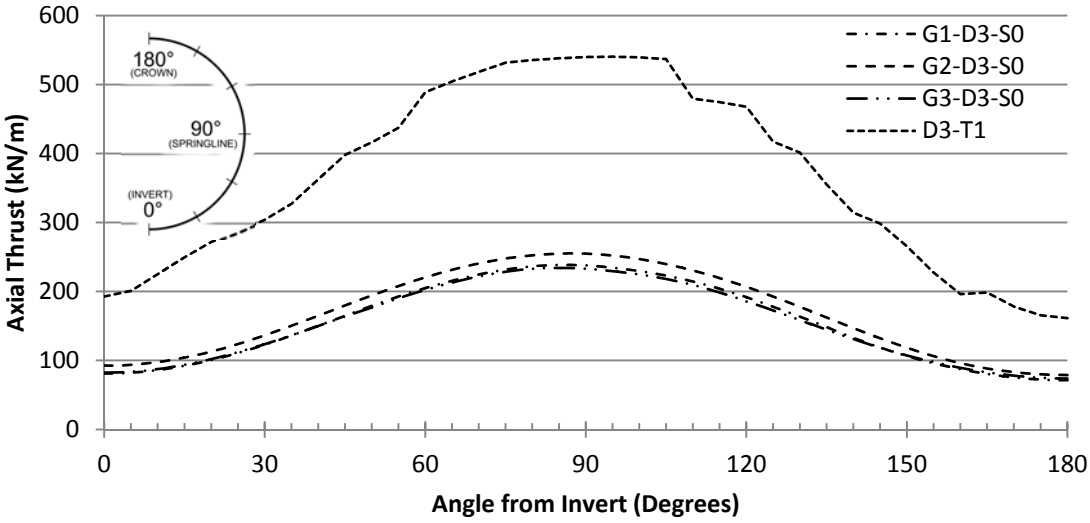

Figure 3.27 – Axial Thrust in Culvert with 12 m Fill (Comparison)

Figure 3.27 presents the variation of the axial thrust around the circumference of culverts having a burial depth of 12 m. It can be seen from Figure 3.27 that SIDD Type 1 results are approximately 127 percent greater than those obtained with the finite-element analysis using Group 1 backfills when compared near the springline. The axial thrusts calculated per SIDD Type 1 are approximately 138 and 126 percent greater at the invert and crown, respectively.

As was observed with the bending moment analysis comparison, the increasing difference with increasing depth of fill again indicates that using a constant value of vertical arching factor may lead to excessively conservative results in installations with higher embankments.

3.4.3 Shear Forces

Comparisons of shear force results using Heger's pressure distribution and the finite element analyses are presented in Figures 3.28 to 3.30.

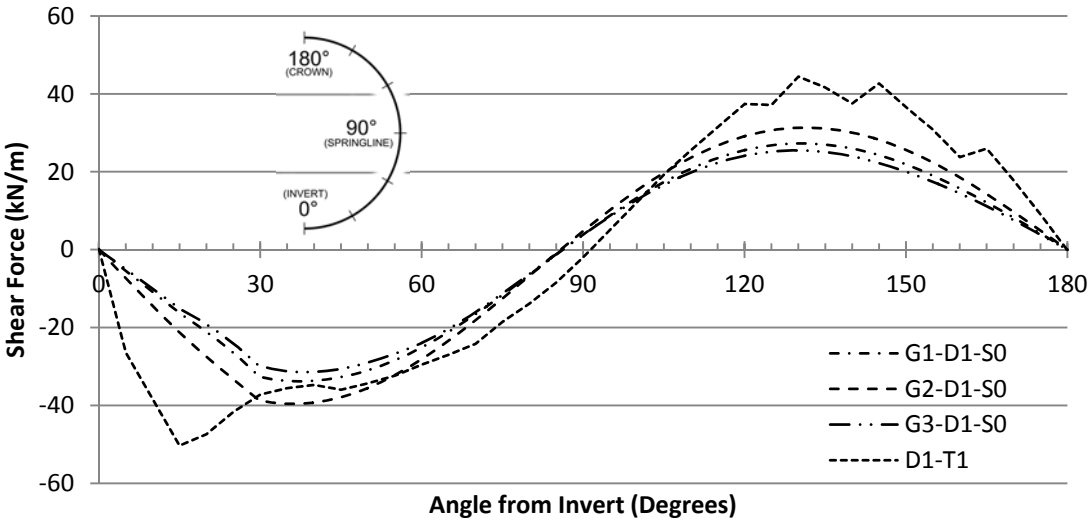

Figure 3.28 – Shear Force in Culvert with 3 m Fill (Comparison)

Figure 3.28 presents the variation of the axial thrust around the circumference of culverts having a burial depth of 3 m. It can be seen from Figure 3.28 that the finite-element analyses show similar patterns. The results obtained using Heger's pressure distribution follow the same general pattern, however the bedding preparation, haunch compaction requirements, and potential voids Heger considered in preparing his pressure distribution results in increased shear forces nearer to the invert. Compared to the Group 1 results, the maximum shear force obtained using a Heger Type 1 installation are approximately forty-nine percent greater. Also, the maxima is located at approximately fifteen degrees from the

invert using Heger Type 1 results, compared with approximately thirty-seven degrees in the Group 1 finite-element analysis.

Figure 3.29 and 3.30 present the variation of the axial thrust around the circumference of culverts having burial depths of 6 m and 12 m, respectively. The same pattern observed in Figure 3.28 is repeated in Figures 3.29 and 3.30 where the Heger Type 1 installation results are approximately 71 percent and 107 percent greater at their respective maxima. Additionally, the location of the maxima moves further from the invert with increasing depth of fill for the finite element results compared with Heger results where the maxima remains at a constant fifteen degrees from the invert.

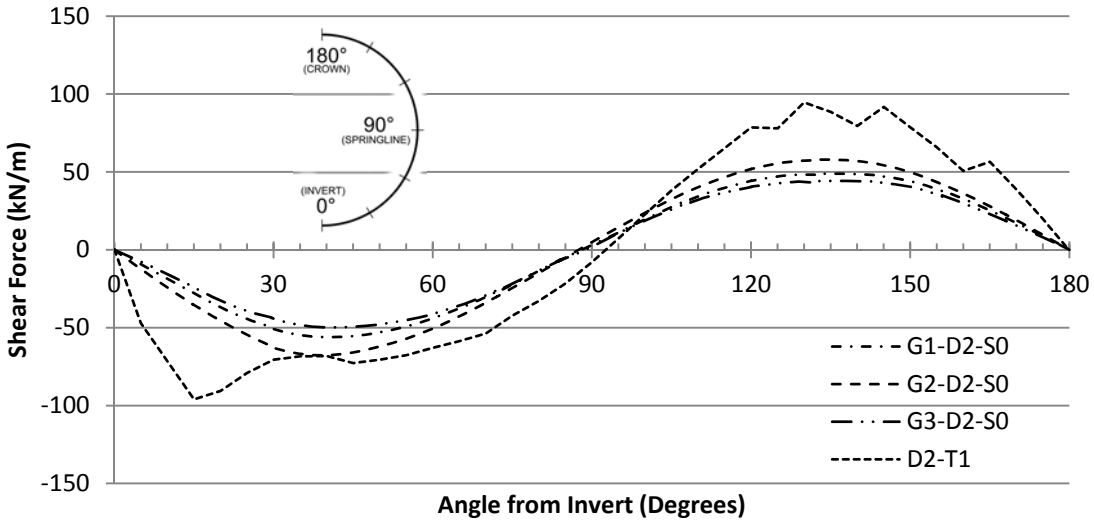

Figure 3.29 – Shear Force in Culvert with 6 m Fill (Comparison)

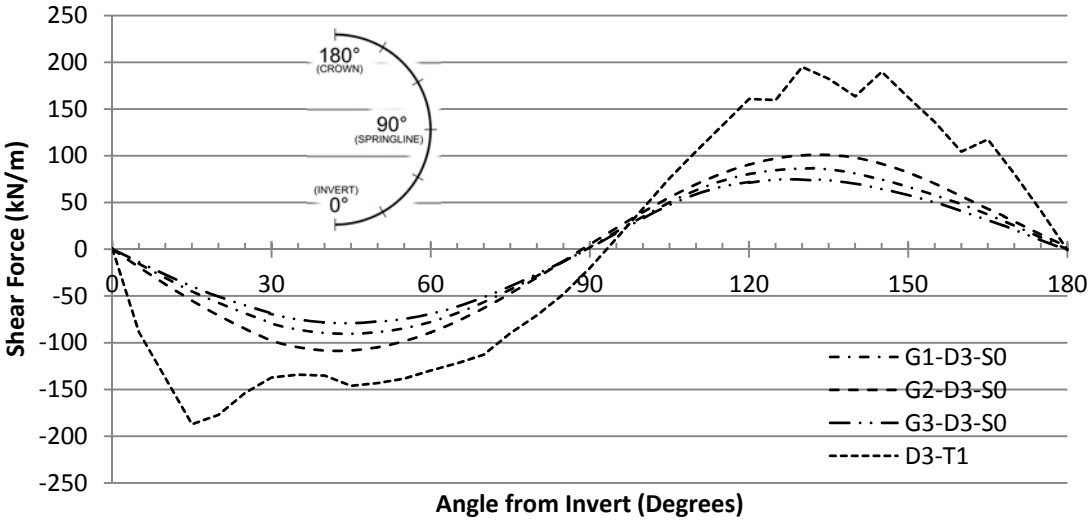

Figure 3.30 – Shear Force in Culvert with 12 m Fill (Comparison)

3.5 Comparison of Required Flexural Reinforcing Steel at Ultimate Limit States

The location that forms the basis for flexural reinforcement design is the invert (0°). As was observed in the parametric studies presented above, bending moments are greatest at that location. As a result, the flexural reinforcement required to satisfy the Ultimate Limit State at that location is a convenient means of comparing the effect of the different pressure distributions. Compared below are the minimum required flexural reinforcement for the finite-element analysis results obtained using the Group 1 backfill materials and those obtained using the Heger Type 1 pressure distribution.

The minimum required flexural reinforcement is calculated per the corrected equation [7] presented in Section 2.3.4 above. The following values represent current industry practices and code requirements for precast concrete pipe and were used for the calculations: $f'_c = 45$ MPa; $f_y = 485$ MPa; $\varphi_s = 0.90$; $\varphi_c = 0.80$; $\alpha_1 = 0.85$, h = 200 mm, and d = 170 mm.

A load factor of 1.25 and an installation factor of 1.1 were applied to the bending moment per the requirements of Clauses 7.5.2 and 7.8.7.1(a) of CHBDC. The load factor for the axial thrust was taken as 1.0 per the requirements Clause 7.8.7.1(b). The value of "d" was calculated by subtracting 25 mm for the concrete cover and 5 mm representing half of the assumed reinforcement diameter from the wall thickness. The maximum permissible area of steel was calculated per the equation presented in CHBDC C7.8.8.1.1, which is reproduced as equation [3.8] below. The purpose of the maximum permissible steel area is to ensure ductile failure behaviour of the structure. Crack control and shear requirements were not considered at this time.

$$A_{s,max} = \left[\frac{380 g' \varphi_s d}{(600+f_y) f_y}\right] - \frac{0.75 N_u}{f_y} \qquad \textbf{[3.8]}$$

Where: $g' = b\, f'_c\, [0.85-0.008\, (f'_c -30)]$

$0.65\, b\, f'_c \leq g' \leq 0.85\, b\, f'_c$

Also presented are approximate equivalent D-Loads calculated with the computer program PipeCAR, which can calculate equivalent D-Loads from inputs of geometry, material properties, and area of reinforcement provided at the inside face of the culvert at the invert. As PipeCAR is based on Load-Resistance Factor Design, which does not consider separate partial factors for the concrete and steel, an equivalent single factor was calculated using the correlation presented in equation [3.9] below (Allard, 2013).

$$\varphi_{r,eq} = 0.9 - 0.08\left(\frac{A_s}{A_{s,max}}\right) \qquad [3.9]$$

Table 3.7 - Comparison of Required Flexural Reinforcement

Burial Depth (m)	Analysis	A_s (mm^2/m)	$A_{s,max}$ (mm^2/m)	D-Load
3	FEA	290	3163	20
	Heger	549	3161	48
6	FEA	535	3154	46
	Heger	1105	3084	102
12	FEA	893	3101	83
	Heger	2405	2928	209

Table 3.7 shows that compared with the finite-element analysis results, designs prepared using the Heger pressure distributions require significantly more reinforcement. Designs prepared using the Heger pressure distribution were found to require 1.90, 2.07, and 2.69 times more reinforcing steel than those prepared using finite-element analysis at burial depths of 3 m, 6 m, and 12 m, respectively. In the case of the 12 m burial depth with Heger's pressure distribution, the required steel is approaching the maximum permissible area. Once crack control requirements are considered, it is possible that the required steel area may exceed the maximum permissible amount.

Table 3.11 also shows that for the burial depth of 12 m, using Heger's pressure distribution may lead to impractical results as the D-Load far exceeds any of the common pipe "classes" with 140-D being the most robust commonly available standard designation.

3.6 Summary and Conclusion

This chapter presented the results of a parametric study that was performed to investigate the appropriateness of using the Heger pressure distribution to predict internal forces in pipe culverts. The main aim is to determine when Heger's pressure distributions can be

expected to yield reasonable results and when it may be advisable to employ more refined analysis methods to obtain more economical designs. In the parametric study, the installation depth as well as the ratio of the stiffness of the backfill to that of the existing embankment material was varied. Based on the results of the parametric study the following conclusions may be drawn:

1. As anticipated, increasing stiffness of the backfill material resulting from increased compaction (better installation quality) results in a decrease in bending moments, shear and axial thrust in the pipe walls.
2. Increased burial depth results in increased soil arching.
3. The constant value of vertical arching factor used in Heger's pressure distributions leads to increasingly conservative results with increasing burial depths.
4. In the case of partial trench installations, Heger's pressure distribution was found to lead to conservative values of bending moments, shear and axial thrusts when compared to FEA methods. In the case of installation in deep embankments, the discrepancy becomes increasingly significant.
5. The required flexural reinforcement calculated using Heger's pressure distributions is significantly greater than that calculated using the finite-element analysis.

The finite-element analysis parametric study demonstrates that Heger's pressure distributions consistently leads to conservative results in partial trench embankments. As a result, in these installations, it may be reasonable to apply more sophisticated analysis methods to achieve a more economical design. The additional cost incurred through the

use of more sophisticated analysis methods, such as finite-element analysis, should be considered in performing the cost comparison.

3.7 References

Allard, E., El Naggar, H. (2013) "Evaluation of PipeCAR per Canadian Highway Bridge Design Code Requirements". GeoMontreal 2013. September 29 to October 3 2013. Montreal, Canada.

American Society for Testing and Materials (ASTM). (2003). *C 76M-03 Standard specification for reinforced concrete culvert, storm drain, and sewer pipe [Metric], 04.05*

American Society of Civil Engineers (ASCE). (2000). *Standard practice for direct design of buried precast concrete pipe using standard installations (SIDD)* American Society of Civil Engineers.

Brinkgreve, R. (2008). *Plaxis 2D - Version 9.0*. Delft, Netherlands: Plaxis.

Canadian Standards Association (CSA). (2006). *CAN/CSA-S6-06 - Canadian highway bridge design code*. Mississauga, Ont.: Canadian Standards Association.

Heger, F. J. (1988). New installation designs for buried concrete pipe. Pipeline Infrastructure, Proceedings, 117-135.

Irving, D. (1985). The LUSAS finite element system with reference to the construction industry. *Proceedings of the 2nd International Conference on Civil and Structural Engineering Computing, London, Volume 2*

Chapter 4 - Numerical Analysis – Seismic Load Case

4.1 General

The Canadian Highway Bridge Design Code (CHBDC) Clause 7.8.4.1 d), mandates including a seismic load combination, in addition to the static load combinations, for evaluation at the Ultimate Limit States (ULS). The mandated seismic load combination includes:

a) The self-weight of the structure;

b) The earth pressure, and;

c) The earthquake load

CHBDC provides a simplified method to evaluate the effect of a seismic event on buried reinforced concrete culvert. This chapter compares results using the simplified method presented in CHBDC with those obtained using a pseudo-static finite-element analysis. Such a comparison is accomplished two ways:

1 - The seismic analysis methods will be compared directly by applying both the CHBDC simplified and pseudo-static finite-element analysis methods to a consistent static starting point. In this case, this starting point will be the static finite-element analysis results obtained in Chapter 3.

2 - Code requirements will be compared to the results of the finite-element analysis by applying the pseudo-static analysis method to the finite-element results and

comparing those results with those obtained by applying the simplified method to results obtained using Heger's pressure distributions.

4.2 Simplified Method per CHBDC

Clause 7.8.4.4 in CHBDC presents a simplified method for calculating seismic effects. It states that: "the additional force effects due to earthquake loads shall be accounted for by multiplying the force effects due to self-weight and earth load […] by the vertical acceleration ratio, A_V, specified in Clause 7.5.5.1". CHBDC Clause 7.5.5.1 states that A_V shall be set equal to two-thirds of the horizontal ground acceleration, A_H, where A_H is the zonal acceleration ratio (A) determined per CHBDC Clause 4.4.3.

Per CHBDC Clause 4.4.3, the zonal acceleration can be obtained directly from Tables A3.1.1 or 4.1 of CHBDC, or directly from the Geological Survey of Canada's website.

As the depth of fill above the structure increases, the dead load rapidly becomes the dominant design force. This observation is largely due to the area over which the live load is applied increasing exponentially with depth, resulting in a matching decrease in the applied live load pressure. As a result of the increasing depth of fill, the seismic load combination, becomes increasingly dominant in governing the structural design. However, Serviceability Limit States design requirements, such as crack control, do not apply to this load combination.

For the purpose of this analysis, three values of "A" were evaluated and are as follows:

1. 0.10g represents areas of low seismicity and is designated as “LSZ”;
2. 0.25g represents areas of medium seismicity and is designated as “MSZ”; and
3. 0.45g represents areas of high seismicity and is designated as “HSZ”.

Following the method presented in CHBDC, the results of the static analyses are subject to a scalar increase of 6.66%, 16.7%, and 30.0% for the LSZ, MSZ, and HSZ, respectively.

4.3 Pseudo-Static Analysis of in-Plane Seismic Stresses

There are two basic approaches to modeling a buried structure’s response to seismic loading using finite-element analysis. The first is to perform a time history analysis, where input motions corresponding to an earthquake signal are applied to the lower boundary of the finite-element model. The pseudo-static analysis method is an alternative approach that involves applying an incremental prescribed static displacement at the lateral boundaries of the model. In this approach, inertia forces are ignored and the earthquake loading is simulated as a static far-field shear stress or strain applied at the boundaries of the model. The magnitude of the prescribed displacement is determined from a site-specific ground response analysis. Current design practice favours the pseudo-static approach (El Naggar, 2008).

The average far-field shear strains for use in the analyses were determined from the ground response analyses presented in Figure 4.1 below (El Naggar, 2008). The ground response analyses were prepared using the program NERA (Bardet and Tobita, 2001) using input ground motions from Atkinson and Beresnev (1998) and scaled in accordance with Adams

(1999) for "Type C" soil per the 2005 National Building Code of Canada. The three ground response analyses are considered to represent low, intermediate, and high seismic events and are designated LSZ, MSZ, and HSZ, respectively. Values of 0.06%, 0.10%, and 0.25% are taken to represent the LSZ, MSZ, and HSZ, respectively at a depth of approximately 7 m. This depth was chosen as it represents an average of the three evaluated burial depths. The prescribed displacements applied to finite-element models vary from 0 at the bottom of the models to 18 mm, 30 mm, and 75 mm at the ground surface for the LSZ, MSZ, and HSZ, respectively. These values represent the peak shear stresses obtained from the ground response analyses multiplied by the height of model.

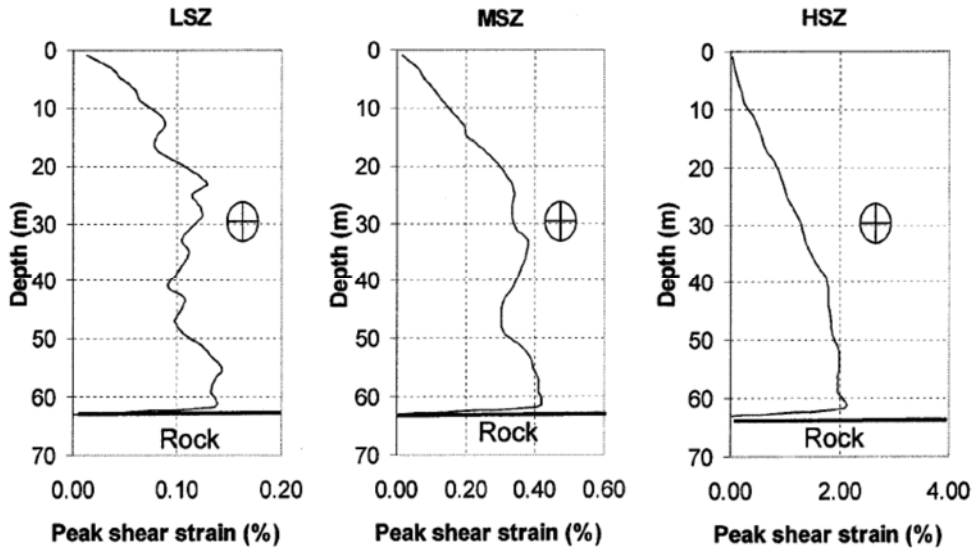

Figure 4.1 - Results of the Ground Response Analyses (El Naggar, 2008).

4.4 Finite-Element Analysis Model

In order to investigate the soil-structure interaction, numerical models were prepared using the two dimensional finite element package Plaxis 2D (Brinkgreve, 2008). With the exception of the addition of two loading stages, the numerical models were identical to

those used for the static analyses, and were described in detail in Chapter 3. Modifications specific to the seismic analyses are described below.

4.4.1 Staged Analysis

In order to simulate the culvert installation procedure and the seismic event, the analysis was performed in six stages. Stages 1 through 4 are common to the both the static and seismic analyses whereas Stages 5a and 5b are specific to the seismic analysis.

Stage 1: Existing, undisturbed soil;

Stage 2: Excavation of the trench;

Stage 3: Installation of the bedding material and culvert;

Stage 4: Backfilling of structure.

Stage 5a: Pseudo-Static Seismic Analysis 1

Stage 5b: Pseudo-Static Seismic Analysis 2

A graphical representation of the staged analysis is presented in Figure 4.2 below.

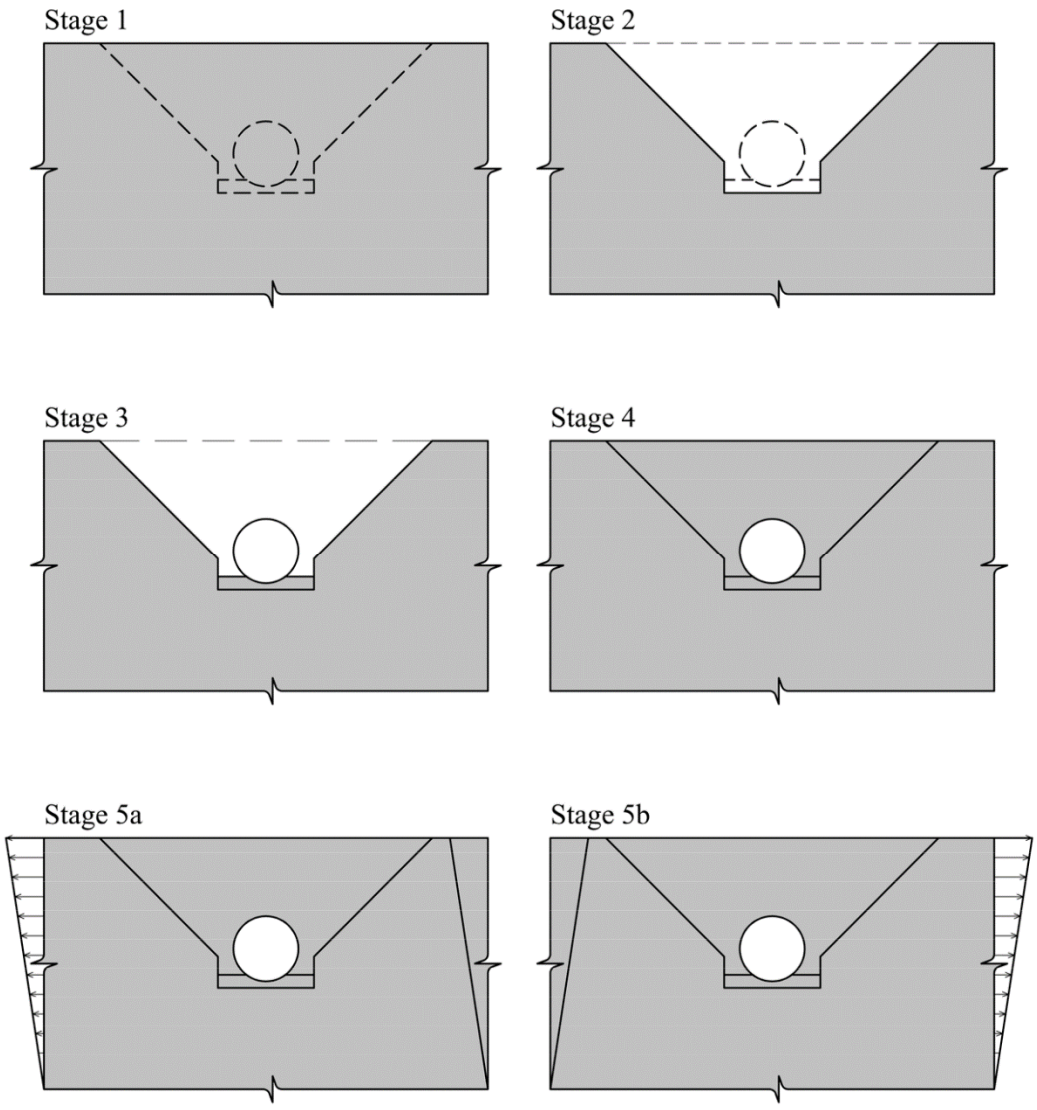

Figure 4.2 - Staged Installation Sequence

Within Plaxis 2D, a staged analysis is accomplished by defining individual stages and activating or deactivating soil "clusters", culvert "geometry lines", or loading conditions and by changing material properties of specified clusters to represent each stage. Pre-existing stresses and strains at the beginning of each of the stages correspond to those present at the end of the previous stage, except where noted below.

4.4.1.1 Analysis Stage 1: Existing, Undisturbed Soil

Stage 1 consists of the entire soil continuum assigned with "Existing" soil properties and the beam elements representing the culvert geometry deactivated. The purpose of this stage is to determine the pre-existing stresses and strains in the soil continuum.

4.4.1.2 Analysis Stage 2: Excavation

Stage 2 is performed by deactivating all of the soil clusters in the areas representing the bedding material, the area enclosed by the culvert, and the backfill area. Its purpose is to determine the changes in strains and stresses in the pre-existing soil as a result of the excavation.

4.4.1.3 Analysis Stage 3: Bedding Material and Culvert Installation

Stage 3 is performed by activating the clusters representing the bedding material and changing their material properties to those representing the respective backfill material used in the analysis. Geometry lines representing the culvert walls are activated. The purpose of this stage is to simulate the installation of the culvert and that it's self-weight is initially supported mostly its invert, causing increased load effects at that location.

4.4.1.4 Analysis Stage 4: Backfilling

Stage 4 is performed by activating the clusters representing the backfill material and changing their material properties to those representing the respective backfill material used in the analysis. While pre-existing stresses are carried over from the previous stage, displacements are reset to zero to isolate soil settlements that occur after backfilling from those that occur prior to backfilling.

4.4.1.5 Analysis Stages 5a and 5b: Pseudo-Static Seismic Analysis

In Analysis Stage 5a, prescribed displacements are incrementally applied at both lateral boundaries to represent the far-field seismic shear stresses.

In Analysis Stage 5b, the prescribed displacements applied in 5a are reversed in direction. For this stage, the starting conditions correspond with those present at the end of Stage 4.

4.4.2 Results

Analysis was performed for each combination of backfill material stiffness, heights of fill, and prescribed displacement magnitude. Bending moments, shear forces, and axial thrust numerical results around the culvert circumference were extracted from each of the Plaxis 2D models following Stages 4, 5a, and 5b and stored in a spreadsheet for ease of manipulation and comparison.

The seismic analyses per the method presented in CHBDC were calculated by increasing the Stage 4 (static) results extracted from the model by the appropriate factors presented in Section 4.2 above. As results are simply scalar multiples of the static results, they are not presented graphically; instead opting to present them in a tabular format comparing multiple analyses.

The pseudo-static analyses were completed by preparing envelopes of maximum and minimum values of bending moments, axial thrusts, and shear forces at each point around the circumference of the culvert with the results of Stages 5a and 5b.

The obtained results were grouped according to depth of fill and presented graphically with the abscissa representing the angle from the invert along the culvert half circumference in degrees and the ordinate representing the bending moment, axial thrust, or shear force in units of kN-m/m, kN/m, and kN/m, respectively.

The legend identifies results as follows: Backfill soil properties are identified with “G1”, “G2”, and “G3”, representing Group 1, 2, and 3 soils, respectively (Table 6, Chapter 3) ; The height of fill above the culvert is identified with “D1”, “D2”, and “D3”, representing 3 m, 6 m, and 12 m height of fill above the culvert, respectively; The seismicity used in the analysis is indicated with “S0”, “S1”, “S2”, and “S3”, representing no seismicity, LSZ, MSZ, and HSZ, respectively.

In order to condense the number of figures required to present the results of the analysis, results are grouped as follows. For each depth of fill the following comparisons will be presented:

1- The level of seismicity will remain constant at S2 (MSZ) while the backfill properties are varied. This comparison is intended to demonstrate the effect of changing the quality and level of compaction of the backfill material.
2- The backfill material will remain constant at G1 (Group 1) while the level of seismicity of varied. This comparison is intended to demonstrate the effect of increasing levels of seismicity.

4.4.2.1 Bending Moments

The bending moments are presented on the ordinate with positive values indicating that the inside face of the culvert is in tension. Conversely, negative values indicate the outside face is in tension. Results are presented in Figures 4.3 through 4.8.

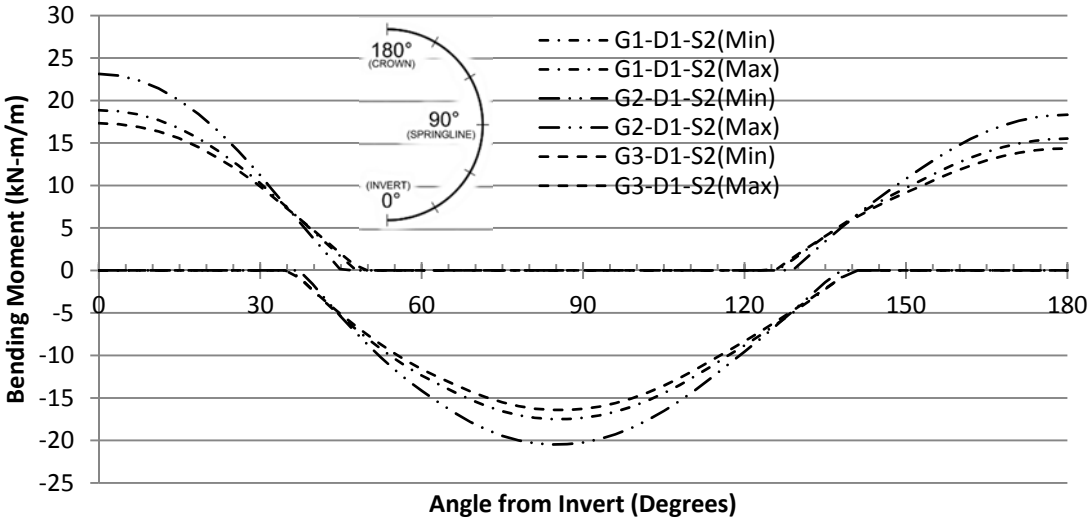

Figure 4.3 - Bending Moments in Culvert with 3 m Fill, MSZ (PS)

Figure 4.3 presents the variation of the bending moments around the circumference of culverts having a burial depth of 3 m calculated per the pseudo-static method. Results are presented with a consistent level of seismicity corresponding to the MSZ and varying levels of backfill quality. Figure 4.3 shows that, as with the static results presented in Chapter 3, increasing level of backfill compaction (quality backfilling) result in reduced bending moments along the entire circumference of the culvert.

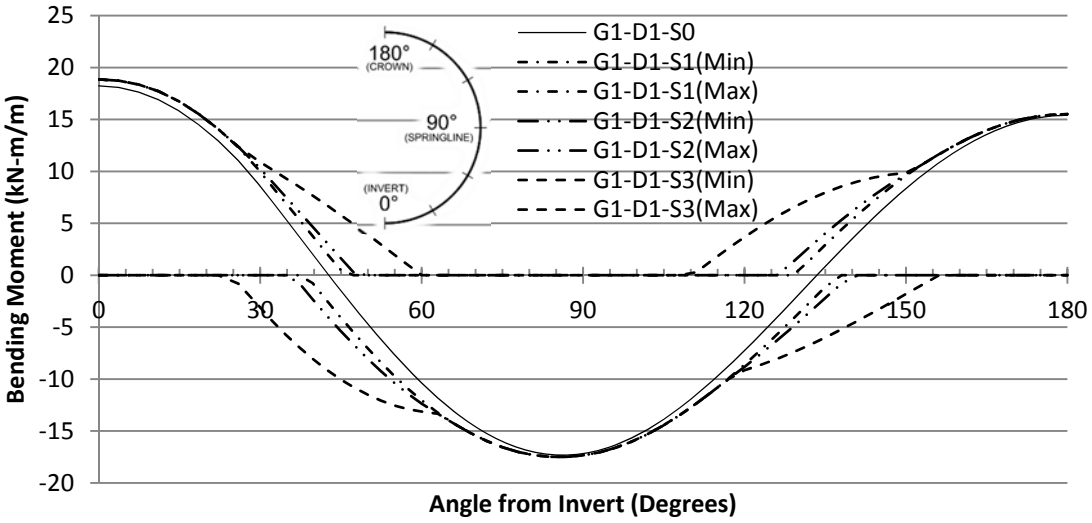

Figure 4.4 - Bending Moments in Culvert with 3 m Fill, G1 (PS)

Figure 4.4 presents the variation of the bending moments around the circumference of culverts having a burial depth of 3 m calculated per the pseudo-static method. Results are presented with a consistent backfill quality and varying levels of seismicity. Figure 4.4 shows that increasing levels of seismicity do not cause a significant increase in the bending moments at the critical areas (invert, springline, and crown). Increasing seismicity however does cause a significant increase in bending moments in the haunch areas from approximately 25 to 60 degrees and 110 to 155 degrees from the invert.

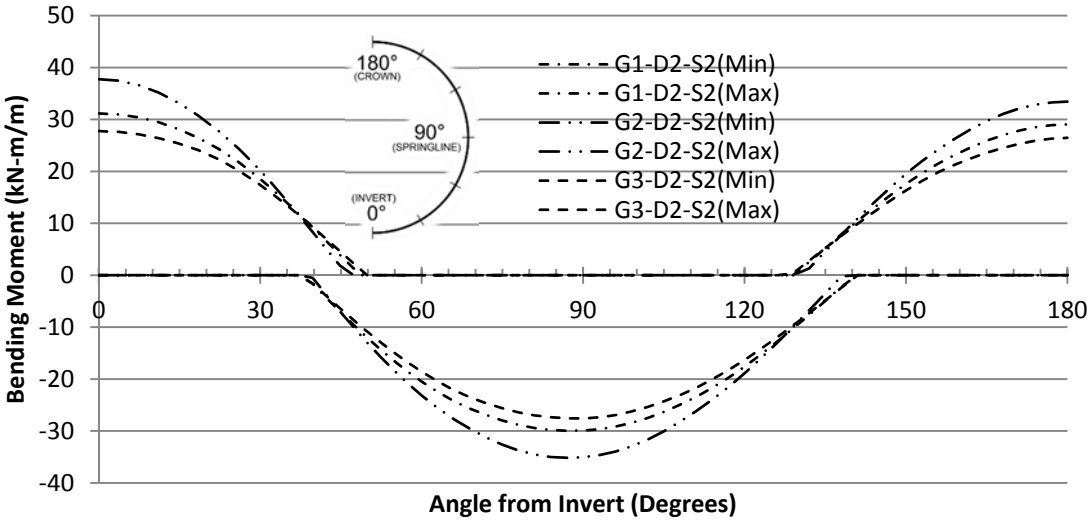

Figure 4.5 - Bending Moments in Culvert with 6 m Fill, MSZ (PS)

Figure 4.5 presents the variation of the bending moments around the circumference of culverts having a burial depth of 6 m calculated per the pseudo-static method. Results are presented with a consistent level of seismicity corresponding to the MSZ and varying levels of backfill quality. Similarly to Figure 4.3, Figure 4.5 shows that, as with the static results presented in Chapter 3, increasing level of backfill compaction result in reduced bending moments along the entire circumference of the culvert.

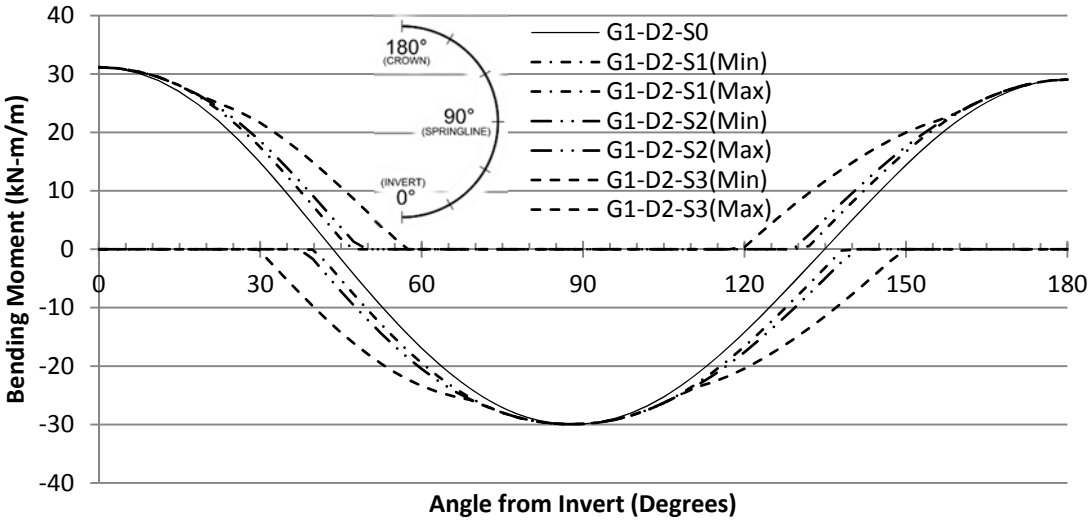

Figure 4.6 - Bending Moments in Culvert with 6 m Fill, G1 (PS)

Figure 4.6 presents the variation of the bending moments around the circumference of culverts having a burial depth of 6 m calculated per the pseudo-static method. Results are presented with a consistent backfill quality and varying levels of seismicity. Similarly to Figure 4.4, Figure 4.6 shows that increasing levels of seismicity do not cause a significant increase in the bending moments at the critical areas (invert, springline, and crown). Increasing seismicity however, does cause a significant increase in bending moments in the haunch areas.

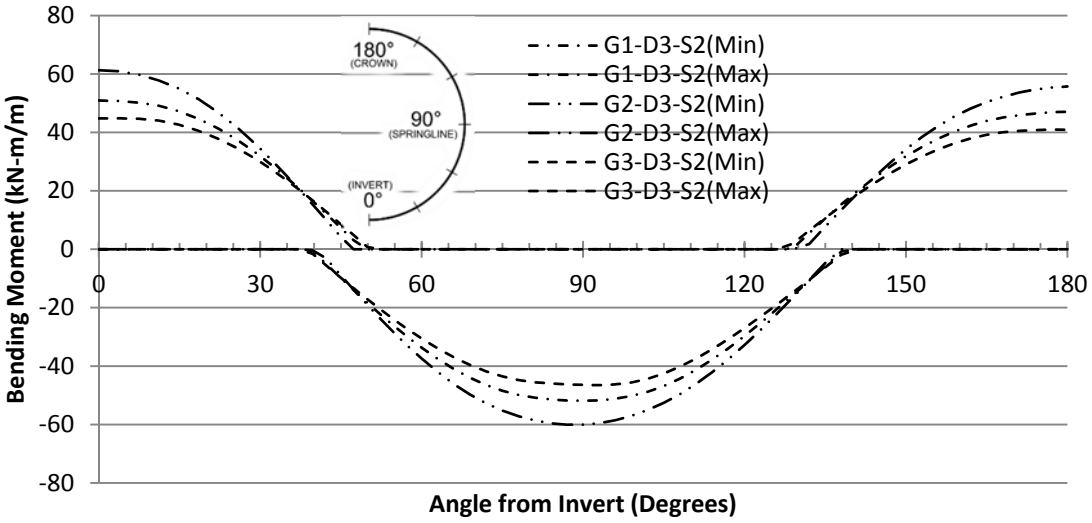

Figure 4.7 - Bending Moments in Culvert with 12 m Fill, MSZ (PS)

Figure 4.7 presents the variation of the bending moments around the circumference of culverts having a burial depth of 12 m calculated per the pseudo-static method. Results are presented with a consistent level of seismicity corresponding to the MSZ and varying levels of backfill quality. Similarly to Figures 4.3 and 4.5, Figure 4.7 shows that, as with the static results presented in Chapter 3, increasing level of backfill compaction result in reduced bending moments along the entire circumference of the culvert.

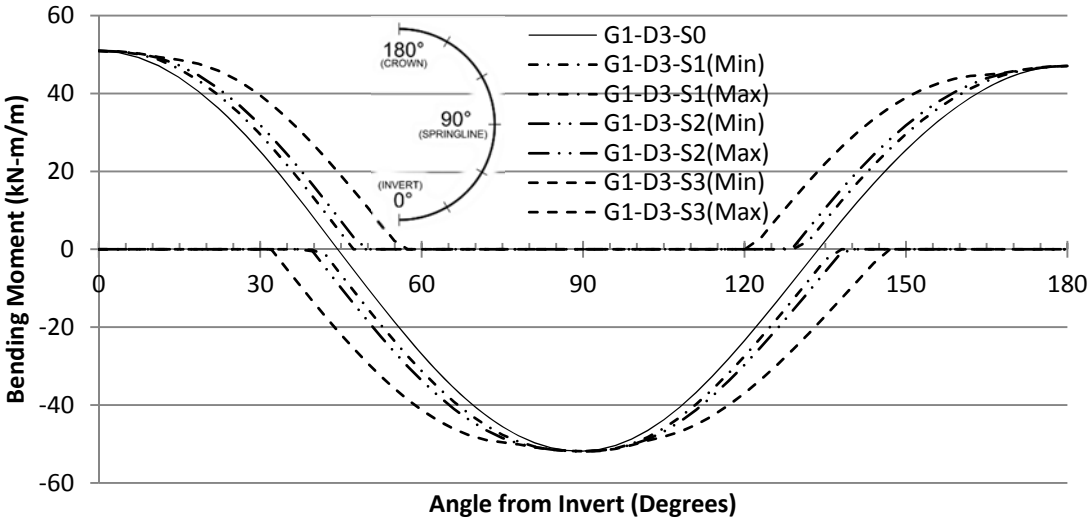

Figure 4.8 - Bending Moments in Culvert with 12 m Fill, MSZ (PS)

Figure 4.8 presents the variation of the bending moments around the circumference of culverts having a burial depth of 12 m calculated per the pseudo-static method. Results are presented with a consistent backfill quality and varying levels of seismicity. Similarly to Figures 4.4 and 4.6, Figure 4.8 shows that increasing levels of seismicity do not cause a significant increase in the bending moments at the critical areas (invert, springline, and crown). Increasing seismicity however does cause a significant increase in the length of the regions of high bending moments, resulting in a significant increase in bending moments in the haunch regions.

4.4.2.1.1 Implications for Structural Design

As the primary basis for structural design is usually the bending moment at the invert, it appears that the seismicity should have negligible impact on the design of the reinforcing steel. However, it may be advisable to avoid elliptical reinforcement where seismicity is a

significant concern. Elliptical reinforcement consists of a single mat that goes from the inside surface of the culvert wall at the crown and invert to the outside surface of the culvert wall at the springline. This results in high flexural resistance in areas where high bending moments are typically expected to occur, however the flexural resistance of the haunch areas are greatly compromised due to the reduced lever arm from the centroid of the reinforcement to the extreme compressive fibres. As increasing levels of seismicity result in increased bending moments in the haunch areas, it may be advisable to avoid elliptical reinforcement where seismicity is a concern.

4.4.2.1.2 Comparison of Seismic Analysis Methods

Tables 4.1 to 4.3 present a comparison of bending moments around the culvert circumference obtained with three methods for evaluating seismic effects. Within each level of seismicity, the column labeled (1) represents the absolute maximum bending moment obtained using the finite-element analysis and the pseudo-static method, (2) represents results obtained by applying the simplified method presented in CHBDC to the static finite-element analysis, and (3) represents results obtained by applying the simplified method presented in CHBDC to static results corresponding to Heger's pressure distribution. Adjacent to the values in (2) and (3) are a percent value representing the relative change as compared to the values in (1). Tables 4.1, 4.2, and 4.3 represent 3 m, 6 m, and 12 m burial depths, respectively. Finite-element results correspond to Group 1 backfill material and Heger results correspond to a Type 1 installation. Results are presented at ten degree intervals along the culvert circumference with "0" representing the invert.

It can be seen from Tables 4.1 to 4.3 that the simplified method of analysis presented in CHBDC (2) overestimates bending moments at the invert, springline and crown and the magnitude of this overestimation increases with increasing seismicity, ranging from approximately three percent for the LSZ to approximately thirty percent for the HSZ. The pseudo-static analysis demonstrated that increasing levels of seismicity increases the range over which the maximum bending moments are located, but not the magnitude of said bending moments. As a result, increasing the static bending moments by scalar multiple as is done with the simplified method results in an overestimation at key areas used for structural design.

Tables 4.1 to 4.3 also show that the simplified method underestimates bending moments in the haunch and shoulder areas. This is simply due to the fact that the result of the simplified method is simply a scalar multiple of the static results and, as such, has an inflection point where bending moments are zero. As a result of this, numerical values for "percent change" presented in the tables are largely meaningless at these locations because, depending on the proximity to the inflection point, the value could be infinitely large. Additionally, while the simplified method does underestimate bending moments in these areas, the magnitudes of said bending moments are very small, and as such, have little to no effect on structural design.

The static analysis presented in Chapter 3 demonstrated that the single value for the vertical arching factor used in Heger's pressure distributions leads to increasingly conservative

results with increasing burial depth. In applying the simplified method presented in CHBDC to results obtained with Heger's pressure distribution (3) results in compounding the conservatism resulting from both methods. Looking at the tables 4.1 to 4.3, this results in overestimations ranging from approximately forty-five percent at the springline for the case of LSZ and 3 m burial depth to approximately 211 percent at the invert for the case of HSZ and 12 m burial depth.

Table 4.1 - Comparison of Seismic Bending Moments with 3 m burial depth.

	LSZ					MSZ					HSZ				
	(1)	(2)		(3)		(1)	(2)		(3)		(1)	(2)		(3)	
	kNm	kNm	%	kNm	%	kNm	kNm	%	kNm	%	kNm	kNm	%	kNm	%
0	18.9	19.5	3.2	33.7	78.5	18.9	21.3	12.8	36.8	95.3	18.9	23.7	25.7	41.0	117.6
10	16.8	16.9	0.6	32.2	91.5	16.8	18.5	10.1	35.3	109.7	16.8	20.6	22.6	39.3	133.5
20	14.5	14.3	-1.5	18.0	23.8	14.5	15.7	7.8	19.7	35.5	14.5	17.5	20.1	21.9	51.0
30	9.9	9.1	-8.4	9.0	-8.7	10.2	9.9	-2.8	9.9	-3.2	10.9	11.1	1.8	11.0	1.4
40	3.6	1.9	-46.0	1.4	-61.8	4.5	2.1	-52.8	1.5	-66.7	8.2	2.4	-71.1	1.7	-79.6
50	7.1	5.0	-29.0	6.1	-14.2	8.1	5.5	-31.9	6.6	-17.8	11.5	6.1	-46.9	7.4	-35.8
60	12.1	11.1	-8.2	13.0	8.0	12.4	12.1	-2.1	14.2	15.1	13.1	13.5	2.8	15.9	20.8
70	15.6	15.7	1.0	19.0	22.2	15.6	17.2	10.5	20.8	33.7	15.5	19.2	23.2	23.2	49.0
80	17.6	18.6	5.6	23.2	31.7	17.6	20.4	15.5	25.4	44.2	17.6	22.7	28.6	28.3	60.5
90	17.3	18.3	5.7	25.1	44.7	17.3	20.0	15.6	27.4	58.3	17.3	22.3	28.8	30.6	76.4
100	15.7	16.3	4.0	23.9	52.6	15.7	17.8	13.7	26.1	66.9	15.7	19.8	26.8	29.1	86.0
110	11.3	11.0	-2.6	19.6	74.1	11.3	12.0	6.7	21.5	90.7	11.3	13.4	19.0	23.9	112.5
120	8.6	7.7	-10.0	13.1	51.7	8.8	8.5	-3.9	14.3	62.0	9.1	9.4	3.3	15.9	74.3
130	3.4	1.7	-49.6	4.7	37.2	4.3	1.9	-55.6	5.2	20.9	7.1	2.1	-70.2	5.7	-18.7
140	7.2	6.0	-17.7	4.3	-40.9	7.8	6.5	-16.3	4.7	-39.9	9.5	7.3	-23.7	5.2	-45.2
150	9.6	8.9	-7.2	12.7	32.1	9.7	9.7	0.1	13.9	42.6	9.9	10.9	10.1	15.5	56.8
160	12.9	13.1	1.7	19.8	53.7	12.9	14.3	11.2	21.7	68.2	12.9	16.0	24.0	24.2	87.5
170	15.4	16.3	5.6	24.4	58.1	15.4	17.8	15.6	26.6	73.1	15.4	19.8	28.7	29.7	92.7
180	15.5	16.4	5.9	25.9	67.1	15.5	18.0	15.8	28.4	82.8	15.5	20.0	29.1	31.6	103.7

Table 4.2 - Comparison of Seismic Bending Moments with 6 m burial depth.

	LSZ					MSZ					HSZ				
	(1)	(2)		(3)		(1)	(2)		(3)		(1)	(2)		(3)	
	kNm	kNm	%	kNm	%	kNm	kNm	%	kNm	%	kNm	kNm	%	kNm	%
0	31.2	33.2	6.7	65.8	111.1	31.2	36.4	16.7	71.9	130.9	31.2	40.5	30.0	80.2	157.2
10	28.2	28.9	2.6	63.2	124.2	28.2	31.6	12.2	69.1	145.1	28.2	35.3	25.1	77.0	173.3
20	24.6	24.4	-1.0	36.4	47.9	25.0	26.7	6.7	39.9	59.3	25.5	29.7	16.7	44.4	74.3
30	17.4	15.7	-9.5	19.4	11.6	18.5	17.2	-6.8	21.2	14.9	21.6	19.2	-11.1	23.6	9.5
40	7.2	4.2	-42.0	4.6	-35.6	8.9	4.6	-48.8	5.1	-43.2	14.7	5.1	-65.5	5.6	-61.7
50	10.4	7.6	-27.1	10.3	-1.0	12.1	8.3	-31.6	11.3	-7.1	18.0	9.3	-48.5	12.6	-30.0
60	19.5	18.1	-7.3	24.9	27.7	20.5	19.8	-3.6	27.2	32.7	23.4	22.0	-5.9	30.3	29.6
70	26.1	26.4	0.9	37.9	45.1	26.3	28.8	9.6	41.5	57.7	26.3	32.1	22.0	46.2	75.5
80	30.0	32.0	6.6	47.6	58.4	30.0	35.0	16.6	52.0	73.2	30.0	39.0	29.9	58.0	93.0
90	29.9	31.9	6.7	52.3	74.9	29.9	34.9	16.7	57.2	91.3	29.9	38.9	30.0	63.7	113.2
100	27.9	29.2	4.6	50.5	80.7	28.0	32.0	14.3	55.2	97.5	28.0	35.6	27.3	61.5	120.0
110	21.3	20.7	-2.9	42.0	96.8	21.9	22.7	3.5	45.9	109.7	22.3	25.2	13.3	51.1	129.5
120	16.6	15.1	-8.7	28.4	71.0	17.6	16.6	-5.8	31.0	76.5	20.4	18.5	-9.6	34.6	69.4
130	7.3	4.6	-37.4	10.8	47.4	9.0	5.0	-43.9	11.8	32.0	14.5	5.6	-61.4	13.2	-9.1
140	11.7	9.5	-19.1	8.3	-29.0	13.1	10.4	-20.4	9.1	-30.1	17.3	11.6	-32.9	10.2	-41.1
150	16.7	15.4	-8.1	26.3	57.2	17.6	16.8	-4.4	28.8	63.4	20.0	18.7	-6.3	32.1	60.3
160	23.8	24.0	1.1	41.7	75.4	23.9	26.3	10.1	45.6	91.0	23.9	29.3	22.6	50.8	112.7
170	28.7	30.6	6.6	51.5	79.1	28.7	33.5	16.6	56.3	95.8	28.8	37.3	29.9	62.7	118.1
180	29.1	31.0	6.7	54.8	88.7	29.1	33.9	16.7	60.0	106.4	29.1	37.8	30.0	66.8	130.0

Table 4.3 - Comparison of Seismic Bending Moments with 12 m burial depth.

	LSZ					MSZ					HSZ				
	(1)	(2)		(3)		(1)	(2)		(3)		(1)	(2)		(3)	
	kNm	kNm	%	kNm	%	kNm	kNm	%	kNm	%	kNm	kNm	%	kNm	%
0	50.9	54.3	6.7	130.0	155.2	50.9	59.4	16.7	142.2	179.1	50.9	66.2	30.0	158.4	210.9
10	46.8	47.2	1.0	125.1	167.6	47.8	51.6	8.1	136.9	186.5	48.2	57.5	19.5	152.5	216.7
20	40.8	40.1	-1.7	73.3	79.6	42.4	43.9	3.5	80.2	89.1	46.5	48.9	5.2	89.3	92.3
30	29.4	26.7	-9.2	40.1	36.5	31.8	29.2	-8.2	43.9	38.1	39.4	32.5	-17.5	48.9	24.0
40	13.0	8.5	-35.0	11.1	-14.6	16.0	9.3	-42.2	12.2	-24.0	26.6	10.3	-61.3	13.6	-49.1
50	15.3	10.7	-29.9	18.8	22.8	18.5	11.7	-36.4	20.6	11.6	29.3	13.1	-55.3	23.0	-21.7
60	31.3	28.7	-8.2	48.6	55.3	33.7	31.4	-6.8	53.1	57.7	41.3	35.0	-15.2	59.2	43.4
70	43.9	43.8	-0.2	75.7	72.6	45.2	47.9	5.9	82.8	83.2	48.4	53.4	10.3	92.3	90.8
80	51.9	54.9	5.9	96.2	85.4	51.7	60.1	16.2	105.2	103.5	51.6	67.0	29.8	117.2	127.3
90	51.8	55.3	6.7	106.7	105.8	51.9	60.5	16.6	116.7	125.0	51.9	67.4	29.9	130.0	150.7
100	49.1	50.8	3.5	103.7	111.0	49.5	55.6	12.4	113.4	129.1	49.7	61.9	24.7	126.3	154.2
110	36.4	35.2	-3.2	86.7	137.9	38.2	38.5	1.0	94.8	148.4	43.2	43.0	-0.7	105.6	144.2
120	27.4	25.0	-8.9	59.0	115.2	29.6	27.3	-7.8	64.5	117.8	36.9	30.5	-17.5	71.9	94.8
130	10.3	6.0	-41.8	23.0	122.2	13.2	6.6	-50.1	25.1	90.5	23.6	7.3	-69.0	28.0	18.6
140	21.9	18.2	-16.8	16.5	-24.9	24.6	19.9	-19.0	18.0	-26.9	33.9	22.2	-34.4	20.1	-40.8
150	29.6	27.2	-8.2	53.6	80.7	31.9	29.7	-6.6	58.6	83.9	38.9	33.1	-14.9	65.3	67.7
160	40.1	40.0	-0.2	85.4	112.9	41.3	43.8	5.9	93.4	126.0	44.2	48.8	10.5	104.1	135.8
170	46.8	49.7	6.3	105.7	125.7	46.7	54.4	16.6	115.6	147.6	46.7	60.6	29.9	128.8	176.0
180	47.1	50.2	6.7	112.7	139.2	47.1	54.9	16.7	123.2	161.6	47.1	61.2	30.0	137.3	191.5

4.4.2.2 Axial Thrusts

The axial thrusts are presented on the ordinate with positive values indicating compression. Results are presented in Figures 4.9 through 4.14.

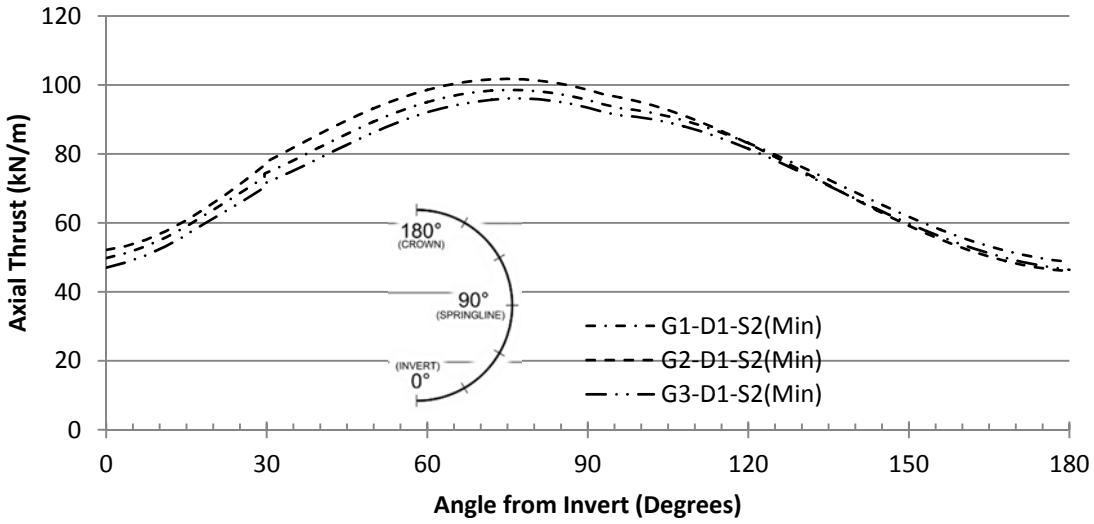

Figure 4.9 – Axial Thrust in Culvert with 3 m Fill, MSZ (PS)

Figure 4.9 presents the variation of the axial thrust around the circumference of culverts having a burial depth of 3 m calculated per the pseudo-static method. Results are presented with a consistent level of seismicity corresponding to the MSZ and varying levels of backfill quality. Figure 4.9 shows that, as with the static results presented in Chapter 3, increasing level of backfill compaction results in reduced axial thrust around the entire circumference of the culvert.

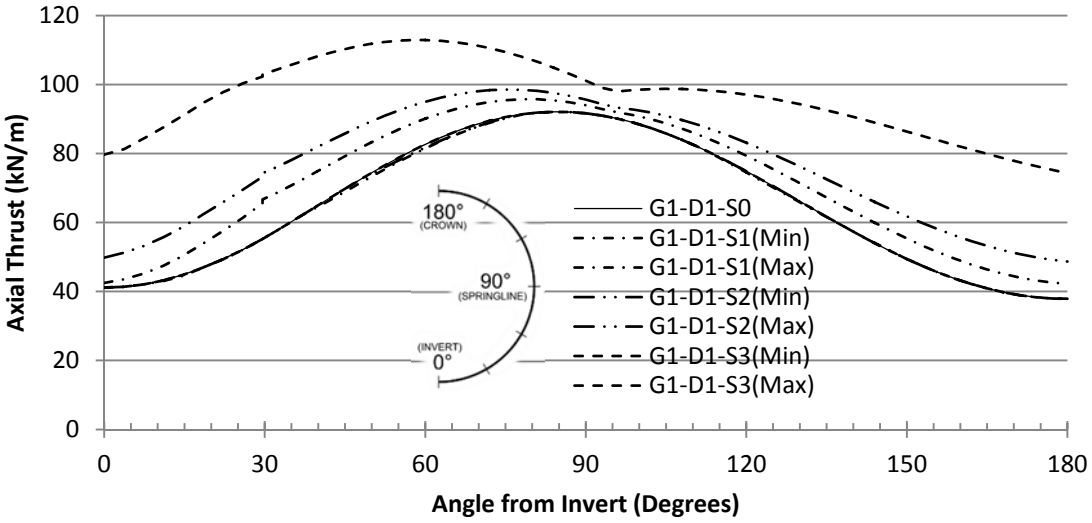

Figure 4.10 – Axial Thrust in Culvert with 3 m Fill, G1 (PS)

Figure 4.10 presents the variation of the axial thrust around the circumference of culverts having a burial depth of 3 m calculated per the pseudo-static method. Results are presented with a consistent backfill quality and varying levels of seismicity. Figure 4.10 shows that increasing levels of seismicity causes the maximum axial load to not only increase, but also to move increasingly away from the springline. Compared to the static results, the LSZ results in an increase approximately four percent and a change in the location of the maximum of approximately six degrees, the MSZ results in an increase approximately seven percent and a change in the location of the maximum of approximately nine degrees, and the HSZ results in an almost twenty-three percent increase and a change in the location of the maximum of approximately twenty-four degrees. The graphs also exhibit two distinct peaks, which are most evident on the HSZ results. This is the result of the analysis where the pseudo-static method was applied alternately in two directions and each peak

representing one direction. The minimum axial thrust values for the seismic load cases are approximately equal to the static load, dropping slightly below the value corresponding to the static analysis in the haunch area.

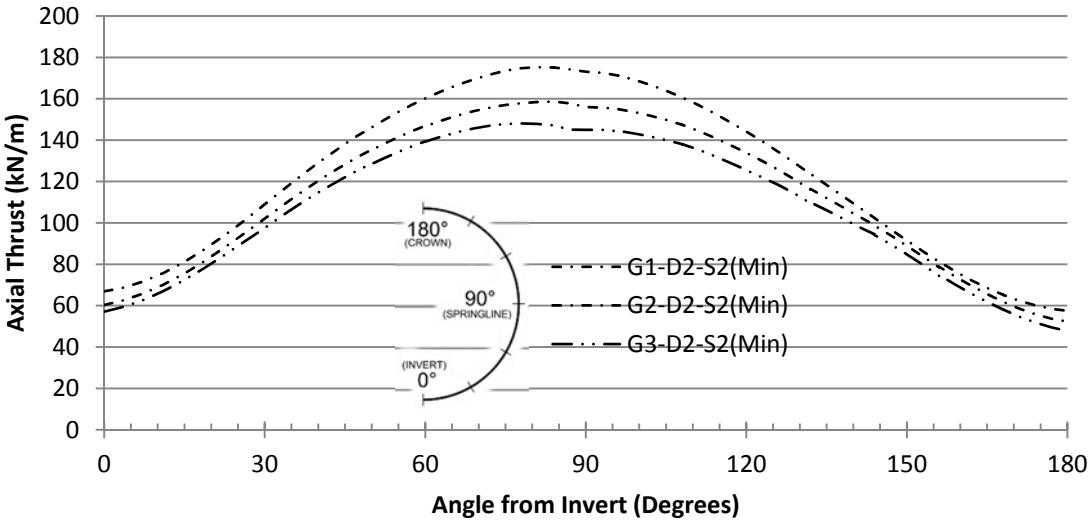

Figure 4.11 – Axial Thrust in Culvert with 6 m Fill, MSZ (PS)

Figure 4.11 presents the variation of the axial thrust around the circumference of culverts having a burial depth of 6 m calculated per the pseudo-static method. Results are presented with a consistent level of seismicity corresponding to the MSZ and varying levels of backfill quality. Similarly to Figure 4.9, Figure 4.11 shows that, as with the static results presented in Chapter 3, increasing level of backfill compaction results in reduced axial thrust around the entire circumference of the culvert.

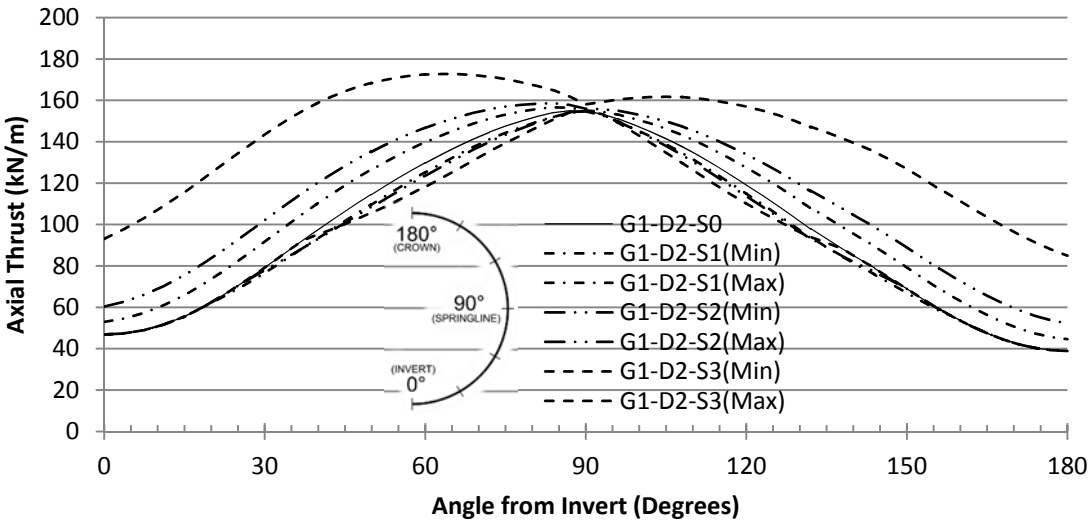

Figure 4.12 – Axial Thrust in Culvert with 6 m Fill, G1 (PS)

Figure 4.12 presents the variation of the axial thrust around the circumference of culverts having a burial depth of 6 m calculated per the pseudo-static method. Results are presented with a consistent backfill quality and varying levels of seismicity. Similarly to Figure 4.10, Figure 4.12 shows that increasing levels of seismicity causes the maximum axial load to not only increase, but also to move increasingly away from the springline. The LSZ and MSZ cause relatively minimal changes in the magnitude and location of the maxima when compared to static results. The HSZ results in an approximately eleven percent increase and a change in the location of the maximum of approximately twenty-four degrees. Also, the two distinct maxima observed in Figure 4.10 are present here as well. At this burial depth, the minimum axial thrust resulting from the seismic load cases are slightly less than that obtained with the static analysis in the haunch and shoulder areas.

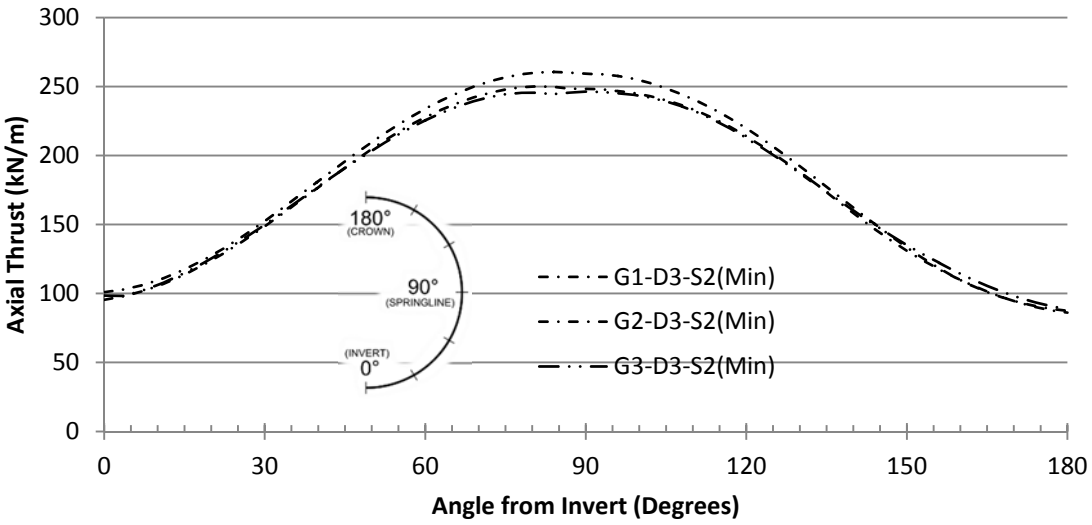

Figure 4.13 – Axial Thrust in Culvert with 12 m Fill, MSZ (PS)

Figure 4.13 presents the variation of the axial thrust around the circumference of culverts having a burial depth of 12 m calculated per the pseudo-static method. Results are presented with a consistent level of seismicity corresponding to the MSZ and varying levels of backfill quality. Similarly to Figures 4.9 and 4.11, Figure 4.13 shows that, as with the static results presented in Chapter 3, increasing level of backfill compaction results in reduced axial thrust around the entire circumference of the culvert.

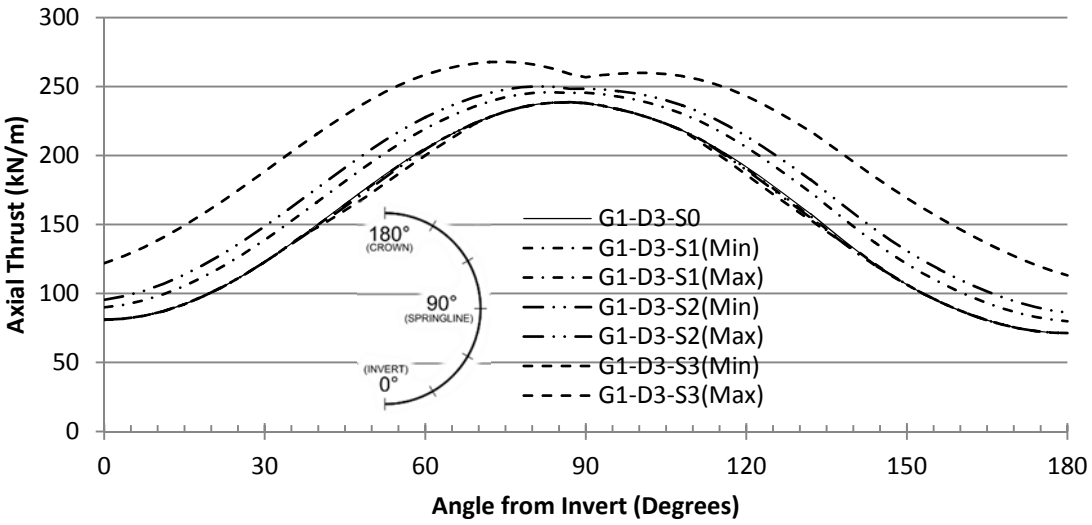

Figure 4.14 – Axial Thrust in Culvert with 12 m Fill, G1 (PS)

Figure 4.14 presents the variation of the axial thrust around the circumference of culverts having a burial depth of 12 m calculated per the pseudo-static method. Results are presented with a consistent backfill quality and varying levels of seismicity. Similarly to Figure 4.10 and 4.12, Figure 4.14 shows that increasing levels of seismicity causes the maximum axial load to not only increase, but also to move increasingly away from the springline. The LSZ and MSZ cause three and five percent increases in axial thrust compared to the static results, respectively. The HSZ results in an approximately twelve percent increase and a change in the location of the maximum of approximately twelve degrees. Also, the two distinct maxima observed in Figures 4.10 and 4.12 are present here as well. At this burial depth, the minimum axial thrust resulting from the seismic load cases are slightly less than that obtained with the static analysis in the haunch and shoulder areas.

4.4.2.2.1 Implications for Structural Design

Equation [2.7] shows that increased axial thrust results in a decrease in the area of required reinforcing steel. As a result, a conservative approach to performing the structural design should be to consider the maximum bending moments and the corresponding minimum axial thrust. Furthermore, Figures 4.10, 4.12, and 4.14 demonstrate that the minimum axial thrust at the invert, springline, and crown are approximately equal to the values obtained with the static analyses regardless of the level of seismicity considered. As these areas are usually the basis for the design of the flexural reinforcement, it should be reasonable to calculate the required area of reinforcing steel using the static axial thrust results. Moreover, the pseudo-static analyses demonstrated that the level of seismicity does not result in a significant increase in the magnitude of the bending moments at these locations. As a result, it should be safe to conclude that the seismicity does not have a significant effect on the design of flexural reinforcing, assuming, of course, that consistent reinforcing steel is provided around the entire circumference of the culvert.

4.4.2.2.2 Comparison of Seismic Analysis Models

Tables 4.4 to 4.6 present a comparison of axial thrusts around the culvert circumference obtained with three methods for evaluating seismic effects. Within each level of seismicity, the column labeled (1) represents the absolute minimum axial thrust obtained using the finite-element analysis and the pseudo-static method, (2) represents results obtained by applying the simplified method presented in CHBDC to the static finite-element analysis, and (3) represents results obtained by applying the simplified method presented in CHBDC to static results corresponding to Heger's pressure distribution. Adjacent to the values in

(2) and (3) are a percent value representing the relative change as compared to the values in (1). Tables 4.4, 4.5, and 4.6 represent 3 m, 6 m, and 12 m burial depths, respectively. Finite-element results correspond to Group 1 backfill material and Heger results correspond to a Type 1 installation. Results are presented at ten degree intervals along the culvert circumference with "0" representing the invert.

It can be seen from Tables 4.4 to 4.6 that the simplified method of analysis presented in CHBDC (2) overestimates axial thrust at the invert, springline and crown and that the magnitude of this overestimation corresponds almost exactly to the scalar multiple by which the static results were increased. While the pseudo-static analysis demonstrated that increasing levels of seismicity cause an increase in the maximum axial thrust, it also demonstrated that the minimum axial thrust are largely unaffected at key areas for structural design. As the basis for structural design should be the minimum axial thrust, the results obtained using the CHBDC simplified method can lead to unconservative results.

The static analysis presented in Chapter 3 demonstrated that the single value for the vertical arching factors used in Heger's pressure distributions leads to increasingly unrealistic results with increasing burial depth. In applying the simplified method presented in CHBDC to results obtained with Heger's pressure distribution (3) results in compounding the potential error resulting from both methods. Looking at the tables, this results in overestimations up to approximately 244 percent approximately twenty degrees from the invert for the case of HSZ, 12 m burial depth.

On the other hand, Heger's pressure distribution results in an underestimation of approximately twelve percent at the crown for the case of the LSZ, 3 m burial depth. This range of values is the result of the unchanging arching factors in Heger's pressure distribution.

Table 4.4 - Comparison of Seismic Axial Thrusts with 3 m burial depth.

	LSZ					MSZ					HSZ				
	(1)	(2)		(3)		(1)	(2)		(3)		(1)	(2)		(3)	
	kN	kN	%	kN	%	kN	kN	%	kN	%	kN	kN	%	kN	%
0	41.1	43.9	6.7	44.8	8.8	41.1	48.0	16.7	49.0	19.0	41.1	53.5	30.0	54.6	32.7
10	44.4	47.9	7.8	47.4	6.8	44.9	52.3	16.7	51.9	15.6	44.9	58.3	30.0	57.8	28.8
20	48.6	51.9	6.7	66.6	36.9	48.6	56.7	16.7	72.8	49.7	48.6	63.2	30.0	81.1	66.8
30	55.7	59.4	6.7	75.2	35.0	55.7	65.0	16.7	82.2	47.6	55.7	72.4	30.0	91.6	64.5
40	64.7	69.4	7.3	89.1	37.7	65.1	75.9	16.7	97.4	49.8	65.1	84.6	30.0	108.6	66.9
50	73.4	79.4	8.2	101.4	38.2	74.1	86.9	17.3	110.9	49.7	74.5	96.8	30.0	123.6	65.9
60	81.5	88.2	8.1	117.4	44.0	81.8	96.4	17.9	128.4	57.1	82.7	107.5	30.0	143.1	73.1
70	88.2	94.8	7.5	123.5	40.1	88.3	103.7	17.4	135.1	53.0	88.9	115.5	30.0	150.6	69.5
80	92.5	98.6	6.5	126.5	36.8	92.4	107.8	16.7	138.4	49.8	92.4	120.1	30.0	154.2	66.9
90	91.7	97.8	6.7	126.4	37.9	91.7	106.9	16.7	138.3	50.8	91.7	119.2	30.0	154.1	68.1
100	88.2	94.1	6.7	125.0	41.7	88.2	102.9	16.7	136.7	55.0	88.2	114.7	30.0	152.4	72.7
110	79.9	85.2	6.7	110.4	38.2	79.9	93.2	16.7	120.7	51.2	79.9	103.8	30.0	134.5	68.5
120	74.5	79.8	7.1	106.3	42.6	74.9	87.3	16.7	116.2	55.3	74.9	97.3	30.0	129.5	73.0
130	65.4	70.0	7.0	90.2	37.8	65.7	76.6	16.7	98.6	50.2	65.7	85.4	30.0	109.9	67.4
140	53.9	57.5	6.7	69.7	29.2	53.9	62.9	16.7	76.2	41.3	53.9	70.1	30.0	84.9	57.4
150	49.4	52.7	6.7	57.8	16.9	49.4	57.7	16.7	63.2	27.9	49.4	64.3	30.0	70.4	42.5
160	43.0	45.8	6.7	41.7	-2.9	43.0	50.1	16.7	45.6	6.2	43.0	55.9	30.0	50.8	18.3
170	38.1	40.7	6.7	37.2	-2.5	38.1	44.5	16.7	40.7	6.7	38.1	49.6	30.0	45.3	18.8
180	37.9	40.4	6.7	33.3	-12.0	37.9	44.2	16.7	36.5	-3.8	37.9	49.3	30.0	40.6	7.2

Table 4.5 - Comparison of Seismic Axial Thrusts with 6 m burial depth.

	LSZ					MSZ					HSZ				
	(1)	(2)		(3)		(1)	(2)		(3)		(1)	(2)		(3)	
	kN	kN	%	kN	%	kN	kN	%	kN	%	kN	kN	%	kN	%
0	46.9	50.0	6.7	98.4	109.9	46.9	54.7	16.7	107.6	129.6	46.9	60.9	30.0	119.9	155.8
10	55.3	59.0	6.7	103.1	86.6	55.3	64.5	16.7	112.8	104.1	55.3	71.9	30.0	125.7	127.4
20	63.6	68.3	7.5	141.0	121.9	64.0	74.7	16.7	154.3	140.9	64.0	83.3	30.0	171.9	168.4
30	76.8	84.7	10.2	158.3	106.0	78.1	92.6	18.6	173.1	121.7	79.4	103.2	30.0	192.9	143.0
40	93.5	104.2	11.4	188.4	101.4	93.2	113.9	22.2	206.1	121.1	95.4	127.0	33.2	229.6	140.8
50	109.7	122.2	11.4	215.6	96.6	108.5	133.7	23.2	235.8	117.4	105.7	148.9	40.9	262.8	148.6
60	125.2	138.4	10.6	252.1	101.4	123.6	151.4	22.5	275.8	123.1	118.3	168.7	42.6	307.3	159.8
70	139.3	152.5	9.5	266.7	91.5	138.1	166.8	20.7	291.7	111.2	133.2	185.8	39.5	325.1	144.1
80	152.4	164.8	8.1	274.8	80.3	152.3	180.2	18.3	300.6	97.4	150.9	200.8	33.0	334.9	121.9
90	154.8	165.1	6.7	276.3	78.5	154.8	180.5	16.7	302.2	95.3	154.8	201.2	30.0	336.7	117.6
100	144.5	156.3	8.2	275.2	90.4	144.1	171.0	18.7	301.0	108.9	142.1	190.6	34.1	335.4	136.1
110	125.4	137.8	9.9	244.2	94.7	124.1	150.7	21.5	267.1	115.3	119.6	167.9	40.4	297.6	148.9
120	114.9	127.0	10.5	237.2	106.5	113.6	138.9	22.2	259.5	128.3	110.1	154.8	40.6	289.1	162.6
130	96.3	107.3	11.4	202.9	110.7	95.7	117.3	22.6	221.9	131.8	95.7	130.7	36.7	247.3	158.4
140	75.6	83.9	11.1	158.2	109.4	76.8	91.8	19.5	173.0	125.4	78.7	102.3	30.0	192.8	145.1
150	67.0	73.5	9.7	132.9	98.4	68.9	80.4	16.7	145.4	111.0	68.9	89.6	30.0	162.0	135.1
160	52.9	56.5	6.7	97.6	84.4	52.9	61.8	16.7	106.8	101.7	52.9	68.8	30.0	119.0	124.7
170	39.7	42.3	6.7	88.1	122.2	39.7	46.3	16.7	96.4	143.0	39.7	51.6	30.0	107.4	170.8
180	38.9	41.5	6.7	79.6	104.6	38.9	45.4	16.7	87.1	123.8	38.9	50.6	30.0	97.1	149.3

Table 4.6 - Comparison of Seismic Axial Thrusts with 12 m burial depth.

	LSZ					MSZ					HSZ				
	(1)	(2)		(3)		(1)	(2)		(3)		(1)	(2)		(3)	
	kN	kN	%	kN	%	kN	kN	%	kN	%	kN	kN	%	kN	%
0	80.9	86.3	6.7	205.6	154.0	80.9	94.4	16.7	224.8	177.8	80.9	105.2	30.0	250.5	209.6
10	92.0	98.1	6.7	214.6	133.3	92.0	107.3	16.7	234.7	155.2	92.0	119.6	30.0	261.6	184.4
20	102.8	109.6	6.7	290.0	182.2	102.8	119.9	16.7	317.2	208.6	102.8	133.6	30.0	353.4	243.9
30	123.1	131.4	6.7	324.5	163.5	123.1	143.7	16.7	354.9	188.2	123.1	160.1	30.0	395.5	221.2
40	150.2	160.6	6.9	387.0	157.7	149.3	175.6	17.6	423.3	183.6	148.5	195.7	31.8	471.7	217.7
50	178.6	191.2	7.1	444.1	148.6	177.1	209.2	18.1	485.7	174.2	173.1	233.1	34.7	541.2	212.7
60	205.1	218.8	6.7	521.6	154.3	204.4	239.3	17.1	570.5	179.0	200.2	266.7	33.2	635.7	217.6
70	225.5	240.5	6.7	553.1	145.3	225.5	263.1	16.7	604.9	168.3	225.2	293.2	30.2	674.1	199.3
80	239.4	255.4	6.7	571.4	138.6	239.4	279.4	16.7	624.9	161.0	239.4	311.3	30.0	696.4	190.8
90	238.0	253.8	6.7	576.0	142.0	238.0	277.6	16.7	629.9	164.7	238.0	309.4	30.0	701.9	195.0
100	229.0	244.3	6.7	575.6	151.3	229.0	267.2	16.7	629.5	174.9	229.0	297.7	30.0	701.5	206.3
110	207.2	221.0	6.7	511.7	147.0	207.0	241.7	16.8	559.7	170.4	203.3	269.3	32.5	623.7	206.8
120	190.5	204.6	7.4	499.1	162.0	189.5	223.7	18.1	545.9	188.1	186.1	249.3	34.0	608.3	226.8
130	160.3	172.9	7.9	428.2	167.2	159.3	189.1	18.8	468.4	194.1	157.0	210.8	34.2	521.9	232.4
140	119.9	129.1	7.6	335.3	179.6	120.0	141.2	17.7	366.7	205.7	122.9	157.3	28.0	408.6	232.6
150	106.4	113.5	6.7	283.2	166.3	106.4	124.2	16.7	309.8	191.0	106.4	138.4	30.0	345.2	224.3
160	86.8	92.6	6.7	209.4	141.3	86.8	101.2	16.7	229.1	163.9	86.8	112.8	30.0	255.2	194.1
170	72.1	76.9	6.7	190.1	163.6	72.1	84.1	16.7	207.9	188.4	72.1	93.7	30.0	231.6	221.3
180	71.4	76.2	6.7	172.2	141.2	71.4	83.3	16.7	188.4	163.9	71.4	92.8	30.0	209.9	194.0

4.4.2.3 Shear Forces

Results of the shear force analyses are presented as Figures 4.15 through 4.20. The legend is identical to that used in the bending moment and axial thrust analyses.

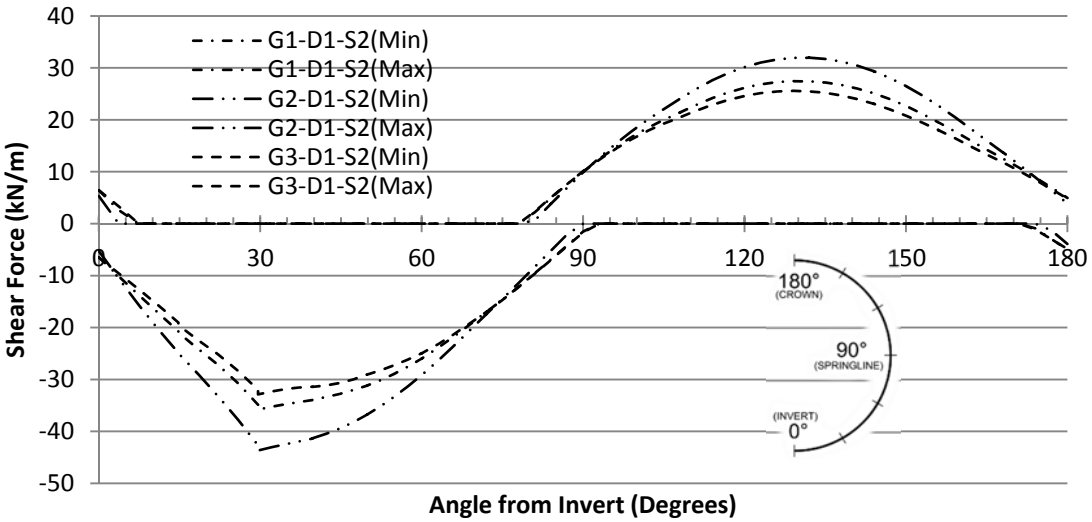

Figure 4.15 – Shear Force in Culvert with 3 m Fill, MSZ (PS)

Figure 4.15 presents the variation of the shear forces around the circumference of culverts having a burial depth of 3 m calculated per the pseudo-static method. Results are presented with a consistent level of seismicity corresponding to the MSZ and varying levels of backfill quality. Figure 4.15 shows that, as with the static results presented in Chapter 3, increasing level of backfill compaction results in reduced shear forces around the entire circumference of the culvert.

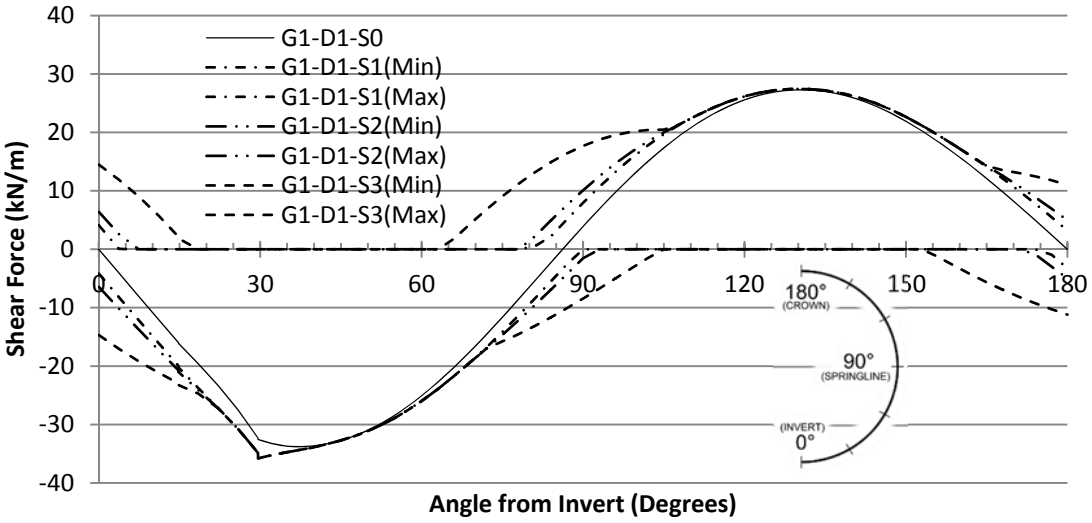

Figure 4.16 – Shear Force in Culvert with 3 m Fill, G1 (PS)

Figure 4.16 presents the variation of the shear forces around the circumference of culverts having a burial depth of 3 m calculated per the pseudo-static method. Results are presented with a consistent backfill quality and varying levels of seismicity. Figure 4.16 shows that applying the pseudo-static seismic loading causes a slight peak in the shear response in the haunch area, but increasing levels of seismicity does not increase the magnitude of this peak. Increasing the level of seismicity causes increases in the magnitude of the shear forces adjacent to the inflection points at the invert, springline, and crown. The magnitude of the peak in the seismic shear response is approximately ten percent greater than the static result.

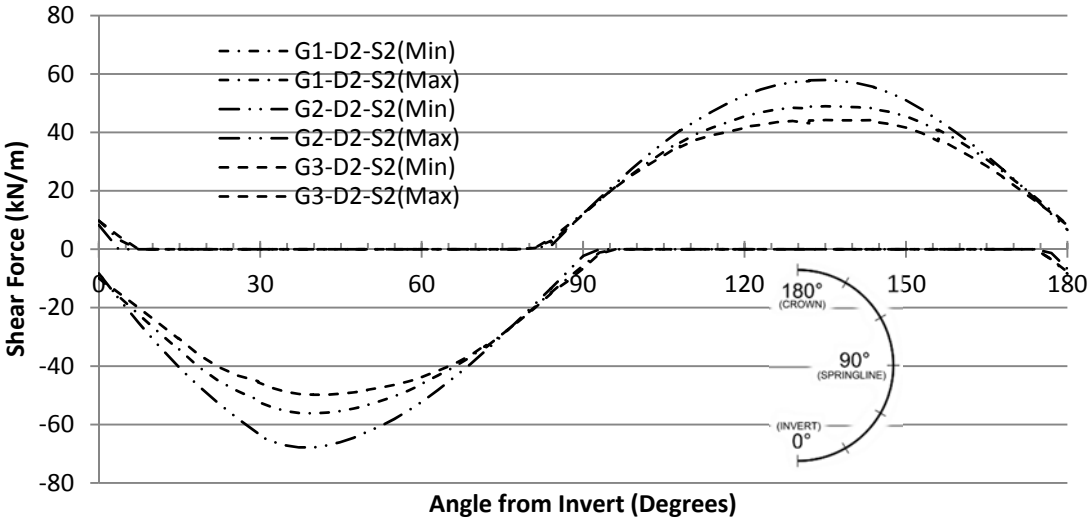

Figure 4.17 – Shear Force in Culvert with 6 m Fill, MSZ (PS)

Figure 4.17 presents the variation of the shear forces around the circumference of culverts having a burial depth of 6 m calculated per the pseudo-static method. Results are presented with a consistent level of seismicity corresponding to the MSZ and varying levels of backfill quality. As with Figure 4.15, Figure 4.17 shows that, as with the static results presented in Chapter 3, increasing level of backfill compaction results in reduced shear forces around the entire circumference of the culvert.

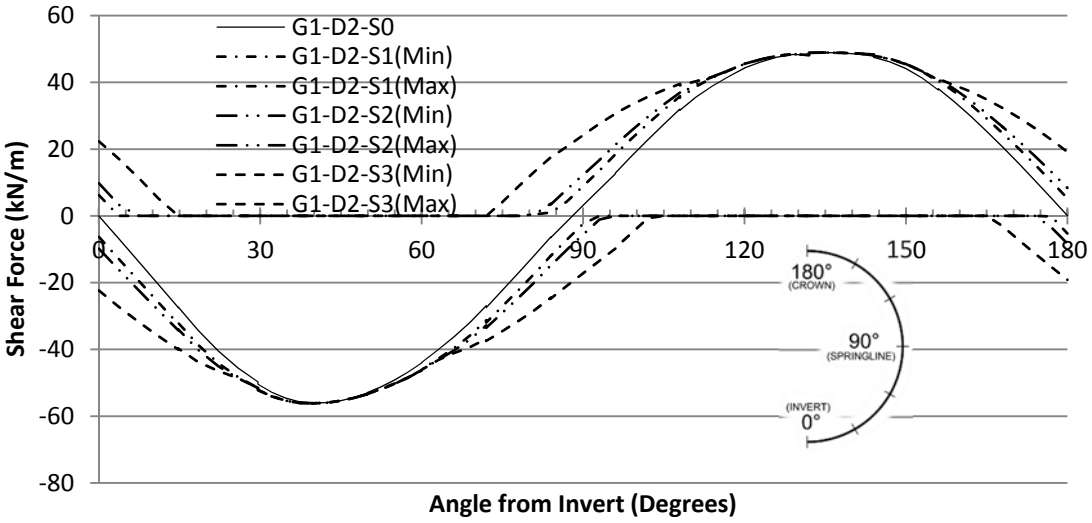

Figure 4.18 – Shear Force in Culvert with 6 m Fill, G1 (PS)

Figure 4.18 presents the variation of the shear forces around the circumference of culverts having a burial depth of 6 m calculated per the pseudo-static method. Results are presented with a consistent backfill quality and varying levels of seismicity. The slight peak in the shear response observed in the haunch area observed in Figure 4.16 is far less pronounced in Figure 4.18. The peak observed in Figure 4.16 may have been caused by the culvert's self-weight, which represents a far smaller portion of the total load when the burial depth increases to 6 m. As with Figure 4.16, Figure 4.18 shows that increasing levels of seismicity causes increases in the magnitude of the shear forces adjacent to the inflection points at the invert, springline, and crown.

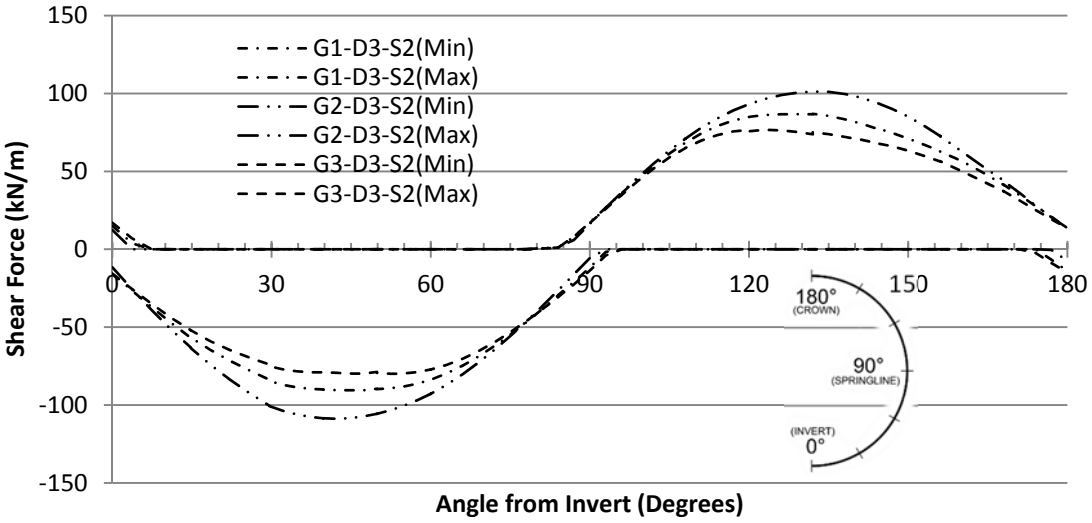

Figure 4.19 – Shear Force in Culvert with 12 m Fill, MSZ (PS)

Figure 4.19 presents the variation of the shear forces around the circumference of culverts having a burial depth of 12 m calculated per the pseudo-static method. Results are presented with a consistent level of seismicity corresponding to the MSZ and varying levels of backfill quality. As with Figures 4.15 and 4.17, Figure 4.19 shows that, as with the static results presented in Chapter 3, increasing level of backfill compaction results in reduced shear forces around the entire circumference of the culvert.

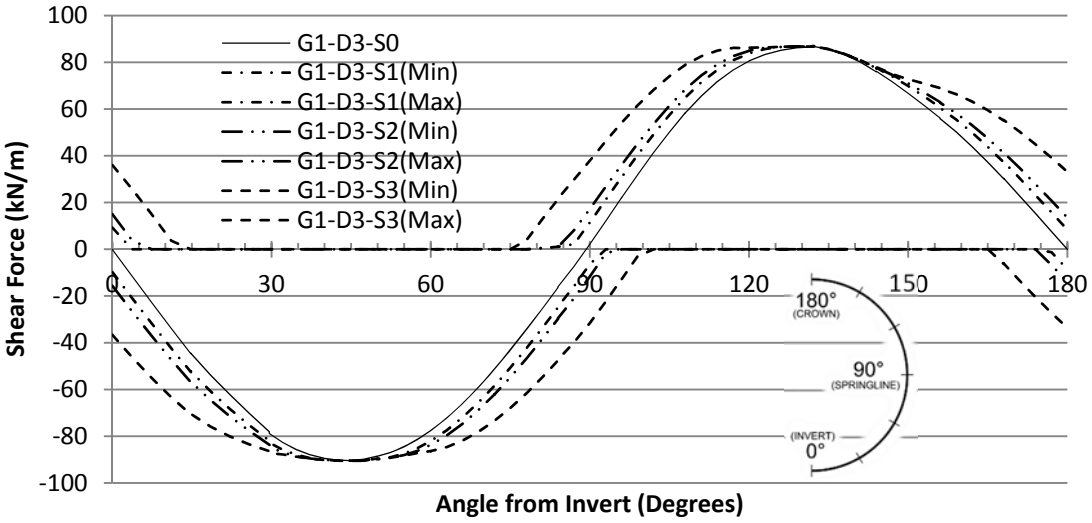

Figure 4.20 – Shear Force in Culvert with 12 m Fill, G1 (PS)

Figure 4.20 presents the variation of the shear forces around the circumference of culverts having a burial depth of 12 m calculated per the pseudo-static method. Results are presented with a consistent backfill quality and varying levels of seismicity. As with Figure 4.18, the slight peak in the shear response observed in the haunch area observed in Figure 4.16 is not evident in Figure 4.20. Again, it is believed that the peak observed in Figure 4.16 may have been caused by the culvert's self-weight, which represents a far smaller portion of the total load when the burial depth increases to 6 m or 12 m. As with Figures 4.16 and 4.18, Figure 4.20 shows that increasing levels of seismicity causes increases in the magnitude of the shear forces adjacent to the inflection points at the invert, springline, and crown.

4.4.2.3.1 Implications for Structural Design

Figures 4.16, 4.18, and 4.20 show that increasing levels of seismicity do not have a significant effect on the magnitude of the maximum shear forces, but do cause increasing shear forces adjacent the inflection points at the invert, springline, and crown. As the shear resistance of the culvert wall is dependent on a number of factors, including the axial thrust, bending moment, shear force, flexural reinforcement ratio, and curvature of the culvert wall, the implications for structural design caused by increasing levels of seismicity are not immediately evident. It is suspected that increasing levels of seismicity likely causes an increase in the range over which stirrups may be required compared with a static analysis, but further study would be required to confirm this.

4.4.2.3.2 Comparison of Seismic Analysis Models

Tables 4.7 to 4.9 present a comparison of shear forces around the culvert circumference obtained with three methods for evaluating seismic effects. Within each level of seismicity, the column labeled (1) represents the absolute maximum shear force obtained using the finite-element analysis and the pseudo-static method, (2) represents results obtained by applying the simplified method presented in CHBDC to the static finite-element analysis, and (3) represents results obtained by applying the simplified method presented in CHBDC to static results corresponding to Heger's pressure distribution. Adjacent to the values in (2) and (3) are a percent value representing the relative change as compared to the values in (1). Tables 4.7, 4.8, and 4.9 represent 3 m, 6 m, and 12 m burial depths, respectively. Finite-element results correspond to Group 1 backfill material and Heger results

correspond to a Type 1 installation. Results are presented at ten degree intervals along the culvert circumference with "0" representing the invert.

Tables 4.7 through 4.9 show that the simplified method of analysis presented in CHBDC (2) overestimates shear forces at the haunch and shoulder areas (at 40˚ and 130˚, respectively) and that the magnitude of this overestimation corresponds very closely to the scalar multiple by which the static results were increased. The tables also show that the simplified method underestimates shear forces at the invert, springline, and crown. This is simply due to the fact that the result of the simplified method is simply a scalar multiple of the static results where shear forces are zero at said locations. As a result of this, numerical values for "percent change" presented in the tables are largely meaningless at these locations because, depending on the proximity to the zero crossing, the value could be infinitely large.

The static analysis presented in Chapter 3 demonstrated that the single value for the vertical arching factors used in Heger's pressure distributions leads to increasingly unrealistic results with increasing burial depth. In applying the simplified method presented in CHBDC to results obtained with Heger's pressure distribution (3) results in compounding the potential error resulting from both methods. Looking at the tables, this results in overestimations up to approximately 192 percent approximately twenty degrees from the invert for the case of HSZ, 12 m burial depth. Another thing to note on the results is that the location of maximum shear is located closer to the invert than was observed in the finite-element results. This is likely due to Heger's pressure distributions, which were

prepared while providing soil clusters having low stiffness in the haunch area in an attempt to better simulate the actual installation conditions and the poor compaction that often occurs in these areas.

Table 4.7 - Comparison of Seismic Shear Forces with 3 m burial depth.

	LSZ					MSZ					HSZ				
	(1)	(2)		(3)		(1)	(2)		(3)		(1)	(2)		(3)	
	kN	kN	%	kN	%	kN	kN	%	kN	%	kN	kN	%	kN	%
0	4.2	0.0	-99.5	0.2	-95.2	6.5	0.0	-99.7	0.2	-96.6	14.7	0.0	-99.8	0.2	-98.3
10	21.5	18.7	-12.8	28.1	31.2	22.1	20.5	-7.4	30.8	39.3	23.8	22.8	-4.3	34.3	43.9
20	26.1	23.7	-9.5	50.5	93.3	26.3	25.9	-1.5	55.3	110.4	26.4	28.8	9.0	61.6	132.8
30	35.7	34.9	-2.3	39.7	11.2	35.7	38.1	6.9	43.4	21.7	35.7	42.5	19.1	48.4	35.6
40	33.9	35.9	5.9	37.1	9.4	33.9	39.2	15.8	40.5	19.7	33.9	43.7	29.1	45.2	33.4
50	31.1	33.0	6.3	36.6	17.8	31.1	36.1	16.3	40.0	28.8	31.1	40.3	29.5	44.6	43.5
60	25.9	26.8	3.1	31.5	21.4	25.9	29.3	12.8	34.4	32.7	25.9	32.6	25.7	38.4	48.0
70	18.1	17.1	-5.2	25.8	42.5	18.2	18.7	3.1	28.2	55.0	18.2	20.9	14.8	31.4	72.7
80	5.5	2.5	-55.5	14.8	167.0	7.0	2.7	-61.2	16.2	132.5	15.1	3.0	-80.1	18.0	19.1
90	8.0	4.1	-48.1	2.1	-73.8	10.1	4.5	-55.2	2.3	-77.5	17.7	5.1	-71.5	2.5	-85.6
100	16.7	14.7	-12.2	13.0	-22.0	17.6	16.0	-8.8	14.2	-19.0	20.3	17.9	-11.9	15.9	-21.8
110	24.3	24.9	2.1	27.2	11.7	24.3	27.2	11.9	29.8	22.4	24.3	30.3	24.7	33.2	36.5
120	26.2	27.3	4.1	39.9	52.3	26.2	29.8	13.9	43.7	66.6	26.2	33.3	26.9	48.6	85.7
130	27.4	29.1	6.0	47.4	72.7	27.4	31.8	15.9	51.8	88.9	27.4	35.4	29.2	57.8	110.5
140	25.4	26.6	4.8	40.0	57.9	25.3	29.1	14.7	43.8	72.8	25.4	32.4	27.7	48.8	92.4
150	22.7	23.4	3.1	39.1	72.3	22.7	25.6	12.8	42.7	88.5	22.7	28.5	25.7	47.6	110.1
160	16.9	16.4	-3.1	25.4	49.9	16.9	17.9	6.0	27.8	64.1	16.9	20.0	18.2	30.9	82.9
170	7.9	5.4	-31.7	19.0	141.0	9.0	5.9	-34.7	20.8	130.6	12.6	6.6	-48.0	23.1	83.8
180	3.2	0.0	-99.9	0.1	-95.5	5.0	0.0	-99.9	0.2	-96.8	11.2	0.0	-99.9	0.2	-98.4

Table 4.8 - Comparison of Seismic Shear Forces with 6 m burial depth.

	LSZ					MSZ					HSZ				
	(1)	(2)		(3)		(1)	(2)		(3)		(1)	(2)		(3)	
	kN	kN	%	kN	%	kN	kN	%	kN	%	kN	kN	%	kN	%
0	6.3	0.0	-99.9	0.4	-93.1	9.8	0.0	-99.9	0.5	-95.2	22.3	0.0	-100.0	0.5	-97.6
10	34.9	32.1	-7.9	50.2	44.1	36.7	35.1	-4.3	55.0	49.7	41.9	39.1	-6.6	61.2	46.2
20	42.4	41.1	-3.0	96.6	127.9	43.5	45.0	3.4	105.7	143.0	45.6	50.1	9.8	117.8	158.2
30	52.6	54.3	3.3	75.2	43.1	52.5	59.4	13.0	82.3	56.6	52.5	66.2	26.0	91.7	74.6
40	56.1	59.8	6.5	72.7	29.5	56.1	65.4	16.5	79.5	41.7	56.1	72.9	29.8	88.6	57.9
50	53.2	56.4	6.1	75.3	41.5	53.2	61.7	15.9	82.3	54.7	53.3	68.8	29.0	91.7	72.1
60	45.9	46.8	2.0	67.1	46.1	46.0	51.2	11.3	73.3	59.4	46.0	57.1	24.0	81.7	77.6
70	33.5	31.4	-6.5	57.2	70.7	34.9	34.3	-1.7	62.6	79.5	38.0	38.2	0.5	69.7	83.4
80	12.2	6.9	-43.2	35.0	188.0	15.1	7.6	-49.9	38.3	154.2	24.9	8.4	-66.2	42.7	71.5
90	9.0	3.4	-62.5	8.4	-6.0	12.4	3.7	-70.2	9.2	-25.3	24.2	4.1	-83.1	10.3	-57.6
100	25.4	21.7	-14.6	24.2	-4.7	27.6	23.7	-14.1	26.5	-4.1	34.5	26.4	-23.4	29.5	-14.5
110	42.2	42.2	0.1	55.4	31.3	42.4	46.2	8.8	60.6	42.8	41.6	51.4	23.8	67.5	62.4
120	45.6	47.3	3.7	83.8	83.9	45.6	51.7	13.4	91.7	101.1	45.6	57.6	26.3	102.2	124.1
130	48.3	51.5	6.5	101.0	109.0	48.3	56.3	16.5	110.5	128.6	48.3	62.7	29.8	123.1	154.7
140	48.4	51.3	5.9	84.8	75.2	48.5	56.1	15.8	92.8	91.5	48.5	62.5	29.0	103.4	113.3
150	45.5	47.1	3.5	83.8	84.3	45.5	51.5	13.1	91.7	101.4	45.5	57.4	25.9	102.1	124.3
160	35.3	34.2	-3.1	54.1	53.3	36.3	37.4	3.1	59.2	63.1	38.2	41.7	9.0	65.9	72.5
170	15.5	11.4	-26.1	41.3	167.1	18.1	12.5	-30.7	45.2	150.4	26.5	13.9	-47.4	50.4	90.0
180	5.3	0.1	-98.7	0.3	-93.4	8.4	0.1	-99.1	0.4	-95.5	19.2	0.1	-99.6	0.4	-97.8

Table 4.9 - Comparison of Seismic Shear Forces with 12 m burial depth.

	LSZ					MSZ					HSZ				
	(1)	(2)		(3)		(1)	(2)		(3)		(1)	(2)		(3)	
	kN	kN	%	kN	%	kN	kN	%	kN	%	kN	kN	%	kN	%
0	9.7	0.1	-98.5	0.9	-90.7	15.6	0.2	-99.0	1.0	-93.7	36.6	0.2	-99.5	1.1	-97.0
10	56.9	52.4	-7.9	94.4	66.0	61.3	57.3	-6.4	103.3	68.6	74.5	63.9	-14.3	115.1	54.4
20	66.0	63.6	-3.6	188.9	186.1	69.4	69.6	0.3	206.6	197.6	78.8	77.5	-1.6	230.2	192.2
30	83.4	84.9	1.9	146.3	75.4	85.0	92.9	9.3	160.0	88.2	87.3	103.5	18.5	178.3	104.1
40	90.0	95.5	6.1	144.0	60.0	90.1	104.4	15.9	157.5	74.8	90.2	116.4	29.0	175.5	94.6
50	89.7	94.5	5.3	152.6	70.1	89.7	103.3	15.2	166.9	86.0	89.8	115.1	28.2	186.0	107.1
60	82.0	82.8	1.0	138.2	68.5	83.7	90.6	8.3	151.2	80.6	86.4	100.9	16.9	168.4	95.0
70	62.0	58.8	-5.1	120.2	93.8	65.4	64.4	-1.6	131.4	100.8	75.7	71.7	-5.3	146.4	93.4
80	25.1	17.7	-29.3	75.5	201.2	30.1	19.4	-35.5	82.6	174.7	48.0	21.6	-55.0	92.0	91.7
90	11.5	2.3	-80.4	21.1	82.8	17.3	2.5	-85.7	23.1	33.4	38.0	2.8	-92.7	25.7	-32.3
100	44.8	39.0	-12.9	46.6	4.1	49.5	42.7	-13.7	51.0	3.1	64.9	47.6	-26.7	56.8	-12.5
110	77.9	77.7	-0.3	111.8	43.5	80.3	84.9	5.8	122.3	52.3	86.3	94.6	9.7	136.2	57.9
120	83.9	86.0	2.5	171.7	104.6	85.1	94.0	10.6	187.8	120.8	86.3	104.8	21.5	209.2	142.6
130	86.7	92.2	6.3	208.2	140.0	86.8	100.8	16.2	227.7	162.4	86.8	112.3	29.4	253.7	192.3
140	78.1	81.9	4.9	174.5	123.5	78.1	89.6	14.7	190.8	144.3	78.3	99.8	27.4	212.6	171.4
150	69.8	71.2	1.9	173.3	148.1	71.0	77.9	9.6	189.5	166.8	72.8	86.8	19.2	211.2	190.2
160	52.8	50.3	-4.7	111.6	111.4	55.7	55.0	-1.3	122.0	119.0	64.9	61.3	-5.5	136.0	109.7
170	23.3	16.4	-29.8	86.0	269.0	28.1	17.9	-36.3	94.1	235.3	45.3	19.9	-56.0	104.8	131.6
180	8.6	0.0	-99.8	0.8	-91.3	14.0	0.0	-99.9	0.8	-94.1	33.7	0.0	-99.9	0.9	-97.3

4.5 Summary and Conclusion

This chapter presented the results of a parametric study that was performed to compare the results of the pseudo-static method of seismic analysis, which is considered more representative to those resulting from the simplified method presented in CHBDC. The primary goal of this study was to determine if and when the simplified method and/or Heger's pressure distributions can be expected to yield reasonable results, and when it may be advisable to employ more refined analysis methods to obtain more economical designs. In the parametric study, the installation depth, the ratio of the stiffness of the backfill to that of the existing embankment material, and the level of seismicity were varied. Based on the results of the parametric study the following conclusions can be drawn:

1. As anticipated, increasing stiffness of the backfill material resulting from increased compaction (better installation quality) results in a decrease in bending moments, shear and axial thrust in the pipe walls.
2. Increased burial depth results in increased soil arching.
3. The constant value of vertical arching factor used in Heger's pressure distributions leads to increasingly conservative results with increasing burial depths.
4. In the case of partial trench installations such as these, Heger's pressure distributions were found to lead to conservative values of bending moments, shear and axial thrusts when compared to FEA methods. In the case of installation in deep embankments, the discrepancy becomes increasingly significant.
5. Increasing levels of seismicity do not cause a significant change in the magnitude of maximum bending moments, shear force and axial thrust for design. It does,

however, cause an increase in the range over which significant bending moments and shear forces are present.

A comparison of required flexural reinforcement as was presented in Section 3.5 was not prepared for this chapter as it is expected to yield very similar results.

The pseudo-static finite element analyses demonstrated that seismicity does not significantly increase bending moments or decrease axial thrusts at areas important for seismic design. As a result, it should be reasonable to conclude that the simplified seismic design combination presented in CHBDC can be safely neglected without decreasing the structural adequacy of the culvert.

4.6 References

Adams, J., Weichert, D., & Halchuck, S. (1999). Lowering the probability level - fourth generation seismic hazard results for Canada at the 2% in 50 year probability level. *Proceedings of the 8th Canadian Conference on Earthquake Engineering,* Vancouver. 6 Pages.

Atkinson, G. M., & Beresnev, I, A. (1998). Compatible ground-motion time histories for new national seismic hazard maps. *Canadian Journal of Civil Engineering, 25*(2), 305-318.

Bardet, J., & Tibita, T. (2001). *NERA: A computer program for nonlinear earthquake site response analysis of layered soil deposits.* (Technical Report). Los Angeles: University of Southern California.

Brinkgreve, R. (2008). *Plaxis 2D - Version 9.0*. Delft, Netherlands: Plaxis.

Canadian Standards Association (CSA). (2006). *CAN/CSA-S6-06 - Canadian highway bridge design code*. Mississauga, Ont.: Canadian Standards Association.

El Naggar, H. (2008). *Analysis and evaluation of segmental concrete tunnel linings - seismic and durability considerations.* (Ph.D., University of Western Ontario (Canada)).

National Research Council of Canada (NRCC). (2005). *National building code of Canada 2005* (Twelfth Edition). Ottawa: Canadian Council on Building and Fire Codes.

Chapter 5 - Chapter 5 – Summary and Conclusions

5.1 General

The objectives of this study were twofold:

The first objective was to determine when Heger's pressure distributions and its associated simplified tools can be expected to yield reasonable results and when more sophisticated, site-specific, finite-element analysis may lead to more appropriate results. This was achieved by performing a finite-element analysis parametric study comparing the effect of the backfill stiffness and the burial depth on the load effects in the culvert. The results of the parametric study were compared with those resulting from Heger's pressure distribution. The analysis, results, and conclusions of this analysis are presented in Chapter 3.

The second objective was to compare the results of the simplified seismic analysis method presented in CHBDC to those resulting from a more sophisticated pseudo-static finite-element analysis to determine if the simplified method leads to reasonable results. This was achieved by performing a finite-element pseudo-static analysis comparing the effect of the backfill stiffness, the burial depth, and the level of seismicity. Results of the parametric study were compared to those resulting from the simplified seismic analysis method presented in CHBDC and Heger's pressure distribution. The analysis, results, and conclusions this analysis are presented in Chapter 4.

5.1.1 Numerical Analysis – Static Load Case

Chapter 3 presented the results of a parametric study that was performed to investigate the appropriateness of using the Heger pressure distribution to predict internal forces in pipe culverts. The main aim is to determine when Heger's pressure distributions can be expected to yield reasonable results and when it may be advisable to employ more refined analysis methods to obtain more economical designs. In the parametric study, the installation depth as well as the ratio of the stiffness of the backfill to that of the existing embankment material was varied. Based on the results of the parametric study the following conclusions may be drawn:

1. As anticipated, increasing stiffness of the backfill material resulting from increased compaction (better installation quality) results in a decrease in bending moments, shear and axial thrust in the pipe walls.
2. Increased burial depth results in increased soil arching.
3. The constant value of vertical arching factor used in Heger's pressure distributions leads to increasingly conservative results with increasing burial depths.
4. In the case of partial trench installations, Heger's pressure distribution was found to lead to conservative values of bending moments, shear and axial thrusts when compared to FEA methods. In the case of installation in deep embankments, the discrepancy becomes increasingly significant.
5. The required flexural reinforcement calculated using Heger's pressure distributions is significantly greater than that calculated using the finite-element analysis.

The finite-element analysis parametric study demonstrates that Heger's pressure distributions consistently leads to conservative results in partial trench embankments. As a

result, in these installations, it may be reasonable to apply more sophisticated analysis methods to achieve a more economical design. The additional cost incurred through the use of more sophisticated analysis methods, such as finite-element analysis, should be considered in performing the cost comparison.

5.1.2 Numerical Analysis – Seismic Load Case

Chapter 4 presented the results of a parametric study that was performed to compare the results of the pseudo-static method of seismic analysis which is considered more representative to those resulting from the simplified method presented in CHBDC. The primary goal was to determine if and when the simplified method and/or Heger's pressure distributions can be expected to yield reasonable results and when it may be advisable to employ more refined analysis methods to obtain more economical designs. In the parametric study, the installation depth, the ratio of the stiffness of the backfill to that of the existing embankment material, and the level of seismicity were varied. Based on the results of the parametric study the following conclusions may be drawn:

1. As with the static load case, increasing stiffness of the backfill material resulting from increased compaction (better installation quality) results in a decrease in bending moments, shear and axial thrust in the pipe walls.
2. Increased burial depth results in increased soil arching.
3. The constant value of vertical arching factor used in Heger's pressure distributions leads to increasingly conservative results with increasing burial depths.
4. In the case of partial trench installations such as these, Heger's pressure distributions were found to lead to conservative values of bending moments, shear

and axial thrusts when compared to FEA methods. In the case of installation in deep embankments, the discrepancy becomes increasingly significant.

5. Increasing levels of seismicity do not cause a significant change in the magnitude of bending moments, shear force and axial thrust for design. It does, however, cause an increase in the range over which significant bending moments and shear forces are present.

The pseudo-static finite element analyses demonstrated that seismicity does not significantly increase bending moments or decrease axial thrusts at areas important for seismic design. As a result, it should be reasonable to conclude that the simplified seismic design combination presented in CHBDC can be safely neglected without decreasing the structural adequacy of the culvert.

5.2 Recommended Further Study

Recommended further study is as follows:

1. Refine analysis to consider voids in the haunch area as a result of poor compaction as was done in preparing Heger's pressure distribution.
2. Refine analysis to consider the effect of changing the excavation geometry, such as the slope of the excavation and the width at the base.

5.3 Practical Considerations

It is acknowledged that the embankment stability of the 6 m and 12 m cases are barely at or less than practical factor of safety for trench excavations (i.e. 1.3) and accordingly should be investigated for design purposes, however these depths were included in the

parametric study solely to show the effect of the high depth of fill on the predictions of the Heger pressure distributions. The extrapolation of the results presented in this thesis should be done cautiously specially for wide trench cases in which the interaction behaviour converge more towards the positive projection case in such case the difference between the FEA results and the Heger predictions are less than the values presented here.

Bibliography

Adams, J., Weichert, D., & Halchuck, S. (1999). Lowering the probability level - fourth generation seismic hazard results for Canada at the 2% in 50 year probability level. *Proceedings of the 8th Canadian Conference on Earthquake Engineering,* Vancouver. 6 Pages.

Allard, E., El Naggar, H. (2013) "Evaluation of PipeCAR per Canadian Highway Bridge Design Code Requirements". GeoMontreal 2013. September 29 to October 3 2013. Montreal, Canada.

Allen, D. (1975). Limit states design - A probabilistic study. *Canadian Journal of Civil Engineering, 2*(36), 36-49.

American Association of State Highway and Transportation Officials (AASHTO). (2004). *AASHTO LRFD bridge design specifications.* (SI Units, Third Edition). Washington, DC: American Association of State Highway and Transportation Officials.

American Concrete Pipe Association (ACPA). (1980). *Concrete pipe design manual*. Vienna, Va.: American Concrete Pipe Association (ACPA).

American Concrete Pipe Association (ACPA). (2011). *Concrete pipe design manual*. Vienna, Va.: American Concrete Pipe Association (ACPA).

American Society for Testing and Materials (ASTM). (2003). *C 76M-03 Standard specification for reinforced concrete culvert, storm drain, and sewer pipe [Metric], 04.05*

American Society of Civil Engineers (ASCE). (2000). *Standard practice for direct design of buried precast concrete pipe using standard installations (SIDD)* American Society of Civil Engineers.

Atkinson, G. M., & Beresnev, I, A. (1998). Compatible ground-motion time histories for new national seismic hazard maps. *Canadian Journal of Civil Engineering, 25*(2), 305-318.

Bardet, J., & Tibita, T. (2001). *NERA: A computer program for nonlinear earthquake site response analysis of layered soil deposits.* (Technical Report). Los Angeles: University of Southern California.

Brinkgreve, R. (2008). *Plaxis 2D - Version 9.0*. Delft, Netherlands: Plaxis.

Canadian Standards Association (CSA). (2003). *CAN/CSA-A257 - Standards for concrete pipe and manhole sections.* CSA Group.

Canadian Standards Association (CSA). (2006). *CAN/CSA-S6-06 - Canadian highway bridge design code*. Mississauga, Ont.: Canadian Standards Association.

El Naggar, H. (2008). *Analysis and evaluation of segmental concrete tunnel linings - seismic and durability considerations.* (Ph.D., University of Western Ontario (Canada)).

Erdogmus, E., Skourup, B. N., & Tadros, M. (2010). Recommendations for design of reinforced concrete pipe. *Journal of Pipeline Systems Engineering and Practice, 1*(1), 25-32.

Galambos, T., & Ravindras, M. (1977). The basis for load and resistance factor design criteria of steel building structures. *Canadian Journal of Civil Engineering, 4*, 178-189.

Heger, F. J. (1985). Proportioning reinforcement for buried concrete pipe. ASCE Proceedings. Advances in Underground Pipeline Engineering, Madison, WI, 543-553.

Heger, F. J. (1988). New installation designs for buried concrete pipe. Pipeline Infrastructure, Proceedings, 117-135.

Heger, F. J., Liepins, A. A., & Selig, E. T. (1985). SPIDA: An analysis and design system for buried concrete pipe. ASCE Proceedings. Advances in Underground Pipeline Engineering, Madison, WI, 143-154.

Heger, F. J., Zarghamee, M. S., & Dana, W. R. (1990). Limit-states design of prestressed concrete pipe. I. Criteria. *Journal of Structural Engineering New York, N.Y., 116*(8), 2083-2104.

Irving, D. (1985). The LUSAS finite element system with reference to the construction industry. *Proceedings of the 2nd International Conference on Civil and Structural Engineering Computing, London, Volume 2*

Kan, F. W., Zarghamee, M. S., & Rose, B. D. (2002). Seismic evaluation of buried pipelines. Paper presented at the *Pipelines 2002 - Beneath our Feet: Challengers and Solutions - Proceedings of the Pipeline Division Specialty Conference,* 13.

Kang, J., Parker, F., & Yoo, C. H. (2007). Soil-structure interaction and imperfect trench installations for deeply buried concrete pipes. *Journal of Geotechnical and Geoenvironmental Engineering, 133*(3), 277-285.

Katona, M. G. (2010). Seismic design and analysis of buried culverts and structures. *Journal of Pipeline Systems Engineering and Practice, 1*(3), 111-119.

Kogut, G. F., & Chou, K. C. (2004). Partial resistance factor design on steel-concrete beam-columns. *Engineering Structures, 26*, 857-866.

Kurdziel, J. M., & McGrath, T. J. (1991). SPIDA method for reinforced concrete pipe design. *Journal of Transportation Engineering, 117*(4), 371-381.

MacEy, C., Cadieux, R., & Braun, A. (2012). *Reinforced concrete pipe design under extreme loading conditions using ASCE standard practice 15-98 and beyond.*

Marston, A. (1930). *The theory of external loads on closed conduits in the light of the latest experiments.* (Bulletin 96, Iowa Engineering Experiment Station).Iowa State College.

Maximos, H., Erdogmus, E., & Tadros, M. (2008). Full scale test installation for reinforced concrete pipe. Paper presented at the *Proceedings of Pipelines Congress 2008 - Pipeline Asset Management: Maximizing Performance of our Pipeline Infrastructure, 321*

McGrath, T., Selig, E., Webb, M., & Zoladz, G. (1999). *Pipe interaction with the backfill envelope.* (No. FHWA-RD-98-191). McLean, VA: US Department of Transportation Federal Highway Administration (FHWA).

McGrath, T. J., Tigue, D. B., & Heger, F. J. (1988). PIPECAR and BOXCAR microcomputer programs for the design of reinforced concrete pipe and box sections. *Transportation Research Record,* (1191), 99-105.

National Research Council of Canada (NRCC). (2005). *National building code of Canada 2005* (Twelfth Edition). Ottawa: Canadian Council on Building and Fire Codes.

Selig, E. T. & Packard, D. L. (1987). Buried concrete pipe trench installation analysis. *Journal of Transportation Engineering, 113*(5), 485-501.

Spangler, M. (1933). *The supporting strength of rigid pipe culverts.* (Bulletin 112, Iowa Engineering Experiment Station). Iowa State College.

Wong, L. S., Allouche, E. N., Baumert, M., Dhar, A. S., & Moore, I. D. (2006). Long-term monitoring of SIDD type IV installations. *Canadian Geotechnical Journal, 43*(4), 392-408.

Curriculum Vitae

Candidate's full name: Eric Yvon Allard

Universities attended (with dates and degrees obtained):

University of New Brunswick, Bachelor of Science in Engineering, 2008

Conference Presentations:

Allard, E., El Naggar, H. (2013) "Evaluation of PipeCAR per Canadian Highway Bridge Design Code Requirements". GeoMontreal 2013. September 29 to October 3 2013. Montreal, Canada.